

**$^{40}\text{Ar}/^{39}\text{Ar}$  Age and Structural Constraints on Permian–Triassic and Jurassic  
Tectono-Metamorphic and Exhumation Phases in the Korean Collision Belt  
and Tectonic Implications**

**Koen de Jong<sup>1</sup>, Gilles Ruffet<sup>2</sup>, and Seokyoung Han<sup>1</sup>**

<sup>1</sup> School of Earth and Environmental Sciences, Seoul National University, 311 ho, 25-1 dong, 1  
Gwanak-ro, Gwanak-gu, Seoul 08826, Republic of Korea

<sup>2</sup> CNRS (CNRS/INSU) UMR 6118, Géosciences Rennes, 35042 Rennes Cedex, France and  
Université de Rennes 1, Géosciences Rennes, 35042 Rennes Cedex, France

Corresponding Author: Koen de Jong (keuntie@yahoo.com)

**Key Points:**

- Korean Collision Belt: a southwards-tapering tectonic wedge with discrete tectono-metamorphic phases at 255–247, 245–237, 225–220 Ma
- 255–247 Ma: fast cooling, rapid exhumation, top-to-SE normal shear; 225–220 Ma: downwards increase retrogression, top-to-N normal shear
- 245–237 Ma: strong reworking; exhumation mid-Triassic eclogite; 194–165 Ma: final metamorphic reactivation and top-to-N normal shear

**Abstract**

The Korean Collision Belt originally constituted a single coherent southwards-thinning tectonic wedge formed by accretion of the Qinling-type Barrovian metamorphic Jingok and Samgot units (Yeoncheon Complex) and Taean Formation onto the Sino–Korean Craton’s southern extension (Precambrian Gyeonggi Massif) while being underthrust by the South China Block. Detailed structural geological study and  $^{40}\text{Ar}/^{39}\text{Ar}$  laser-probe dating of 47 mineral single-grain and 2 whole-rock samples with both syn-collisional peak metamorphic and retrograde mineral assemblages reveal a prolonged tectonic evolution from the Devonian–Carboniferous pre-collisional stage (375–370 Ma; ~315 Ma) to the Middle–Late Jurassic reactivation of the Permian–Triassic wedge during the second major exhumation phase of the Gyeonggi Massif (194–165 Ma). The latest Permian to Late Triassic main orogeny comprises three distinct correlated tectono-metamorphic phases. Essentially concordant (pseudo-)plateau ages ( $255.2\text{--}249.9 \pm 0.4\text{--}0.9$  Ma,  $1\sigma$ ) for main-phase-fabric-forming muscovite and biotite in the garnet, staurolite and kyanite zones and discordant late-stage andalusite-quartz veins (Jingok Unit) show fast cooling during exhumation from ~30 km to  $\leq 12.5$  km. Hornblendes ( $248.8\text{--}247.0 \pm 0.6\text{--}1.6$  Ma,  $1\sigma$ ) in the underlying higher-grade metamorphic, deeper underthrust Samgot Unit show later cooling. Fabric asymmetry implies cooling and age differences stem from (S)SE-ward exhumation along low-angle ductile normal faults. Incipient exhumation of mid-Triassic eclogites (Hongseong Belt) induced strong tectono-metamorphic reworking of the overriding plate (242–237 Ma; Yeoncheon Complex, Taean Formation, Gyeonggi Massif). Structurally downwards increasing resetting of mica (225–220 Ma), retrogression and overprinting by top-to-the-north post-main-phase-shear constrains the Gyeonggi Massif’s further exhumation and cooling.

45

46 **Plain Language Summary**

47 The Korean Collision Belt was a tectonic wedge to the south of the Sino–Korean Craton that  
48 formed by collision with the South China Block. Detailed structural geological investigations  
49 and radiometric age determination of mineral grains and whole-rock samples with a laser-probe  
50 reveal a prolonged tectonic evolution from the Devonian–Carboniferous pre-collisional stage  
51 (375–370 million years ago (myrs) and ~315 myrs) to the Middle–Late Jurassic post-collisional  
52 stage (194–165 myrs). The wedge was formed during the main collision from the latest Permian  
53 to the Late Triassic (255–220 myrs) and experienced three distinct phases of deformation and  
54 metamorphic recrystallization. During this main tectonic period the rocks cooled fast in the 650–  
55 400°C temperature range, while being exhumed from about 30 km to less than 12.5 km. The  
56 asymmetry of structures formed in this process reveals (S)SE-ward movement along low-angle  
57 extensional faults (255–247 myrs). The movement sense reversed around 225–220 myrs  
58 concomitant with structurally downwards increasing retrograde recrystallization. Final  
59 metamorphic reworking and tectonic reactivation occurred in Early–Middle Jurassic time when  
60 an Andean-type magmatic arc was created and extensional sedimentary basins formed, further  
61 partially exhuming the collision belt’s deeper part.

62

## 1. Introduction

Due to its particular location in the eastward extension of two Late Paleozoic to Early Mesozoic orogenic belts towards the Pacific Ocean the continental crust of Korea was affected by tectonism and magmatism linked to Permian–Triassic collisional and post-collisional processes. In addition, being located in the East Asian continental margin, the Korean Peninsula’s crust also bears the marks of deformational and/or igneous events related to subduction of Paleo-Pacific oceanic lithosphere in the Permian–Triassic, Jurassic and Cretaceous. Accordingly, deformation, metamorphism and magmatism during the entire Mesozoic Era combined to create Korea’s great geological complexity. The peninsula’s tectonic evolution is subdivided into the Songnim (Late Permian to Middle/Late Triassic), Daebong (Early Jurassic to Early Cretaceous) and Bulguksa (Late Cretaceous to Paleogene) orogenies, separated by more quiet periods (e.g., [Chough, 2013](#); [S.I. Park et al., 2019](#)). Yet, mainly because suitable isotopic dating methods have yet to be applied to appropriate targets combined with their detailed structural study, both tectonic architecture and evolution of Korea is only fairly crudely known, so that many fundamental tectonic questions remain unanswered. As a consequence a multitude of widely different and sharply conflicting models have been put forward that generally high-light and try to explain just a single aspect of the geological data ([M. Cho et al., 2007, 2013](#); [M. Cho, Kim, Yang, & Yi, 2017](#); [M. Cho, Lee, Kim, Cheong, Kim, & Lee, 2017](#); [Cho & Kim, 2005](#); [D.K. Choi et al., 2012](#); [Jeong et al., 2021](#); [S.W. Kim et al., 2006, 2008, 2015](#); [S.W. Kim, Kwon, Park, Yi, Santosh, & Kim, 2017](#); [S.W. Kim, Park, Jang, Kwon, Kim, & Santosh, 2017](#); [J.M. Kim et al., 2008](#); [Kwon et al., 2009, 2013](#); [B.C. Lee et al., 2019](#); [Oh et al., 2015, 2017](#); [Oh & Kusky, 2007](#); [Ree et al., 1996](#); [Sajeev et al., 2010](#); [Suzuki, 2009](#); [Yengkhom et al., 2014](#)).



The Korean Peninsula's geological time line shows a cluster of isotopic dates between ca. 290 Ma and 210 Ma, the relation of which to specific major tectonic events remains, however, unclear. Geochronological studies applying the chemical Th–U–total Pb isochron method (CHIME), Laser Ablation Inductively Coupled Plasma Mass Spectrometry (LA-ICP-MS) and the Sensitive High-Resolution Ion Micro Probe (SHRIMP) have flourished during the past two decades (D.L. Cho, 2014; de Jong et al., 2014; Jeong et al., 2021; B.C. Lee et al., 2019; H.S. Kim et al., 2022; J.M. Kim et al., 2008; S.W. Kim et al., 2006, 2008; Oh et al., 2015, 2017; S.-I. Park, Kim, Kwon, Thanh, Yi, & Santosh, 2014; S.-I. Park, Kwon, Kim, Yi, & Santosh, 2014; Suzuki, 2009; Suzuki et al., 2006; Yengkhom et al., 2014; Yi, 2010; Yi & Cho, 2009). Although many of these studies yielded Permo-Triassic isotopic dates, it often appeared difficult to link U–Th–Pb data of sub-millimeter grains of polygenetic zircon, allanite and monazite to the metamorphic evolution or to fabric forming tectonic events. In contrast to SHRIMP dating of Th- and U-bearing accessory minerals  $^{40}\text{Ar}/^{39}\text{Ar}$  geochronology can be applied to a wide range of common K-bearing fabric-forming minerals, like micas or amphiboles, whose growth, deformation and recrystallization can be straightforwardly correlated to major phases of the tectono-metamorphic evolution of rocks. The  $^{40}\text{Ar}/^{39}\text{Ar}$  method permits to identify different age components in recrystallized minerals so that meaningful geochronological information can even be extracted from rocks and regions with a complex geological history (Alexandrov et al., 2002; Daoudene et al., 2013; de Jong et al., 1992, 2006, 2009; Lister & Baldwin, 1996; Pitra et al., 2010; Viete et al., 2011). Indeed, the widely varying K–Ar mineral dates ranging from 675 Ma to 136 Ma (Cho & Kim, 2005; Kee, 2011; S.W. Kim, 2005; S.W. Kim et al., 2008, and references therein) illustrate Korea's complex thermo-tectonic history underscoring the need for state-of-the-art  $^{40}\text{Ar}/^{39}\text{Ar}$  dating. The  $^{40}\text{Ar}/^{39}\text{Ar}$  dating method has before our own studies (de Jong & Ruffet,

2014a, 2014b; de Jong et al., 2014, 2015) only been occasionally applied to Korean material (R. Han et al., 2014; S.W. Kim, 2005; S.I. Park et al., 2019). Research results on the Yeoncheon Complex, the main target of our study, are regrettably very rarely published; the limited number of isotopic ages referred to in the literature, is unfortunately mainly from unpublished sources, hence not providing isotopic data and statistical procedures, nor location, characteristics and context of samples, rendering their meaning fairly limited. Together with our earlier publications the present paper is part of the first systematic  $^{40}\text{Ar}/^{39}\text{Ar}$  study in the foremost Korean metamorphic litho-tectonic units to the north and west of the Precambrian Gyeonggi Massif (Fig. 1). With these new isotopic age constraints mainly provided by laser-probe dating of muscovite, biotite and hornblende single-grains from samples with peak tectono-metamorphic as well as with retrograde mineral assemblages, combined with the structural study of these units and additional metamorphic data from the literature, we are in a position to discuss the different stages of the tectonic evolution of the Korean Collision Belt from the latest Permian to middle Jurassic. We use the chart of the International Commission on Stratigraphy (Cohen et al., 2013) to transfer isotopic dates to chronostratigraphical ages.

## 2. Regional Geology of the Central Korean Peninsula

The Korean Collision Belt is developed to the south of the Sino–Korean Craton, represented by the Nangrim Massif (Fig. 1) and comprises Neoproterozoic–Paleoproterozoic granite–gneiss basement terranes (massifs) separated by belts of polyphasely deformed Paleozoic and Neoproterozoic meta-sedimentary and meta-volcanic series. From North to South the: Imjingang Belt, Gyeonggi Massif, Okcheon Belt and Yeongnam Massif (Fig. 1). In addition, a mélange zone, the Hongseong Belt, occurs along the Gyeonggi Massif's western margin (Fig. 1).

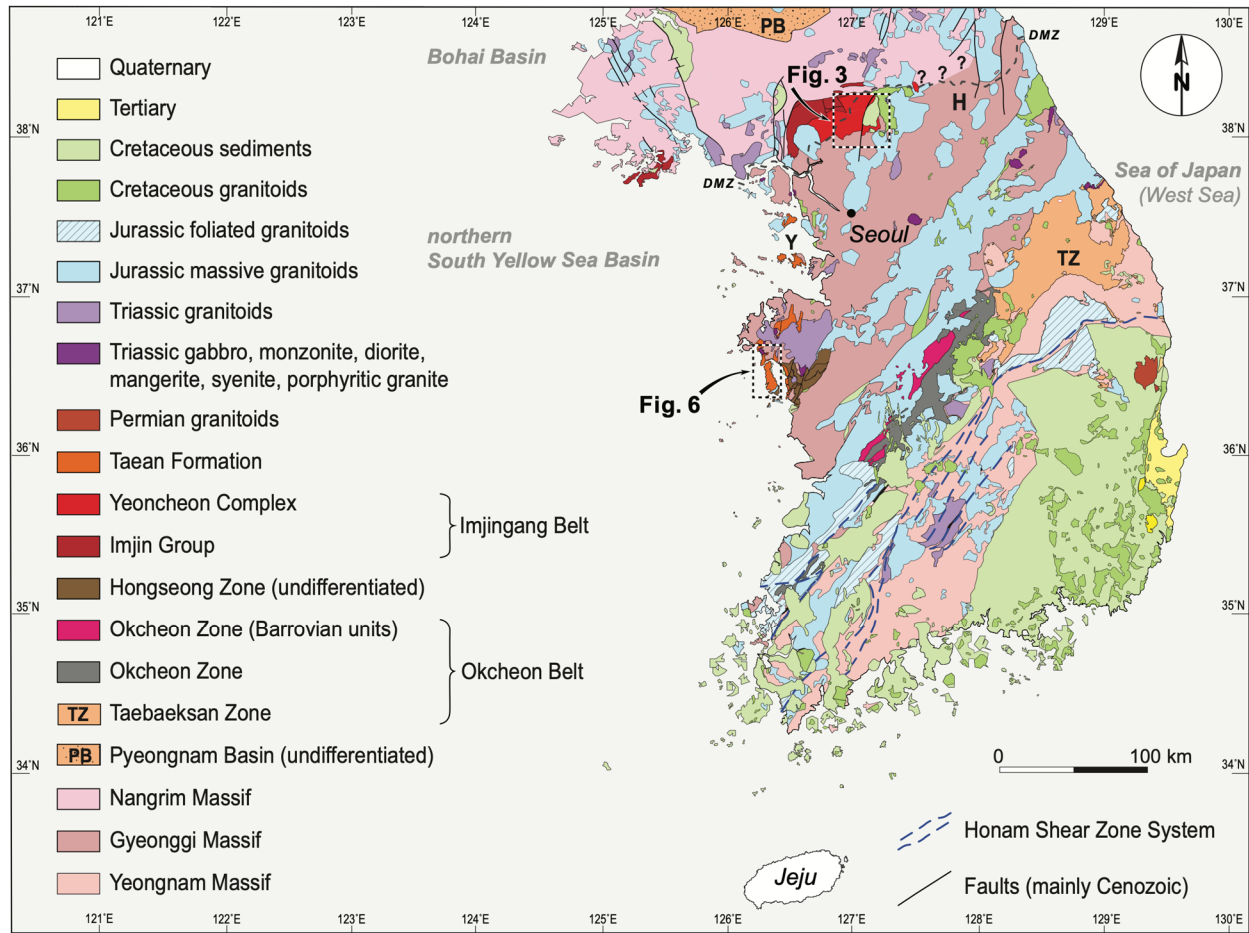


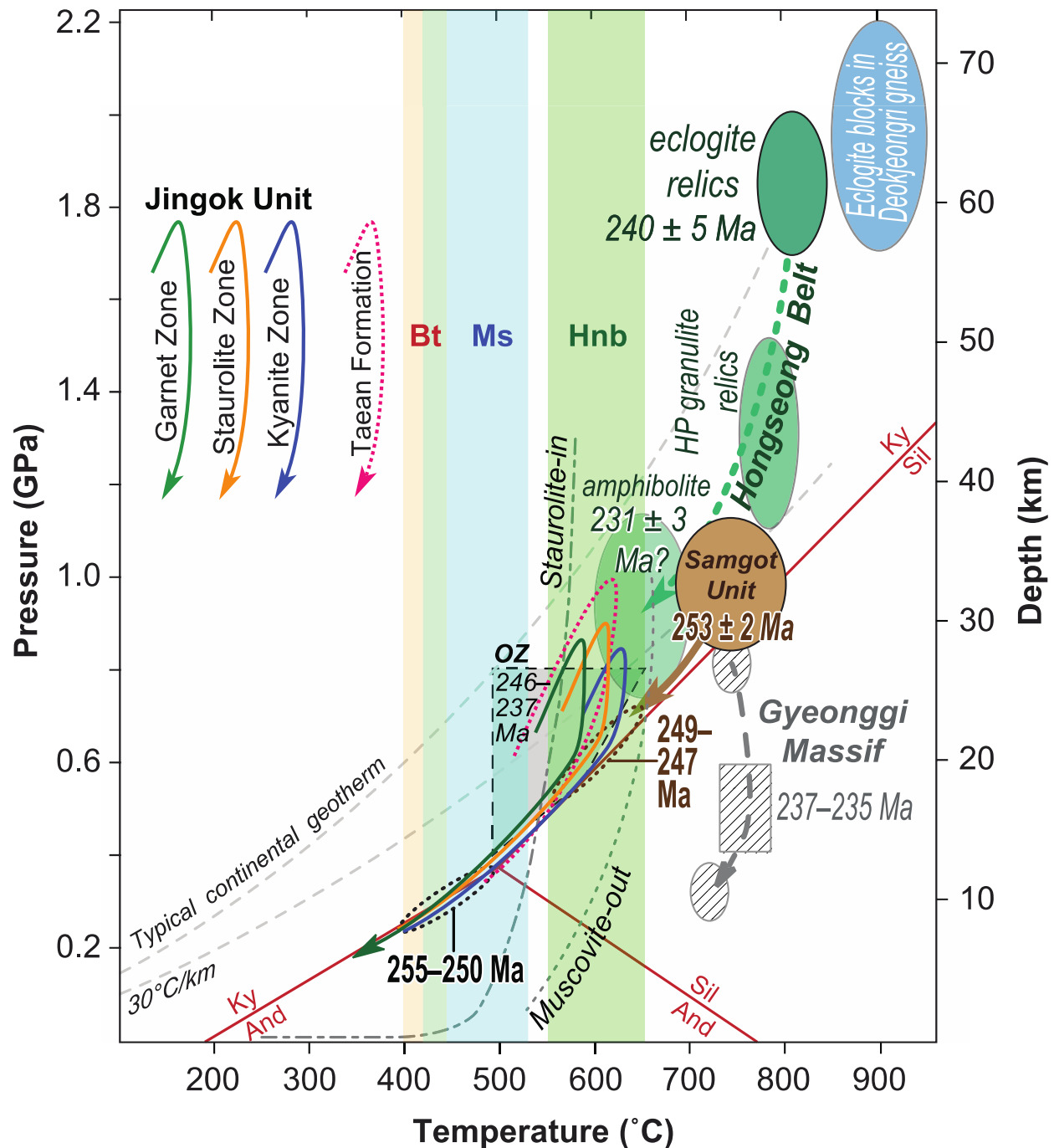
**Figure 1** - Tectonic sketch map of the Korean Peninsula's southern part based on [de Jong et al. \(2015\)](#), [S.Y. Han et al. \(2017\)](#) and [Kee \(2011\)](#). Maps of sampling areas in the Juksung–Yeoncheon–Baengmagoji–Cheorwon area ([Fig. 3](#)) and Anmyeon Island ([Fig. 6](#)) are outlined. Small isolated fault-bounded outcrops of the Jurassic Daedong Supergroup omitted for clarity. DMZ, Demilitarized Zone; H, Hwacheon Granulite Complex; Y, Yeongheung–Seonjae–Daebu Islands.

The material of the three basement terranes was extracted from the mantle at about 2.7 Ga, with major additions around 2.5 Ga, and was deformed, metamorphosed up to upper amphibolite- to granulite-facies and migmatized to varying degrees around 1.88–1.85 Ga, subsequently affected locally by Early Neoproterozoic (ca. 0.9 Ga) rift-related magmatism; an evolution comparable to that of the Sino–Korean Craton ([M. Cho, Kim, Yang, & Yi, 2017](#); [Jeong et al., 2021](#); [Lee & Cho, 2012](#); [B.C. Lee et al., 2014](#); [Sagong et al., 2003](#); [Yengkhom et al.,](#)

2014). The Gyeonggi Massif is the only Precambrian basement terrane seriously affected by strong regional Permo–Triassic tectono-metamorphic reworking and ductile shearing during collision (B.C. Lee et al., 2014; Oh & Kusky, 2007; Yengkhom et al., 2014). Early, probably collision-related metamorphism occurred in the late Middle Permian to Early Triassic (D.L. Cho, 2014; Jeong et al., 2021; Sagong et al., 2003). However, the characteristic high-temperature–low-pressure metamorphic recrystallization (700–750°C; 0.35–0.8 GPa; Fig. 2) is of Late Triassic age, and generally resulted in cordierite-bearing assemblages, accompanied by moderate but widespread anatexis and local granulite-facies metamorphism (M. Cho, Kim, Yang, & Yi, 2017; B.C. Lee et al., 2014; Oh & Kusky, 2007; Oh et al., 2015; Yengkhom et al., 2014).

The Imjingang Belt crops out in the area straddling the de facto border between North and South Korea. The belt comprises the Barrovian-type (medium-pressure, medium-temperature; medium P/T) metamorphic Yeoncheon Complex, extensively cropping out in South Korea, and the Imjin Group (Rimjin System), exclusively developed in North Korea (Fig. 1). The strongly ductilely deformed sedimentary and volcanic series of the Yeoncheon Complex (Fig. 3) are of inferred Neoproterozoic to Devonian age and experienced Permian–Triassic medium-grade metamorphism (500–780°C; 0.5–1.2 GPa; Fig. 2) (D.L. Cho et al., 2005; M. Cho et al., 2007; S.Y. Han et al., 2017; Kim & Jung, 2010; S.W. Kim, Park, Jang, Kwon, Kim, & Santosh, 2017; B.C. Lee et al., 2019). The probable equivalent of the Yeoncheon Complex in North Korea is a series of quartzites and mica schists with biotite, garnet, staurolite, kyanite and andalusite, as well as intercalated amphibolite and rare carbonates. These Barrovian-type metamorphic rocks occur amongst lesser metamorphic pelites and psammities in the uppermost 500–1300 m of the Imjin Group (Om et al., 1996). The lower part of the Imjin Group is formed by 1–2 km thick

166 Middle–Late Devonian epicontinental to shallow-water terrigenous clastic sediments with minor  
 167 carbonates (D.C. Lee et al., 2017; Om et al., 1996).



168

169

170 **Figure 2** - *P-T-t* paths for the Korean Collision Belt's main litho-tectono units in the late Paleozoic to early  
 171 Mesozoic constrained by the main  $^{40}\text{Ar}/^{39}\text{Ar}$  dating results for the Yeoncheon Complex (this study, bold  
 172 face), as well as isotopic ages (italics) and thermo-barometric data from the literature. *P-T* paths for the

three Barrovian zones of the Jingok Unit (Yeoncheon Complex) slightly modified after Kim and Jung (2010). *P-T* conditions for the Samgot Unit (Yeoncheon Complex) from M. Cho et al. (2007); U–Pb zircon rim age from D.L. Cho et al. (2005). *P-T-t* path for the amphibolite-facies Taeon Formation on the islets of Gukhwa and Ippa (Fig. 1) from H.S. Kim et al. (2021). *P-T-t* path for the Hongseong Belt reconstructed by the authors based on literature data (S.W. Kim et al., 2006, 2008, S.W. Kim, Kwon, Park, Yi, Santosh, & Kim, 2017; Oh et al., 2017; S.-I. Park, Kwon, Kim, Yi, & Santosh, 2014). The metamorphic conditions of Okcheon Zone (OZ; triangular shaded area; Cho and Kim, 2005) are comparable to those of the Yeoncheon Complex; isotopic ages from Suzuki et al. (2006) and S.W. Kim (2005). Note that the *P-T* path for the Gyeonggi Massif (grey ruled boxes and arrow, after M. Cho, Kim, Yang, & Yi (2017); age range discussed in de Jong et al., 2015) evolves under much higher thermal gradients than the belt's other litho-tectonic units and reflects mid-Triassic post-collisional decompression and reheating. The adopted cooling temperature ranges (sources and details, see text) for biotite (Bt), muscovite (Ms) and hornblende (Hnb) are also indicated. Mineral stability fields adapted from Jamieson et al. (1998). And, andalusite; Ky, kyanite; Sil, sillimanite.

The Okcheon Belt to the south of the Gyeonggi Massif (Fig. 1) is a Triassic collision belt reactivated and transformed into a fold-and-thrust belt in the Jurassic, comprising polyphasely-deformed, low- to medium-grade metamorphic, mainly Paleozoic sedimentary and minor Neoproterozoic volcanic rocks (Cho & Kim, 2005; M. Cho et al., 2013; D.K. Choi et al., 2012; Chough, 2013; R. Han et al., 2014; S.W. Kim, 2005). It is subdivided into the southwestern Okcheon Zone (also known as Okcheon Metamorphic Belt), with a tectonically disrupted Barrovian metamorphic zonation with maximum pressure–temperature conditions of 0.4–0.8 GPa and 490–650°C (Fig. 2), and the northeastern Taebaeksan Zone (also known as Taebaeksan Basin) that is intimately linked to the Yeongnam Massif (Fig. 1; Cho & Kim, 2005; M. Cho et al., 2013; Oh & Kusky, 2007; S.W. Kim, 2005; S.W. Kim, Park, Jang, Kwon, Kim, & Santosh, 2017). <sup>40</sup>Ar/<sup>39</sup>Ar, Rb–Sr and CHIME dates in the 246–219 Ma range of (errors 1–6%) on metamorphic minerals (Cliff et al., 1985; S.W. Kim, 2005; Suzuki et al., 2006) constrain the timing of the Songnim Orogeny in the Okcheon Zone.

The Hongseong Belt (Fig. 1) comprises a *mélange* of lens-shaped, strongly deformed lithologies of different age, provenance and metamorphic grade, including highly serpentized

ultramafic rocks (S.Y. Han et al., 2017; S.W. Kim, Kwon, Park, Yi, Santosh, & Kim, 2017; Kwon et al., 2013; Oh et al., 2017; S.-I. Park, Kwon, Kim, Yi, & Santosh, 2014). It is also referred to as Hongseong Suture Zone (Kwon et al., 2013), Hongseong Collision Belt (Oh et al., 2017), or Hongseong–Imjingang Belt (S.W. Kim, Kwon, Park, Yi, Santosh, & Kim, 2017). This heterogeneous lithological assemblage is subdivided, from west to east, into the Gonam Complex, the Paleozoic Weolhyeonri Complex and the Neoproterozoic Deokjeongri Gneiss Complex (S.Y. Han et al., 2017; Oh et al., 2017; S.-I. Park, Kwon, Kim, Yi, & Santosh, 2014, and references therein). The belt is affected by Triassic regional metamorphism in its western and eastern parts (Oh et al., 2017). To date the only occurrences in the Korean Collision Belt of rocks with convincing relics of Triassic high-pressure metamorphism are in or along the Hongseong Belt's eastern margin. Blocks of Paleoproterozoic augen gneiss in the Deokjeongri Gneiss Complex experienced metamorphic conditions of 1.7–2.2 GPa and 840–960°C (Fig. 2; Oh et al., 2017). The Bibong body in the boundary zone with the Gyeonggi Massif farther east (Fig. 1) mainly comprises amphibolite-facies metamorphic ( $P = 0.7\text{--}1.1$  GPa) mafic rocks, in which garnet with relictic omphacite records early eclogite-facies metamorphism ( $P = 1.7\text{--}2.0$  GPa) overprinted by a HP granulite-facies stage ( $P = 1.1\text{--}1.5$  GPa) during exhumation (Fig. 2; S.W. Kim et al., 2006, 2008; S.W. Kim, Kwon, Park, Yi, Santosh, & Kim, 2017; Oh & Kusky, 2007; Oh et al., 2017; S.-I. Park, Kwon, Kim, Yi, & Santosh, 2014).

Isolated outcrops of the Taean Formation occur in the islands of central western Korea, located to the west of the Hongseong Belt or partially tectonically overlying it, or tectonically covering the Gyeonggi Massif in coastal areas (Fig. 1). These rhythmically layered, graded-bedded meta-sedimentary series are usually less deformed and of lower metamorphic grade than their tectonic substratum (S.Y. Han et al., 2017). Rare amphibolite-facies meta-sediments



(garnet–staurolite–kyanite assemblages in meta-pelites; scapolite in meta-calc-silicate rocks) assigned to the Taean Formation crop out in the isolated Gukhwa and Ippa Islands (Fig. 1). Their maximum P–T conditions of 0.9–1.1 GPa at 600–620°C and P–T path are similar to Yeoncheon Complex (Fig. 2; H.S. Kim et al., 2022, and references therein). S.Y. Han et al. (2017) regarded the Taean Formation as related to the Yeoncheon Complex and the amphibolite-facies upper Pibanryeong Unit of the Okcheon Zone. This correlation was based on comparable sedimentological characteristics and strikingly similar populations of prominent mid-Paleozoic and early Neoproterozoic, but only relative rare basement-aged, detrital zircons (Cho et al., 2013; S.Y. Han et al., 2017; H.S. Kim et al., 2022; S.W. Kim, Park, Jang, Kwon, Kim, & Santosh, 2017; So et al., 2013).

### 3. Available Geochronological Constraints on the Tectonic Evolution

U–Pb dating on mid-Paleozoic meta-sediments of the Gyeonggi Massif (Guryong Group) yielded ages of  $265 \pm 8$  Ma (garnet; Sagong et al., 2003) and  $247 \pm 6$  Ma (SHRIMP on a metamorphic rim on detrital zircon; D.L. Cho, 2014), whereas early Neoproterozoic metabasites gave  $255\text{--}254 \pm 1\text{--}12$  Ma (LA-ICP-MS on zircon; Jeong et al., 2021).

An amphibolite in the lowermost tectonic unit of the Yeoncheon Complex, the Samgot Unit, yielded  $249 \pm 31$  Ma (Sm–Nd) and  $222 \pm 31$  Ma (Rb–Sr) garnet–plagioclase–whole-rock error-chrons (Ree et al., 1996). From garnet–biotite paragneisses of this unit Jeon and Kwon (1999) obtained an Sm–Nd mineral isochron age of  $263 \pm 6$  Ma, whereas metamorphic overgrowths on detrital zircon gave SHRIMP U–Pb ages of  $253\text{--}249 \pm 1\text{--}3$  Ma (D.L. Cho et al., 2005; B.C. Lee et al., 2019). Monazite from a kyanite–staurolite–mica schist in the Yeoncheon Complex’ tectonically uppermost Jingok Unit yielded a  $255 \pm 8$  Ma CHIME age (D.L. Cho et al.,



1996). Without providing visuals, contextual information and errors M. Cho et al. (2007) mentioned  $^{40}\text{Ar}/^{39}\text{Ar}$  “inverse isochron and plateau” ages of about 230 and 223 Ma (hornblende, Samgot Unit), as well as 205 Ma (muscovite), 220 and 160 Ma (biotite) in the Jingok Unit. Metasediments in the heterogeneous zone between the Samgot Unit and the underlying Gyeonggi Massif yielded single-grains of muscovite with  $^{40}\text{Ar}/^{39}\text{Ar}$  (pseudo-) plateau ages of 242.8, 240.3 and 219.7 Ma (errors  $\leq 1.0$  Ma at  $1\sigma$ ) (Fig. 3; de Jong & Ruffet 2014b; de Jong et al., 2015).

SHRIMP U–Pb geochronology in the Taean Formation yielded weighted mean  $^{206}\text{Pb}/^{238}\text{U}$  ages on metamorphic zircon of  $250.9 \pm 0.5$  Ma (metapelite) and  $252.4 \pm 1.1$  Ma (amphibolite) in amphibolite-facies rocks in Gukhwa and Ippa (H.S. Kim et al., 2022), and concordant ca. 277–260 Ma ages for metamorphic overgrowth rims on detrital zircon from more typical low-grade meta-pelites in Anmyeon Island (S.W. Kim, Park, Jang, Kwon, Kim, & Santosh, 2017).  $^{40}\text{Ar}/^{39}\text{Ar}$  single grain laser step-heating of muscovites in metasediments of the island revealed age components of 243 Ma to 237 Ma (de Jong et al., 2014, 2015). However, the main metamorphism in these rocks is clearly of early Late Triassic age shown by concordant  $^{40}\text{Ar}/^{39}\text{Ar}$  muscovite pseudo-plateau ages (230.7 and 228.8 Ma, errors 1.0 Ma at  $1\sigma$ , de Jong et al., 2014) and SHRIMP U–Pb ages of titanite from meta-calc-silicate rocks ( $232.5 \pm 3.0$  Ma, de Jong et al., 2014, 2015;  $234.1 \pm 6.4$  and  $238.8 \pm 5.4$  Ma, S.W. Kim, Kwon, Park, Yi, Santosh, & Kim, 2017; S.W. Kim, Park, Jang, Kwon, Kim, & Santosh, 2017) (Fig. 6). Zircons with age components of about 230 Ma (H.S. Kim et al., 2022) demonstrate that amphibolite-facies meta-sediments recorded this Late Triassic event too. Analogous concordant  $^{40}\text{Ar}/^{39}\text{Ar}$  plateau ages (230.1 Ma to 228.1 Ma, errors 1.0 Ma at  $1\sigma$ ) were obtained for hornblende and biotite single grains from amphibolites in the Hongseong Belt (de Jong and Ruffet, 2014a; de Jong et al., 2015). 243–229 Ma SHRIMP U–Pb zircon ages (average: ca. 235 Ma) occur regionally in other parts of the

Hongseong Belt and the neighboring western Gyeonggi Massif (de Jong et al., 2015; S.W. Kim, Park, Jang, Kwon, Kim, & Santosh, 2017, and references therein). de Jong et al. (2014, 2015) pointed out that these tightly clustered mineral ages overlap with the timing of mantle-sourced Mg-rich potassic syenite–granite and gabbro–monzonite magmatism (237–224 Ma) occurring throughout the Precambrian crystalline basement terranes and most bordering belts (Fig. 1; Cheong et al., 2015; S.G. Choi et al., 2009; de Jong & Ruffet, 2014a; de Jong et al., 2015; Jeong, Yi, Kamo, & Cheong, 2008; Seo et al., 2010; Williams et al., 2009). Local granulites with spinel–cordierite–corundum assemblages (900–1150°C at 0.9–1.1 GPa; Oh & Kusky, 2007) were produced at less than 2 km from a ca. 229-Ma-old hypersthene-bearing monzonite intrusion (Jeong, Yi, Kamo, & Cheong, 2008). de Jong et al. (2014, 2015) pointed out that syenite with mafic enclaves and associated mafic dikes truncate folds and associated tectonic foliations in the Taean Formation showing the post- or late-collisional nature of this magmatism. The early Late Triassic bimodal magmatic event was interpreted as due to slab break-off and/or lower crust and uppermost mantle delamination (Cheong et al., 2015; S.G. Choi et al., 2009; de Jong & Ruffet, 2014a; de Jong et al., 2015; Jeong, Yi, Kamo, & Cheong, 2008; Seo et al., 2010; Williams et al., 2009). This process produced the typical high-temperature–low-pressure metamorphism and anatexis in the Gyeonggi Massif and is linked to its transformation into a post- to late collisional metamorphic core complex (de Jong et al., 2015). The tight clustering of metamorphic ages of minerals with highly different cooling temperatures, namely, micas, hornblende, titanite and zircon, points to very fast cooling in the early Late Triassic after the thermal pulse (de Jong et al., 2014, 2015).

Metamorphic rims around magmatic zircons in enclaves with relics of high-pressure metamorphism in the Deokjeongri Gneiss Complex in the eastern Hongseong Belt yielded a

weighted mean  $^{206}\text{Pb}/^{238}\text{U}$  age of  $230 \pm 4$  Ma (MSWD = 3.9), which [Oh et al. \(2017\)](#) took as the timing of high-pressure metamorphism. Mafic rocks in the principally amphibolite-facies metamorphic Bibong body ([Fig. 1](#)) contain magmatic zircon with metamorphic rims yielding SHRIMP U–Pb dates of  $231 \pm 8$  Ma (MSWD = 2.2) and  $240 \pm 5$  Ma (MSWD = 0.62) ([S.-I. Park, Kwon, Kim, Yi, & Santosh, 2014](#)). We question, however, that the ca. 230 Ma ages refer to the high-pressure metamorphic event because the MSWD values are much greater than unity, pointing to the presence of non-analytical scatter. Earlier, [de Jong et al. \(2015\)](#) pointed out that ca. 230–235 Ma dates in the Bibong body would reflect recrystallization of the original eclogitic mineralogy, corroborated by [Kwon et al. \(2020\)](#), during the Late Triassic thermal pulse. We, thus, regard the age of  $240 \pm 5$  Ma as the best estimate for the timing of the eclogite metamorphism in the Korean Collision Belt.

Common Jurassic and very rare Cretaceous isotopic ages in the Yeoncheon Complex, Gyeonggi Massif and Okcheon Zone were as a rule regarded as due to magmatism-related resetting (e.g., [Cliff et al., 1985](#); [S.W. Kim, 2005](#)).

#### **4. Geological Context and Deformation Features of Sampled Litho-Tectonic Units**

This section outlines the main characteristics and structural evolution of the sampled litho-tectonic units, namely, the different units of the Yeoncheon Complex, the Taean Formation, the Gonam Complex, the Gyeonggi Shear Zone and the sheared and low-grade meta-sediments of the lowermost part of the Jurassic Daedong Supergroup covering the shear zone ([Fig. 3](#)).



#### 4.1. Yeoncheon Complex

In its type locality (Fig. 3) the Yeoncheon Complex is subdivided into the Jingok Unit and the tectonically underlying Samgot Unit (M. Cho et al., 2007; S.Y. Han et al., 2017; Kim & Jung, 2010; Ree et al., 1996; Sajeev et al., 2010). M. Cho et al. (2007) argued that differences in metamorphic conditions between both litho-tectonic units point to the presence of a low-angle ductile normal fault sub-parallel to their main tectonic foliations. Poor outcrop conditions preclude firm demonstration but our dating results shed light on this issue. The Jingok Unit is a several-kilometers-thick monotonous series of rhythmically alternating meta-pelites and meta-psammities. The Samgot Unit forms a well-bedded sequence of meta-calc-silicate and biotite-rich rocks, with intercalated quartzite, meta-pelite and minor marble (M. Cho et al., 2007; Kee et al., 2008; D. Kim et al., 2009), and amphibolites with mid-Neoproterozoic (860 Ma; D.L. Cho et al., 2005; Ree et al., 1996) and Late Devonian (ca. 361–371 Ma; B.C. Lee et al., 2019) basaltic protoliths. Some of the amphibolites contain relics of granulite-facies metamorphism (Kwon et al., 2009; Sajeev et al., 2010). Rarely occurring are lenses of metaluminous A-type granite (372–373 Ma, zircon, SHRIMP U–Pb; S.W. Kim, Kwon, Park, Yi, Santosh, & Kim, 2017; S.W. Kim, Park, Jang, Kwon, Kim, & Santosh, 2017; B.C. Lee et al., 2019) transformed into mylonitic hornblende–biotite gneiss. The intensely deformed and lithologically heterogeneous lower part of the Samgot Unit with rocks of different type, age and derivation forms a tectonic mélange (S.Y. Han et al., 2017).

The Yeoncheon Complex experienced polyphase penetrative ductile deformation under prograde, peak and retrograde metamorphic conditions (M. Cho et al., 2007; Jung et al., 1999, 2002; Kee et al., 2008; Kim & Cho, 2008; Kim & Jung, 2010; Ree et al., 1996). These authors adopted the approach set out by Bakker et al. (1989) of using the deformation phase producing

the main tectonic fabric ( $D_m$ ) as reference and labeling older and younger phases as  $D_{m-1}$  and  $D_{m+1}$ , respectively, which we follow in this paper enabling easier comparison with the literature. The Jingok Unit shows a partial, normal Barrovian zonal sequence with garnet, staurolite and kyanite zones, overall showing a downward increasing medium-pressure (0.5–1.0 GPa) and medium- to high-temperature (500–650°C) metamorphism (Fig. 2; M. Cho et al., 2007; Kim & Jung, 2010). Psammitic schist and garnet-amphibolites in the Samgot Unit recorded peak temperatures of 660–780°C and pressures of 0.8–1.2 GPa (Fig. 2; M. Cho et al., 2007; B.C. Lee et al., 2019), whereas meta-calc-silicate rocks experienced metamorphic recrystallization at temperatures around 750°C (D. Kim et al., 2009). Far more severe metamorphic conditions of about 2.0 GPa and 900°C claimed for mafic granulites in this unit (Kwon et al., 2009; Sajeev et al., 2010) stem from incorrect pseudo-section calculations (Oh et al., 2015). This casts doubt on the plea by M. Cho et al. (2007) for early eclogite-facies metamorphism.

#### 4.1.1. Jingok Unit: Structural Features and Sample Selection

The fine-grained meta-pelites and intercalated laminated meta-psammities of the garnet zone have a moderately northward dipping penetrative bedding-parallel main phase foliation ( $S_m$ ) (Fig. 4a). It contains a well-developed muscovite–biotite platelet lineation that parallels the long axes of quartz-filled pressure fringes on garnet porphyroblasts, averaging 330/40 (Fig. 4a). Poikiloblastic biotite and subhedral garnet have an internal fabric ( $S_{m-1}$ ) of aligned inclusions of elongated quartz, feldspar, clinozoisite, ilmenite, apatite and tourmaline. Such internal fabrics are: (1) straight and oblique to the external foliation  $S_m$ , implying that both minerals grew after  $D_{m-1}$  and before  $D_m$ , or (2) sigmoidal curving into  $S_m$ , pointing to growth during the early stages of  $D_m$ . Kim & Cho (2008) demonstrated that garnet blastesis outlasted  $D_m$  as well. The main

foliation is locally deformed in chlorite-rich brittle–ductile shear zones ( $S_{m+1}$ ). Rare strongly curvi-linear folds ( $D_{m+1}$ ), deforming the main foliation, are found in particular layers that also contain discordant boudinaged quartz lenses. To constrain the timing of  $D_m$  we sampled metapelites with the well-developed main tectonic fabric (biotite 13JK53, mica schist; whole-rock 13JK58, phyllite).

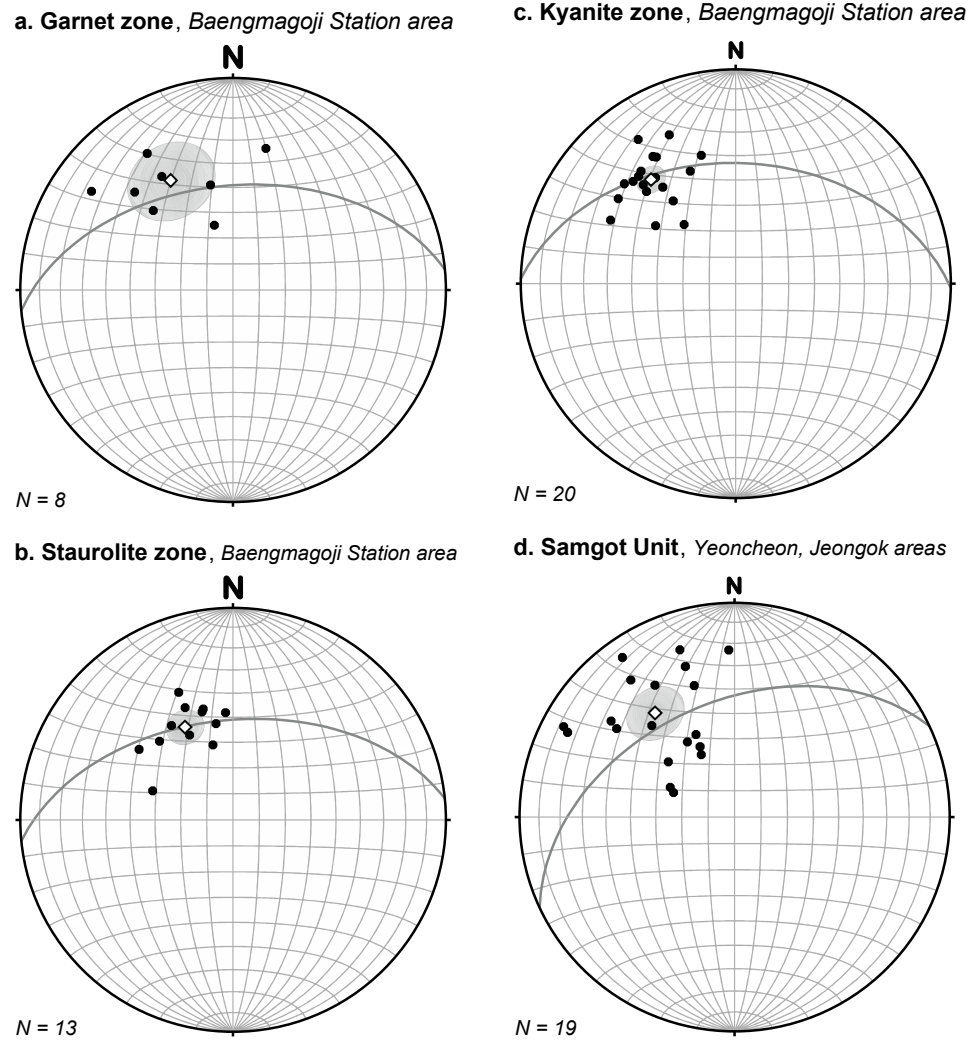


**Figure 4** - Lower hemisphere equal area projections of linear fabric elements in the Yeoncheon Complex (dots) formed during the first deformation phases in the (a) garnet, (b) staurolite and (c) kyanite zones of the Jingok Unit and (d) Samgot Unit, with mean lineations (open diamond) and their 95% confidence cones (greyed area); great circles represent the average foliation plane bearing the plotted lineations.



Typical meta-pelites of the staurolite and kyanite zones are garnet–biotite–muscovite–plagioclase–quartz schists with a penetrative, differentiated main phase foliation dipping moderately to the north (Fig. 4b and c). Rocks with  $S_m$  have well-developed parallel lineations formed by elongated grains and aggregates of quartz, muscovite–biotite platelets and the long axes of quartz-filled pressure fringes on garnet porphyroblasts, averaging 333/49 and 321/38 in the staurolite and kyanite zones, respectively (Fig. 4b and c). The main foliation is axial planar to rare isoclinal folds of layering or ptygmatically folded quartz veins, demonstrating intense transposition; their hinges are sub parallel to the above-mentioned main phase lineations. Locally,  $S_m$  refracts on more quartz-rich mica schist layers forming an oblique foliation with quartz-rich micro-lithons containing a crenulated older foliation  $S_{m-1}$ . Garnets have internal fabrics of elongated quartz, opaque and accessory minerals ( $S_{m-1}$ ) that are straight and oblique to the external foliation  $S_m$  and truncated at crystal margins, or sigmoidal and curving into  $S_m$ . This implies that, like in the garnet zone, the mineral grew before and during the early stages of  $D_m$ , corroborating work by Jung et al. (1999), Kim and Cho (2008) and Kim and Jung (2010). Frequently randomly orientated, up to 2-cm-long staurolite and kyanite porphyroblasts overgrew the quartz–mica foliation, also wrapping garnet, but also occurs as, sometimes boudinaged, crystals aligned parallel to the main lineations, especially the smaller grains (Fig. 5a). The main foliation is overprinted by a shear band cleavage formed during  $D_{m+1}$ , also wrapping staurolite (Fig. 5b) and kyanite crystals with inclusions patterns that are straight in their interiors but sigmoidal in rims. Hence, both minerals grew after  $D_m$  until the early stages of the strong shear deformation  $D_{m+1}$ . Aiming to constrain the timing of the main tectono-metamorphic phase in the staurolite (13JK63, 67) and kyanite (13JK77) zones, we sampled biotite and/or muscovite from mica schist with  $S_m$  for  $^{40}\text{Ar}/^{39}\text{Ar}$  dating.



**Figure 5 a-f** - Field photographs of deformation structures in the Yeoncheon Complex, Jingok Unit (a–c, f) and Samgot Unit (d, e) (locations, Fig. 3). Planes of pictures b, c, e, f parallel to the muscovite–biotite–quartz shape fabric and stretching lineations; d oblique view to structures. Coins, pencils or rulers for scale.



**(a)** Various oriented staurolite porphyroblasts on the main foliation of a garnet–staurolite–kyanite–mica schist with a well-developed stretching lineation (muscovites 13JK71 and 72 from this outcrop).



**(b)** garnet–staurolite–mica schist with shear band cleavages wrapping staurolite indicating top-to-the-SSE  $D_{m+1}$ ; (kyanite zone).



**Figure 5 (ctd)**



**(c)** sigmoid-shaped quartz vein forming a shear band boudin in garnet–staurolite–kyanite–mica schist indicating top-to-the-SE  $D_{m+1}$  shear (muscovite 13JK86 from this outcrop).



**(d)** tight to isoclinal  $D_m$  folds in meta-calc-silicate rocks transected by a cleavage in biotite-rich layers ( $S_{m+2}$ ) not related to folding, the sigmoidal CS-like aspect of which appears in the lower right part of the picture (Samgot Unit).



**Figure 5 (ctd)**



**(e)** quartz–alkali-feldspar–plagioclase mylonite; top-to-the-ESE  $D_{m+1}$  shear shown by CC' structures in ultra-mylonite bands (hornblende 13JK96 from this outcrop at Gungshin Bridge, Samgot Unit).



**(f)** foliation formed during dominant top-to-the-SE  $D_{m+1}$  shear (kyanite zone) wraps an older shear band boudin with stair-stepping showing top-to-the-(N)NW  $D_m$  shear, same outcrop as [Fig. 5b](#).

Irregular centimeter- to meter-thick, variably ductilely deformed quartz veins cut  $S_m$  and  $S_{m+1}$ , and may be folded and/or boudinaged (Fig. 5c); the thinner ones are more or less parallel to the main foliation. Such late-stage discordant veins have margins with large crystals of muscovite randomly grown against mica schist, and may in the staurolite zone contain centimeter-size euhedral andalusite crystals, without preferred orientation relative to vein margins, and in the kyanite zone occasionally large idiomorphic kyanite.  $^{40}\text{Ar}/^{39}\text{Ar}$  dating of such muscovite was undertaken aiming to constrain the timing of this fluid flow event during decompression with respect to  $D_m$  and  $D_{m+1}$  (13JK62, 65, 69, staurolite zone; 13JK71, 75, 86, kyanite zone). To establish the timing of late-stage retrogression, we also sampled biotite and/or muscovite from garnet–biotite–muscovite schist in the staurolite zone with  $S_m$ , in which biotite was partially (13JK68) or completely (13JK69) chloritized. With the same objective we analyzed both minerals from kyanite zone mica schists with strongly chloritized garnet (13JK93) and from a zone with dominant late top-to-the-north shear associated with brittle–ductile shearing (13JK72), regarded as  $D_{m+2}$  (see section 4.1.3).

#### 4.1.2. Samgot Unit

The meta-calc-silicate rocks have a fairly uniformly grained matrix composed mainly of elongated quartz, diopside, scapolite, clinozoisite, calcite and biotite with a moderately NNW-dipping penetrative planar fabric and an aggregate and stretching lineation, averaging 323/39 (Fig. 4d), paralleling hinges of cm-scale intrafolial  $D_{m-1}$  folds. This lineation may be parallel to a linear structure of millimeter to centimeter-sized frequently elongated, occasionally pulled-apart garnet crystals or aggregates with high aspect ratios, often rimmed by oriented hornblende. Amphibolites generally display a well-developed hornblende lineation that may parallel

elongated aggregates of garnet in meta-calc-silicate rocks. Sample 10JK07 with such an early fabric was taken for dating. The principal tectono-metamorphic layering in meta-calc-silicate rocks is deformed by meter-scale tight to isoclinal folds ( $D_m$ ) (Fig. 5d), which only have a locally developed axial planar fabric oblique to the tectono-metamorphic foliation in the limbs. C-axis fabrics of quartz grains with a shape-preferred orientation oblique to the main tectono-metamorphic foliation suggest temperatures of 500–600°C (D. Kim et al., 2009), probably referring to the conditions when these folds were produced during cooling and initial exhumation. Such temperatures are similar to those estimated by B.C. Lee et al. (2019) for amphibolite (ca. 575 °C) and psammitic schist (ca. 665 °C) during retrogression and decompression. The main phase transposition foliation  $S_m$  is cut by local, low-angle ductile shear bands ( $S_{m+1}$ ). Locally,  $D_m$  folds are transected by a sigmoidal CS-like cleavage not related to folding that is exclusively developed in biotite-rich layers but not in the intercalated meta-calc-silicates (Fig. 5d), considered as  $D_{m+2}$  (see next section).

A lens of Late Devonian alkali-granite (4.1) has a dominant platy  $D_{m+1}$  foliation of thoroughly recrystallized quartz–alkali-feldspar–plagioclase (Fig. 5e) with isoclinal and sheath folds. Linear fabric elements are a stretching lineation of elongated quartz and feldspar grains and alkali-feldspar porphyroclasts, and well-crystallized occasionally boudinaged hornblendes sometimes rimming garnet; these are parallel to the linear fabric in the encasing meta-calc-silicates (Fig. 4d). Hornblende 13JK96 was used to date this  $D_{m+1}$  fabric.

Coarse-grained amphibolite/meta-gabbro with a poorly developed deformation fabric (10JK06), which may contain granulite relics and later discordant garnet-bearing granitic leucosomes, formed during exhumation (Sajeev et al., 2010), occurs as lenses in banded



orthogneiss. Elsewhere coarse-grained biotite-rich augen gneiss (13JK102) with up to 3-cm-long garnets, crosscut by amphibole-filled extension cracks, occurs interlayered with meta-calc-silicate rocks.

#### 4.1.3. Kinematics of the Polyphase Deformation

The obliquity of the straight internal fabric and the sigmoidal inclusion patterns in garnets, as well as the asymmetry of quartz-rich pressure fringes on them points to top-to-the-SE to SSE shear during  $D_m$  in all mineral zones of the Jingok Unit, confirming earlier studies (Jung et al., 1999; Kim & Cho, 2008; Ree et al., 1996). Top-to-the-(S)SE shearing continued during  $D_{m+1}$  as implied by shear band cleavages, CS fabrics, fish-like foliation boudins and stair-stepping of quartz boudins (Figs. 5a and c), some of which contain andalusite. A large randomly oriented muscovite crystal from the margin of such a quartz boudin was dated (13JK86). Conjugate  $D_{m+1}$  shear band cleavage systems with top-to-the-SE and top-to-the-NW kinematics have been observed as well; mica schist sample 13JK77 for  $^{40}\text{Ar}/^{39}\text{Ar}$  dating is from this zone. The dominant  $D_{m+1}$  shear direction may be overprinting an earlier movement with an opposite shear direction illustrated by a shear band boudin with stair-stepping indicating a northerly shear that is wrapped by the external foliation (Fig. 5f) that was formed during dominant top-to-the-SE shear in the same outcrop (Fig. 5b). Cm- to dm-spaced low-angle shear band cleavages with top-to-the-NNW kinematics occur locally superimposed on the prominent  $S_m$  and  $S_{m+1}$ , pointing to a younger  $D_{m+2}$  shear event with northerly kinematics in the staurolite and kyanite zones. Shear band boudins indicating top-to-the-NW kinematics in local fine-grained mylonites in the kyanite zone, contain biotite with a diameter well below 1 mm, but no garnet, staurolite or kyanite. These

502 tectonites are associated with near layer-parallel cataclasite zones that truncate the main  
 503 mylonitic foliation.

504 Although hornblende aggregates rimming garnet crystals or aggregates in meta-calc-  
 505 silicate rocks of the Samgot Unit are usually symmetrical, sometimes their asymmetry points to  
 506 top-to-the-NW  $D_{m-1}$  or  $D_m$  shear. The asymmetry of the outcrop-scale lens of quartz–alkali-  
 507 feldspar–plagioclase mylonite (from which hornblende 13JK96 was dated) indicates top-to-the-  
 508 (E)SE shear, agreeing with the deflection of both the main internal and external foliations, and  
 509 discrete shear zones in fine-grained ultra-mylonitic rocks, resembling CC' structures (Fig. 5e),  
 510 within the lens. We correlate this shear phase that is also dominant in platy meta-calc-silicates  
 511 surrounding the gneisses (S.Y. Han et al., 2017) with  $D_{m+1}$  in the Jingok Unit. A younger  
 512 northerly shear, correlated with  $D_{m+2}$  in the Jingok Unit, is indicated by a more discrete CS-like  
 513 cleavage exclusively developed in biotite-rich layers alternating with meta-calc-silicate layers  
 514 (Fig. 5d).  $D_{m+2}$  is much more pronounced in fine-grained garnet free meta-calc-silicate rocks in  
 515 the lowermost Samgot Unit that have a strongly platy and linear mylonite fabric with shear band  
 516 boudins and antithetic shears. Such northerly shear thus seems to increase in intensity  
 517 structurally downward in the Samgot Unit too, and is similarly observed in the underlying  
 518 Gyeonggi Shear Zone (see below).

## 519 520 **4.2. Taeon Formation**

521 The Taeon Formation (Fig. 6) comprises a rhythmic alternation of dark-grey meta-pelites  
 522 and lighter coloured, normal-graded, in part calcareous, meta-sandstone, with locally intercalated  
 523 layers of meta-calc-silicate rocks that alternate with biotite-rich meta-pelites (not unlike the  
 524 lithological association found in the Samgot Unit), as well as rare impure marble, amphibolite

and thin tuffs (de Jong et al., 2014; S.Y. Han et al., 2017; H.S. Kim et al., 2022; So et al., 2013).

In Anmyeon Island a well-developed bedding-parallel quartz-mica differentiation foliation ( $S_1$ ) is

almost exclusively developed in low-grade meta-pelites, locally as axial planar cleavage of rare

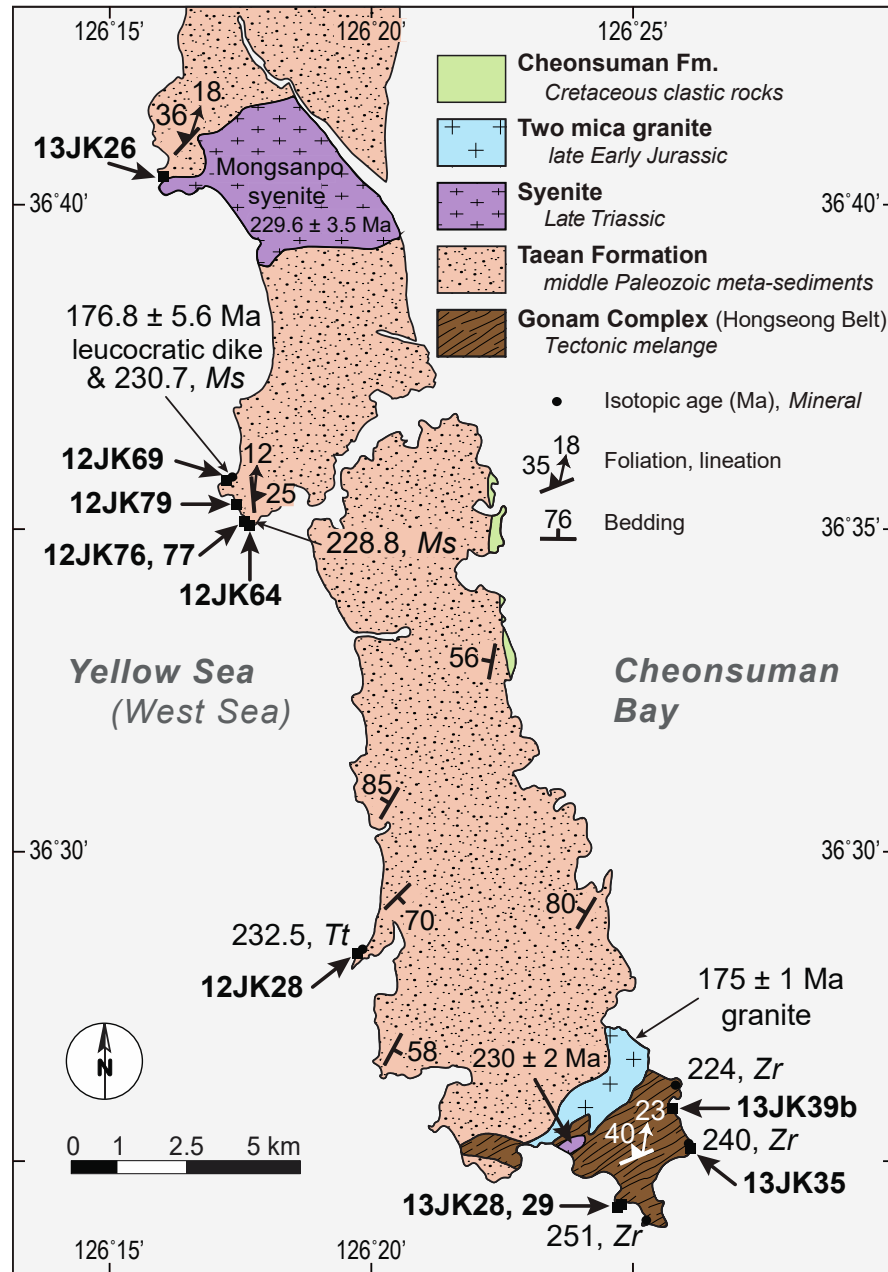


**Figure 6** - Geological sketch map of Anmyeon Island and adjacent areas modified after de Jong et al. (2015) and S.Y. Han et al. (2017) with sampling locations in the Tae'an Formation. U–Pb zircon ages (Zr) from Kee (2011);  $^{40}\text{Ar}/^{39}\text{Ar}$  muscovite ages (Ms) and SHRIMP U–Pb titanite ages (Tt) from de Jong et al. (2014). Ages of magmatic intrusions (SHRIMP U–Pb, zircon) from S.Y. Han et al. (2017) and Kee (2011).



recumbent isoclinal folds (de Jong et al., 2015; S.Y. Han et al., 2017). Only some meta-calc-silicate rocks reveal NNE-trending amphibole and biotite aggregates lineations, whereas biotite-rich meta-pelites occasionally display a rodding lineation (Fig. 6); otherwise  $L_1$  is ill developed with a highly variable orientation (S.Y. Han et al., 2017). The chlorite–biotite–muscovite mineral assemblage in meta-pelites, occasionally with garnet, suggests metamorphic temperatures not much higher than about 450°C (Fig. 2; de Jong et al., 2014, 2015). Farther north, in Yeongheung Island (Fig. 1) the metamorphic grade is higher and garnet-bearing biotite–mica schist was formed, whereas layer-parallel quartz veins may contain rare andalusite or kyanite.  $D_1$  structures include NNE- or S-ward plunging mica and quartz shape fabric lineations, oriented quartz-filled pressure shadows on garnet and rare non-cylindrical recumbent folds.

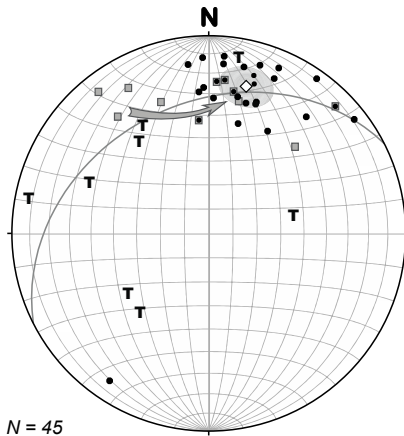
While, the main metamorphism of the fairly low-grade rocks in Anmyeon Island is of early Late Triassic age with relics of an earlier, mid-Triassic metamorphic event (de Jong et al., 2015), the amphibolite-facies metamorphism on the islets of Gukhwa and Ippa (section 2; Fig. 1) took place around the Permian–Triassic boundary (section 3). To better constrain the timing of the tectono-metamorphic evolution of the Taeon Formation we sampled additional meta-sandstones (12JK28, 64, 69, 76, 77, 79), and a dolerite dyke (13JK26) for  $^{40}\text{Ar}/^{39}\text{Ar}$  dating of metamorphic muscovite and/or biotite on Anmyeon Island (Fig. 6) and pluri millimeter randomly oriented muscovite from a layer-parallel quartz vein (13JK20) from the east coast of Yeongheung Island.

### 4.3. Gonam Complex

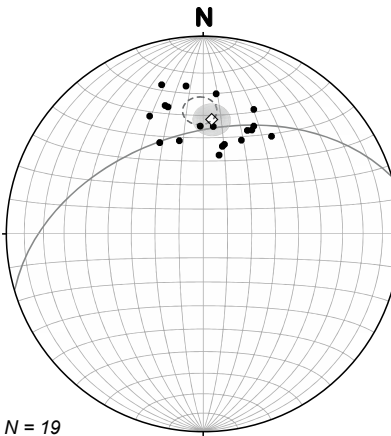
The Gonam Complex, exposed on Anmyeon Island's southern tip (Fig. 6), constitutes the westernmost subduction-accretion complex of the Hongseong Belt. It consists of a strongly

deformed, highly heterogeneous mélange-like assemblage of Paleo- Meso- and Neoproterozoic gneisses and meta-sediments (S.Y. Han et al., 2017; Kee, 2011; S.W. Kim, Kwon, Park, Yi, Santosh, & Kim, 2017; S.W. Kim, Park, Jang, Kwon, Kim, & Santosh, 2017; Kwon et al., 2013; S.-I. Park, Kim, Kwon, Thanh, Yi, & Santosh, 2014; S.-I. Park, Kwon, Kim, Yi, & Santosh, 2014), including associated carbonate, red chert, (ultra) mafic rocks, graphitous metapelites and meta-sandstones that represent a dismembered ocean plate stratigraphy (de Jong et al., 2015).

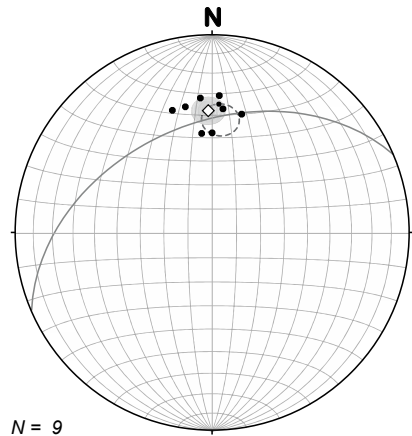
The principal quartzite–mica schist series shows well-developed by asymmetric, plunging inclined folds with steep to overturned western limbs. These are D<sub>2</sub> structures as they deform an earlier tectonic fabric with isoclinal intrafolial folds, also locally showing indications for top-to-the-SSW shear. The lower part of the complex has an intense planar and linear mylonitic deformation fabric with highly curvi-linear folds (S.Y. Han et al., 2017) and NNE-plunging mineral and stretching lineations (av. 014/24; Fig. 7a). Sigma-type porphyroclasts, CS-fabrics and shear band boudins indicate top-to-the-NNE shear. Small granitic bodies and veins of a 232–228-Ma-old bimodal intrusive suite (Fig. 6; Kee, 2011) truncate D<sub>2</sub> folds, associated cleavages and mylonitic foliations in the lower part of the complex (de Jong et al., 2015). Thinner granitic veins are sub-parallel to the mylonitic foliation and show a pinch-and-swell structure or are boudinaged. Up to a meter thick Late Triassic granitic veins have crude margin-parallel deformation fabrics. Stringers of oriented and boudinaged tourmaline (de Jong et al., 2015) in margins of ductilely deformed veins that truncate the mylonites at a low angle have an orientation close the average foliation plane and make an angle of up to about 90 degrees with the average lineation in the ductilely deformed country rocks (Fig. 7a). In individual outcrops the angle between tourmaline crystals in vein margins and the extension lineation in the country rocks is 40–50 degrees. Tourmalines in veins without margin-parallel deformation fabric have

**a. Gonam Complex, Anmyeon Island**

N = 45

**b. Gyeonggi Shear Zone, Jeongok area**

N = 19

**c. Gimpo Group, basal part, Jeongok area**

N = 9

**Figure 7** - Lower hemisphere equal area projections of linear fabric elements (dots) in the **(a)** Gonam Complex, Anmyeon Island (greyed squares: hinges  $D_2$  folds; T: long axes tourmaline crystals in granitoid veins; greyed arrow: increasing  $D_3$  strain) and **(b)** the Gyeonggi Shear Zone and **(c)** foliated and lineated phyllite in the Gimpo Group's basal part on top of the shear zone in the area to the south of Jeongok (**Fig. 3**). Mean lineations (open diamond) and their 95% confidence cones (greyed area) are shown; great circles represent the average foliation plane bearing the plotted lineations. Note the overlapping 95% confidence cones around the mean lineations of gneisses in the Gyeonggi Shear Zone (dashed ellipse in **(c)**) and sheared phyllite in the basal part of the Gimpo Group (dashed ellipse in **(b)**).

highly different orientations (**Fig. 7a**). Clearly the leucocratic bodies have taken up considerably less ductile strain than the country rocks. Hence, the dominant northerly shear took place, at least partly, after the intrusion of the ca. 235–230-Ma post- or late-collisional bimodal rocks. We, therefore, regard the top-to-the-NNE shear as a third phase of ductile deformation. The  $D_3$  strain intensity increases to the west and structurally downwards, shown by: 1) diminishing interlimb angle of deformed  $D_2$  folds from 70–90 degrees to 20–30 degrees; 2) their axial plane's cleavage intensification and dip decrease; 3) the concomitant reorientation of hinge plunge from NW to NNE, approaching the stretching lineation in  $D_3$  mylonites (**Fig. 7a**). 251–262-Ma-old metamorphic rims around detrital zircons could constrain the timing of early tectono-

metamorphic events, whereas ca. 320-Ma-old crystals suggest an earlier event (Kee, 2011). The ca. 175-Ma-old two-mica granite (Kee, 2011; Fig. 6) at the contact with the Taean Formation constrains the timing of termination of all collisional-related tectonic activity. To test this tentative tectonic calendar, we dated hornblende and biotite from amphibolites (13JK28, 29, 35), including from a section with pervasive top-to-the-NNE shear and highly attenuated D<sub>2</sub> folds, as well as muscovite from quartzite (13JK39).

#### 4.4. Gyeonggi Shear Zone

The ca. 4–5 km thick Gyeonggi Shear Zone (Fig. 3) is developed in the lower part of the heterogeneous zone that de Jong et al. (2015) and S.Y. Han et al. (2017) incorporated into the mélange zone between the Gyeonggi Massif and the overriding mélange-like Samgot Unit (Yeoncheon Complex) and not to the Gyeonggi Massif, contrary to other workers (M. Cho et al., 2007; J.N. Kim et al., 2000; S.W. Kim, Kwon, Park, Yi, Santosh, & Kim, 2017; S.W. Kim, Park, Jang, Kwon, Kim, & Santosh, 2017; S.I. Park et al., 2019). It comprises strongly retrogressed and ductilely deformed biotite gneisses (Gyeonggi Massif type), quartz–biotite–muscovite–chlorite schists and well-foliated micaceous quartzite, with hecto- to pluri-kilometer long lenses of fine-grained, in part, garnet-bearing amphibolite and biotite-rich augen gneiss ( $731 \pm 20$  Ma, zircon, SHRIMP U–Pb; Kee, 2011), including the variably deformed Gamaksan syenite to alkali granite suite (Fig. 3;  $742 \pm 7$  Ma, zircon, SHRIMP U–Pb; S.R. Lee et al., 2003). The latter was transformed into retrograde muscovite-bearing augen gneiss and (ultra) mylonite (Figs. 8a and b). Tectonites in the NNW-dipping shear zone have northerly plunging mineral and stretching lineations (av. 005/43; Fig. 7b) and are overprinted by late low-angle brittle-ductile shear bands (Fig. 8b).



**Figure 8 a-d** - Field photographs of deformation structures in the Gyeonggi Shear Zone (**a, b**) and the foliated and lineated basal part of the directly overlying Gimpo Group (**c, d**) (locations, **Fig. 3**). Planes of pictures parallel to the stretching lineation, except (**c**) having an oblique view to the lineation. Pencils for scale.



**(a)** Top-to-the-North shear indicated by sigma-type porphyroclasts, CS fabrics and CC' shears in mylonitic augen gneiss.



**(b)** late low-angle brittle-ductile shear bands in mylonite.



**Figure 8 (ctd)**



**(c)** internal gneissosity of a gneiss boulder cut off by the strong deformation fabric in metapelites of the Gimpo Group's basal part (same outcrop as [Fig. 8b](#)).



**(d)** isolated shear band boudins and low-angle shear bands in lowermost Gimpo Group (whole-rock sample 12JK42 from this outcrop).

Top-to-the-North shear is indicated by: (1) sigma-type porphyroclasts, (2) CS fabrics, (3) CC' shears and (4) late-stage shear bands (Figs. 8a and b), agreeing with J.N. Kim et al. (2000), who regarded the Gyeonggi Shear Zone as an extensional structure. Microstructures of quartz and feldspar in the mylonites suggest temperatures of 500°C during ductile deformation, the timing of which is constrained by an Rb–Sr mineral–whole-rock isochron age of  $226 \pm 1$  Ma on muscovite formed during shearing (J.N. Kim et al., 2000). Applying  $^{40}\text{Ar}/^{39}\text{Ar}$  dating of single muscovite and biotite grains from three tectonites in the Gyeonggi Shear Zone (12JK35, 36, 39) we test the proposed Late Triassic timing of its activity.

#### 4.5. Gimpo Group

The Gimpo Group crops out along the western and northwestern margin of the Gyeonggi Massif (Kee, 2011; Kee et al., 2008) and forms the northernmost occurrence of the Daedong Supergroup in South Korea. The Daedong Supergroup in central South Korea comprises post-collisional, non-marine conglomerates, sandstones and coal-bearing shales with intercalated tuffs and tuffaceous rocks deposited in structurally controlled, fault-bounded (intra-arc) basins on a metamorphic basement (Egawa, 2013; H.-j. Lee et al., 2021; Lim & Cho, 2012). Sediments of the Supergroup's lower part are metamorphosed and experienced ductile deformation (Egawa, 2013; Lim & Cho, 2012). The maximum illite crystallinity values indicate a high thermal maturity with average temperatures of the order of 320–340°C (Egawa, 2013). Local additional re-heating by fault-channeled flow of hot fluids linked to Jurassic igneous activity seems to have occurred after diagenesis agreeing with deposition in a continental arc setting with an elevated geothermal gradient (Egawa, 2013). Whereas plant fossils suggest that these sediments could be as old as latest Triassic (Rhaetian), the age of the supergroup's higher parts is well constrained as

mid-Early to early-Late Jurassic by tuffs and tuffaceous rocks yielding 187–172-Ma-old zircons, as well as by the youngest populations (ca. 164 Ma) and individual grains (ca. 158 Ma) of detrital zircon (H.-j. Lee et al., 2021; and references therein). Some rocks acquired primary remanent magnetization around 180 Ma during sedimentation (Kee, 2011). This timing agrees with the 195–160 Ma timespan (peak: ca. 172 Ma) of Jurassic granitic magmatism in the peninsula (Cheong et al., 2014; K.H. Park et al., 2010; Sagong et al., 2005).

The Gimpo Group is in part spatially associated with the Gyeonggi Shear Zone in small outcrops mainly to the north of it, but also on top (Fig. 3). To the north of the shear zone this series comprises dull, dark grey to black shales with lenses of medium to coarse-grained sandstones and conglomerates (Fig. 3). In the lowermost 100 meters dull slates without a deformation fabric give progressively way to shiny phyllites with a well-developed bedding-parallel tectonic foliation and lineation, whereas psammites at this level are quartzitic, suggesting incipient mylonitization. Although estimates of metamorphic conditions are unavailable, the observed ductile deformation structures in the Gimpo Group's basal part would be compatible with temperatures of about 330°C established for the Daedong Supergroup. Large K-Fsp crystals, rare elongated pebbles and boulders of (augen)gneiss, which resemble lithologies in the Gyeonggi Shear Zone, are wrapped by this strong deformation fabric, truncating the internal gneissosity (Fig. 8c; from the same outcrop as Fig. 8b). Planar and linear fabric elements (Fig. 7c; average lineation: 358/38) are parallel to the foliation and lineation in Gyeonggi Shear Zone (Fig. 7b). The asymmetry of isolated shear band boudins and low-angle shear bands (Fig. 8d) demonstrate the same top-to-the-North kinematics as the underlying ductile shear zone. We applied whole-rock  $^{40}\text{Ar}/^{39}\text{Ar}$  laser step-heating dating to the lowermost linear phyllites in



contact with the Gyeonggi Shear Zone (12JK42) in order to constrain the age of ductile deformation.

## 5. $^{40}\text{Ar}/^{39}\text{Ar}$ Geochronology

### 5.1. $^{40}\text{Ar}/^{39}\text{Ar}$ Analytical Procedures and Methodology

Following thorough ultrasonic rinsing in distilled water, single mineral grains obtained by handpicking the 0.3–2.0 mm size fraction of crushed rock under a binocular zoom microscope were wrapped in  $11 \times 11 \times 0.5$  mm Al foil envelopes and stacked in an irradiation can with neutron flux monitors inserted after every 10 samples. Processing of the samples with fast neutrons occurred in three distinct irradiations (IR19, IR21 and IR23) with two distinct flux monitors, namely, amphibole Hb3gr [(Jourdan et al., 2006);  $1081.0 \pm 1.2$  Ma; Renne et al., 2010, 2011)] for IR19 and IR21, and sanidine TCRs ( $28.608 \pm 0.033$  Ma; Renne et al., 1998, 2010, 2011) for IR23. Irradiation IR19 (all 10JK samples) in the Cd-shielded Rodeo P3 facility of the European Commission High Flux Reactor at Petten (The Netherlands) lasted 72h with a  $J/h \approx 2.54 \times 10^{-4} \text{ h}^{-1}$ . IR21 and IR23 were processed under Cd-shielding in location 8E of the McMaster reactor (Hamilton, Canada) for about 298 hours with a  $J/h$  of ca.  $5.85 \times 10^{-5} \text{ h}^{-1}$  for IR21 (samples 12JK28, 61, 64, 69, 77, 79 and 81) and around 127.5 hours with a  $J/h$  of ca.  $4.77 \times 10^{-5} \text{ h}^{-1}$  for IR23 (samples 12JK35, 36, 38, 39, 42 and 76 and the entire 13JK series). The sample arrangement allowed monitoring of the neutron flux gradient with a precision of  $\pm 0.2\%$ . Single-grains were  $^{40}\text{Ar}/^{39}\text{Ar}$  step-heated with a Synrad<sup>®</sup> CO<sub>2</sub> continuous laser, following the protocol outlined by Ruffet et al. (1991, 1995). Using a MAP215<sup>®</sup> noble gas mass spectrometer, the five argon isotopes and the background baselines were measured in eleven cycles, in peak-jumping mode. Blanks were performed routinely at the start of an experiment and repeated typically after

each third run, and subtracted from the subsequent sample gas fractions. All isotopic measurements are corrected for mass discrimination and atmospheric argon contamination, following [J.Y. Lee et al. \(2006\)](#) and [Mark et al. \(2011\)](#), as well as K, Ca and Cl isotopic interferences. Plateau ages were calculated if 70% or more of the  $^{39}\text{Ar}_\text{K}$  was released in three or more contiguous steps, the apparent ages of which agreeing to within  $1\sigma$  of the integrated age of the plateau segment. Pseudo-plateau ages meet these criteria for less than this threshold. Plateau ages can be validated by inverse isochron ( $^{36}\text{Ar}/^{40}\text{Ar}$  vs.  $^{39}\text{Ar}_\text{K}/^{40}\text{Ar}^*$ ) calculation with least-squares fitting of the best straight line according to [York \(1969\)](#) and [York et al. \(2005\)](#). However, importantly, [Fleck et al. \(1977\)](#) pointed out that "*The criteria for determining the presence or extent of an age plateau, however, remain somewhat subjective*", underscoring that the amount of  $^{39}\text{Ar}_\text{K}$  released is not a disqualifying criterion. To visualize the degassing kinetics of argon during the step-heating procedure of samples from multiphase systems, [De Putter and Ruffet \(2020\)](#) developed  $^{40}\text{Ar}^*$  degassing kinetics analysis ( $(^{40}\text{Ar}^*/\Delta T^\circ)/(^{40}\text{Ar}^*/\Delta T^\circ)_{\text{Max}}$  versus  $\%^{39}\text{Ar}_\text{K}$ ) and weighted age spectrum processing, which resizes apparent ages according to their respective  $^{39}\text{Ar}_\text{K}$  degassing rate ( $\%(^{39}\text{Ar}_\text{K}/\Delta T^\circ)/(^{39}\text{Ar}_\text{K}/\Delta T^\circ)_{\text{Max}}$ ) rather than their absolute amount of  $^{39}\text{Ar}_\text{K}$ . A weighted age spectrum allows weakly expressed but clearly identified radiogenic components (associated with degassing peaks) to be represented in proportion to their degassing rates. All errors are quoted at the  $1\sigma$  level; those on (pseudo)-plateau ages or on apparent ages individually cited include the errors on the  $^{40}\text{Ar}^*/^{39}\text{Ar}_\text{K}$  ratio and age of the monitor, the decay constant and the J-parameter, but the tabulated apparent ages do not. For the parameters used in calculations (decay constants ([Renne et al., 2011](#)), atmospheric argon ratios ([J.Y. Lee et al., 2006](#); [Mark et al., 2011](#)), mass discrimination, isotopic ratios measured on K, Ca and Cl pure

salts and J parameter) we refer to the Supporting Information data at  
<https://data.mendeley.com/datasets/x2x5h8p6wj/1>

## 5.2. K–Ar Isotopic Closure Temperature Estimates

Generally, mineral ages in metamorphic rocks are interpreted within the closure temperature concept envisaging that during cooling a threshold is passed below which radiogenic isotopes start to accumulate in crystal lattices. However, the estimation of the closure temperatures of minerals in the K–Ar isotopic system is a quite delicate exercise. Calibrating K–Ar ages against metamorphic grade, isotopic closure of muscovite and biotite were first estimated to occur around 350°C and 300°C, respectively (e.g., [Purdy & Jäger, 1976](#)); values that are still widely used. However, since then several studies implied that for muscovite (more generally K–white mica) in absence of deformation and fluid-enhanced recrystallization, which both will lower the temperature for isotopic closure as they generally reduce the effective radius for argon diffusion of affected minerals, isotopic closure temperatures may be as high as 500°C ([Bosse et al., 2005](#); [Villa, 1998](#)). Applying the experimental muscovite diffusion coefficients estimated by [Harrison et al. \(2009\)](#), [Pitra et al. \(2010\)](#) calculated a closure temperature range of 425–540°C for K–white micas with effective diffusion radii of 100–1000 µm and for cooling rates of 10–100°C/Ma. Similarly, the closure temperature of biotite was reappraised to a value as high as about 450°C (e.g., [Villa & Puxeddu, 1994](#)). For hornblende with an effective diffusion radius of 80 µm in geological systems cooling with rates between 10 and 500°C/Ma the closure temperature range is estimated at 500–590°C ([Harrison, 1981](#); [Lister & Baldwin, 1996](#)), revised upward to 550–650°C by [Villa \(1998\)](#).

### 5.3. $^{40}\text{Ar}/^{39}\text{Ar}$ Results

Our  $^{40}\text{Ar}/^{39}\text{Ar}$  laser-probe step-heating dating of hornblende, and/or muscovite and biotite single-grains yielded different plateau ages (PA) and pseudo-plateau ages (PPA), but also complicated age spectra with coinciding frequently measured individual steps, forming distinct clusters in density probability diagrams that agree with (P)PAs. We take this as reflecting distinct geological events in a prolonged and complex tectono-metamorphic and thermal evolution from Late Permian to mid-Jurassic time. The analytical data and  $^{40}\text{Ar}/^{39}\text{Ar}$  ages are listed in Supplementary Data S1 and portrayed as age spectra in Figs. 9–13.

#### 5.3.1. Yeoncheon Complex: Garnet Zone of the Jingok Unit

Biotite 13JK53 from a garnet–mica schist with a well-developed main foliation and a biotite platelet lineation yielded a PA of  $254.6 \pm 0.9$  Ma (Fig. 9a). In contrast, single phyllite whole-rock fragment 13JK58 from a thick-bedded laminated quartzite gave a sigmoid-shaped age spectrum with increasing apparent ages from about 170 to 500 Ma for the fusion step, and a PPA of  $237.1 \pm 0.5$  Ma in the intermediate temperature degassing domain (Fig. 9a). This could suggest partial resetting of an old inherited component ( $> \text{ca. } 500$  Ma) around 237 Ma.  $^{40}\text{Ar}^*$  degassing kinetics analysis reveals several peaks in the low-temperature domain (Fig. 9b) suggesting the disturbance is probably related to degassing of newly crystallized secondary white mica components. Weighted age spectrum processing clearly reveals a secondary component that crystallized around 237 Ma (Fig. 9b) at the cost of an early to pre-Triassic primary component, the age of which cannot be more precisely constrained due to the presence of an apparent Early Paleozoic inherited constituent. The estimated metamorphic peak temperature for garnet zone meta-pelites ( $570\text{--}585 \pm 30^\circ\text{C}$ ; Kim & Jung, 2010) is far in excess of the maximum estimate of

the K–Ar isotopic closure temperature of biotite (see above). Therefore, the ca. 255 Ma PA of biotite 13JK53 necessarily is a cooling age. Nevertheless, the "old" apparent ages for the final degassing steps of phyllite whole-rock 13JK58 raises some concerns because metamorphic peak temperatures would preclude the survival of an older isotopic component in mica. This could mean that degassing in the high temperature steps is dominated by "contaminants" such as included accessory minerals.

### 5.3.2. Yeoncheon Complex: Staurolite Zone of the Jingok Unit

Overall, dating of biotite and muscovite from the staurolite zone resulted in concordant PAs or PPAs in the 255–250 Ma range, also clearly demonstrated by a huge peak in the density probability diagram expressing the relative occurrence of apparent ages from all samples from this zone (Fig. 9h). However, the frequency plot also reveals additional clusters around 243–238 Ma and 223 Ma implying a more complex history; we discuss these results in detail in the following part.

The asymmetric hump-shaped age spectrum of the largest biotite grain (400–1000  $\mu\text{m}$  size fraction) from mica schist 13JK63 (Fig. 9c) shows the effect of  $^{39}\text{ArK}$  recoil during irradiation linked to chloritization (cf., Ruffet et al., 1991). The smallest biotite grain (250–400  $\mu\text{m}$  size fraction) from this sample, however, yielded a PA of  $250.9 \pm 0.8$  Ma, implying it was less chloritized. Results from mica schist 13JK67 are more complex (Fig. 9d). The small biotite grain (250–400  $\mu\text{m}$ ) yielded a slightly staircase-shaped age spectrum with a PA of  $240.7 \pm 0.7$  Ma for the intermediate to high temperature steps and an older fusion step of ca. 246 Ma. The larger biotite (400–1000  $\mu\text{m}$ ) and the muscovite in this sample display staircase-shaped age spectra, but with older PPAs for intermediate to high temperature steps of  $251.7 \pm 0.6$  Ma and  $250.2 \pm 0.5$



Ma, respectively, which agree with the PA of small biotite 13JK63. However, also the fusion step for the larger biotite in 13JK67 is older (ca. 262 Ma), whereas the final high-temperature steps of the muscovite increase up to about 282 Ma (Fig. 9d). Consequently, despite the near concordant ca. 252–250 Ma PPAs, both biotite and muscovite single grains contain an apparent inherited/contaminant component, as previously concluded for the garnet zone. The staircase-shape of the age spectra of the larger biotite and the muscovite implies that sample 13JK67 experienced a disturbance probably slightly younger than ca. 241 Ma, as similarly implied by the PA of the smaller biotite in this sample (Fig. 9d).

The grain-size dependent interpretation is also consistent with results on large randomly oriented muscovite grains from late quartz veins that cross cut the main tectonic foliation in the mica schists from which biotites 13JK63 and 13JK67 were obtained. Such muscovites yielded almost identical PAs of  $252.9 \pm 0.5$  Ma (13JK62) and  $252.5 \pm 0.4$  Ma (13JK65) (Fig. 9e) that are slightly older than the ca. 252–250 Ma PPAs of main fabric forming biotite and muscovite grains discussed above. It must nevertheless be underscored that an apparent inherited/contaminant component also seems preserved in high-temperature steps of muscovite 13JK62, possibly representing tiny parts of the vein margin's host rock on which the mica crystal grew. However, despite its large grain size muscovite is also affected by subsequent disturbance(s). Another muscovite grain from a quartz vein in mica schist 13JK69 yielded a saddle-shaped age spectrum with a mean age for the saddle sidewall steps of  $253.6 \pm 0.6$  Ma and a saddle minimum PPA of  $249.9 \pm 0.6$  Ma (Fig. 9f). Biotite grain 13JK68 from the strongly chloritized mica schist close to the vein yielded a PA of  $222.9 \pm 0.8$  Ma (Fig. 9g). We interpret the saddle-shaped age spectrum of 253.5-Ma-old muscovite 13JK69 by its recrystallization probably related with chloritization of the quartz vein's host rock around 223 Ma. This explanation follows the interpretation of saddle-

shaped age spectra by mixing of two generations of chemically distinct muscovite formed by partial recrystallization of the original white mica (Alexandrov et al., 2002; Tartèse et al., 2011).

**Figure 9 a-h** (caption: two pages below)

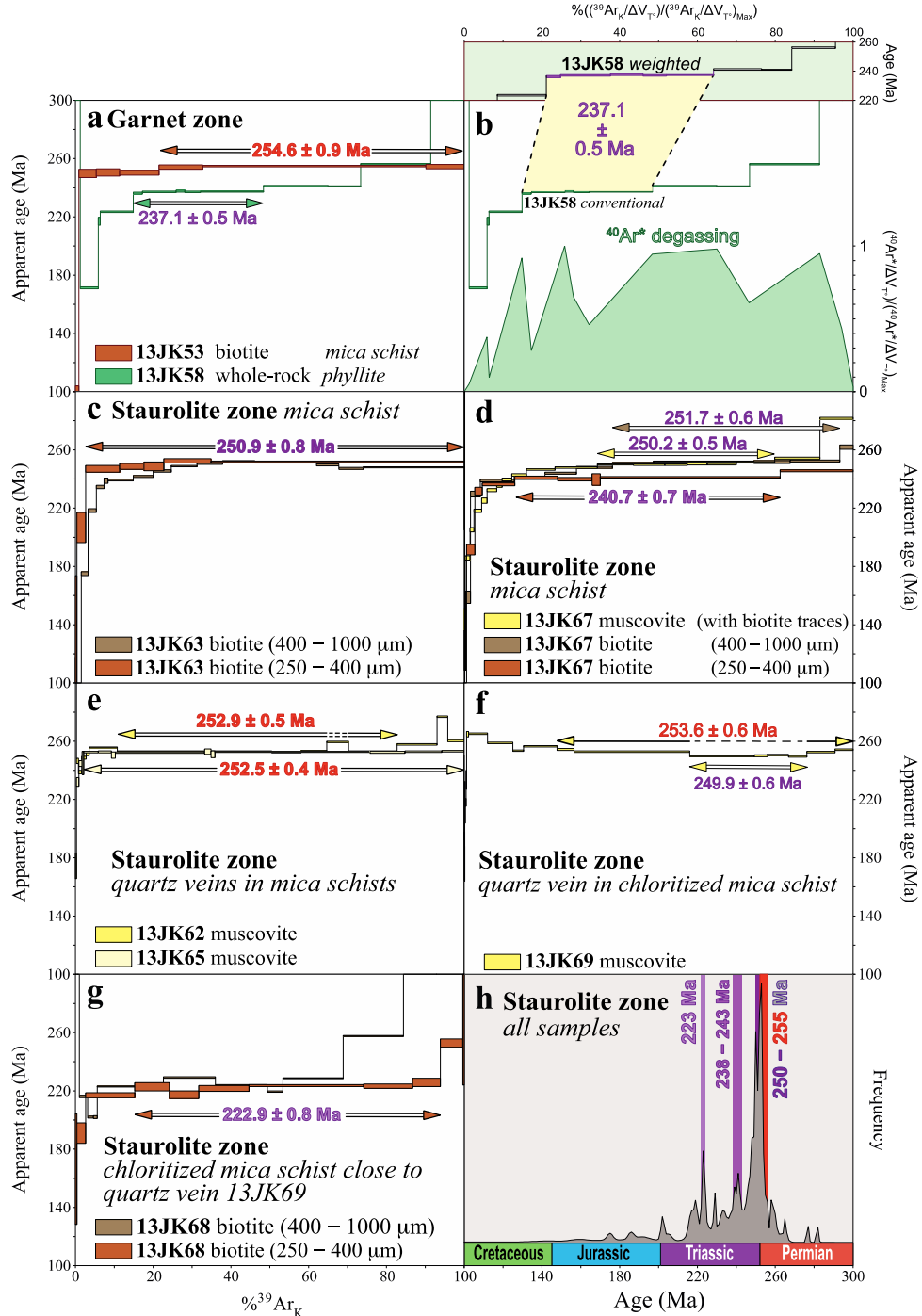




**Figure 9** -  $^{40}\text{Ar}/^{39}\text{Ar}$  laser step-heating age spectra for muscovite, biotite and hornblende single-grains and a whole-rock fragment from different rocks of the Yeoncheon Complex in the Juksung–Yeoncheon–Baengmagoji area (**Fig. 3**); error bars at  $1\sigma$ . **(a)** Garnet, **(c–g)** staurolite, **(i–k)** kyanite zones of the Jingok Unit, **(m)** Samgot Unit; **(b, n)** conventional age spectra and degassing diagrams displaying  $(^{40}\text{Ar}^*/\Delta V_{T^*})/(^{40}\text{Ar}^*/\Delta V_{T^*})_{\text{Max}}$  vs.  $\%^{39}\text{Ar}_K$  (lower panels) compared with corresponding weighted age spectra of  $\%((^{39}\text{Ar}_K/\Delta V_{T^*})/(^{39}\text{Ar}_K/\Delta V_{T^*})_{\text{Max}})$  vs. apparent ages (upper panels);  $\Delta V_{T^*}$  corresponding to laser power control voltage increment (see text for explanation). Double-lined arrows for plateau ages (thick lines, boldfaced numbers) and pseudo-plateau ages (thin lines, lightface numbers); dashed-lined arrows for mean ages of saddle sidewall steps and saddle base minimum apparent ages for saddle-shaped spectra (uncertainties at  $1\sigma$ ). **(h, l, o)** Density probability diagrams with the relative occurrence of apparent ages for the staurolite and kyanite zones, and the Samgot Unit. Colors of isotopic dates, periods and epochs are according to the scheme of the International Commission on Stratigraphy (ICS) (Cohen et al., 2013). Structural aspect of samples illustrated in **Fig. 5a** (13JK71, 72), **Fig. 5c** (13JK 86) (kyanite zone) and **Fig. 5e** (13JK96) (Samgot Unit).

### 5.3.3. Yeoncheon Complex: Kyanite Zone of the Jingok Unit

The grouping of apparent ages from the samples of the kyanite zone results in three main peaks of about 255–250, 242–237 and 225–221 Ma in the density probability diagram, highly similar to the staurolite zone, and an additional peak at ca. 183 Ma (**Fig. 9l**). Again, most samples gave strikingly different age spectra, once more underlining the complexity of the tectono-metamorphic and thermal history.

Mica schist 13JK77 from a zone with conjugate  $D_{m+1}$  shear band cleavage systems has a well-developed lineation of elongated biotite and muscovite grains and quartz aggregates; kyanite porphyroblasts have a random orientation, whereas late andalusite-bearing quartz veins cross cut the main foliation. Muscovite gave a PA of  $250.7 \pm 0.4$  Ma, but biotite has a significantly older PPA of  $255.2 \pm 0.4$  Ma (**Fig. 9i**). The age spectrum of the muscovite is nearly perfectly flat with younger apparent ages only for the first couple of steps, but that of biotite has

a slight staircase shape in the low to intermediate steps, probably expressing a younger disturbance.  $^{40}\text{Ar}^*$  degassing kinetics analysis with age spectrum weighting indicates that this may be related to degassing of a ca. 239–237-Ma-old secondary component, suggesting partial recrystallization around that time, which also affected the garnet and staurolite zones. Quartz–mica schist 13JK72 is from a zone in which staurolite crystals are both randomly orientated within the foliation and aligned parallel to the main lineation (Fig. 5a). In this zone folded quartz–mica foliations  $S_m$  and  $S_{m+1}$  are locally overprinted by well-developed cm- to dm-spaced low-angle  $D_{m+2}$  shear bands with top-to-the-(N)NW kinematics, opposite to main phase shear. Muscovite 13JK72 displays a saddle-shaped age spectrum (Fig. 9j), with a mean age for the saddle sidewall steps of  $240.5 \pm 0.6$  Ma and the saddle minimum pseudo-plateau age of  $224.5 \pm 0.8$  Ma. We interpret this age spectrum, as previously discussed, by the mixing of two muscovite generations formed by partial recrystallization of an at least ca. 241-Ma-old component during an event around 225 Ma, which is related to  $D_{m+2}$ . In contrast, chlorite–mica schist 13JK93 has strongly retrogressed garnet, kyanite and staurolite, with muscovite and biotite both yielding disturbed age spectra (Fig. 9j). Muscovite has a saddle-shaped age spectrum with a minimum apparent age of  $224.5 \pm 0.8$  Ma; biotite has a less disturbed age spectrum with a PPA of  $221.3 \pm 0.5$  Ma for the intermediate to high temperature steps. Coincidence of both ages and the pronounced disturbance of the muscovite age spectrum are probably not fortuitous since traces of biotite were observed within the analyzed muscovite grain. The minimum apparent age of the muscovite is identical to the saddle minimum pseudo-plateau age of  $224.5 \pm 0.8$  Ma of muscovite 13JK72 (Fig. 9j).

Large randomly oriented muscovite grains present in the margins of two late discordant andalusite-bearing quartz veins yielded distinct age spectra (Fig. 9k). Muscovite 13JK86 from a



sigmoid-shaped vein indicating  $D_{m+1}$  top-to-the-(S)SE shearing (Fig. 5c) has a well-developed PA of  $251.4 \pm 0.4$  Ma (Fig. 9k). In contrast, muscovite 13JK71 yielded a saddle-shaped age spectrum with sidewall steps having a mean age of  $242.2 \pm 0.4$  Ma (Fig. 9k), which resembles muscovite 13JK72, taken from the same outcrop, both in shape and ages of the sidewalls (ca. 241 Ma). It is likely that the saddle minimum pseudo-plateau age of  $236.6 \pm 0.5$  Ma (13JK71) is also related to the Late Triassic disturbance demonstrated for other samples.

The marked hump-shape age spectrum of the youngest biotite from sample 13JK72 (Fig. 9j) clearly points to chloritization (see above). Its Jurassic apparent ages may suggest a post-Triassic resetting, also recorded by biotite 13JK75 from a concordant andalusite-bearing quartz-rich pod, which gave a slightly hump-shaped age spectrum likewise pointing to limited chloritization, yet yielding a PPA of  $182.9 \pm 0.4$  Ma (Fig. 9k).

#### 5.3.4. Yeoncheon Complex: Samgot Unit

Hornblende crystal 13JK96 forming part of the linear fabric of a mylonitic hornblende–biotite gneiss with a top-to-the-(E)SE  $D_{m+1}$  fabric occurring as an asymmetric lens within meta-calc-silicate rocks showing the same kinematics gave flat  $^{37}\text{Ar}_{\text{Ca}}/^{39}\text{Ar}_{\text{K}}$  and age spectra and a PA of  $248.8 \pm 0.6$  Ma (Fig. 9m). In contrast, the two analyzed amphibole grains from coarse-grained amphibolite/meta-gabbro 10JK06 with granulite relics and a poorly developed deformation fabric display saddle-shaped age and  $^{37}\text{Ar}_{\text{Ca}}/^{39}\text{Ar}_{\text{K}}$  spectra (Fig. 9m). The saddle shaped  $^{37}\text{Ar}_{\text{Ca}}/^{39}\text{Ar}_{\text{K}}$  points to partial recrystallization of both amphiboles, the timing of which is best estimated by the concordant PPAs of the saddle bases of  $248.5 \pm 1.5$  Ma (grain a) and  $247.0 \pm 1.6$  Ma (grain b) (Fig. 9m). The perfect agreement of the hornblende (P)PAs in both samples, well expressed in the density probability diagram (Fig. 9o) as a huge sharp peak, suggests they

registered the same main tectono-metamorphic event around 249–247 Ma. Ca. 253–249-Ma-old metamorphic overgrowths (errors  $\pm 1\text{--}3$  Ma) occur on mid-Devonian detrital zircons in neighboring meta-sediments (D.L. Cho et al., 2005; B.C. Lee et al., 2019). We regard the Early Triassic  $^{40}\text{Ar}/^{39}\text{Ar}$  age we obtained as constraining the cooling of the Samgot Unit after  $D_{m+1}$  because the estimated maximum metamorphic temperatures for garnet-amphibolites (660–780°C; M. Cho et al., 2007; B.C. Lee et al., 2019) are well above the hornblende closure temperature estimates. This interpretation agrees with the occurrence of quartz lattice preferred orientations in meta-calc-silicate rocks formed during  $D_m$  that suggest temperatures of 500–600°C.

Hornblende–biotite gneiss featuring a lineation of elongated garnet aggregates (10JK07) yielded an amphibole with a strongly disturbed age spectrum that is difficult to interpret, and a biotite with a staircase age spectrum with a slope break at ca. 375 Ma and apparent ages up to ca. 407 Ma for the final steps (Fig. 9n). Also, biotite from garnet-bearing augen gneiss 13JK102 displays a staircase-shaped age spectrum with apparent ages increasing up to about 380 Ma at fusion and a PPA of  $371.6 \pm 1.2$  Ma (Fig. 9n).  $^{40}\text{Ar}^*$  degassing kinetics analysis clearly shows a peak for the first 30–40% of  $^{39}\text{Ar}_K$  release (Fig. 9n). Age spectrum weighting would suggest a disturbance related to degassing of a ca. 372-Ma-old secondary component (partial recrystallization?), in good agreement with the PPA and the slope break at about 375 Ma in the age spectrum of biotite 10JK07, which could suggest a similar process. The density probability diagram of the biotite in both samples shows a number of significant peaks in the 380–365 Ma range (Fig. 9o). Interestingly, the mylonitic gneiss lens with ca. 249-Ma-old hornblende 13JK96 has a ca. 372–373-Ma-old granite protolith.

### 5.3.5. Yeoncheon Complex: Interpretative Summary of Results

All  $^{40}\text{Ar}/^{39}\text{Ar}$  results from the Yeoncheon Complex clearly demonstrate a principal latest Permian to Early Triassic event and smaller, but important, incidents in the Middle and Late Triassic, visualized in density probability diagrams of apparent ages and PA/PPAs, and a cumulative diagram of PAs and PPAs (Fig. 10).

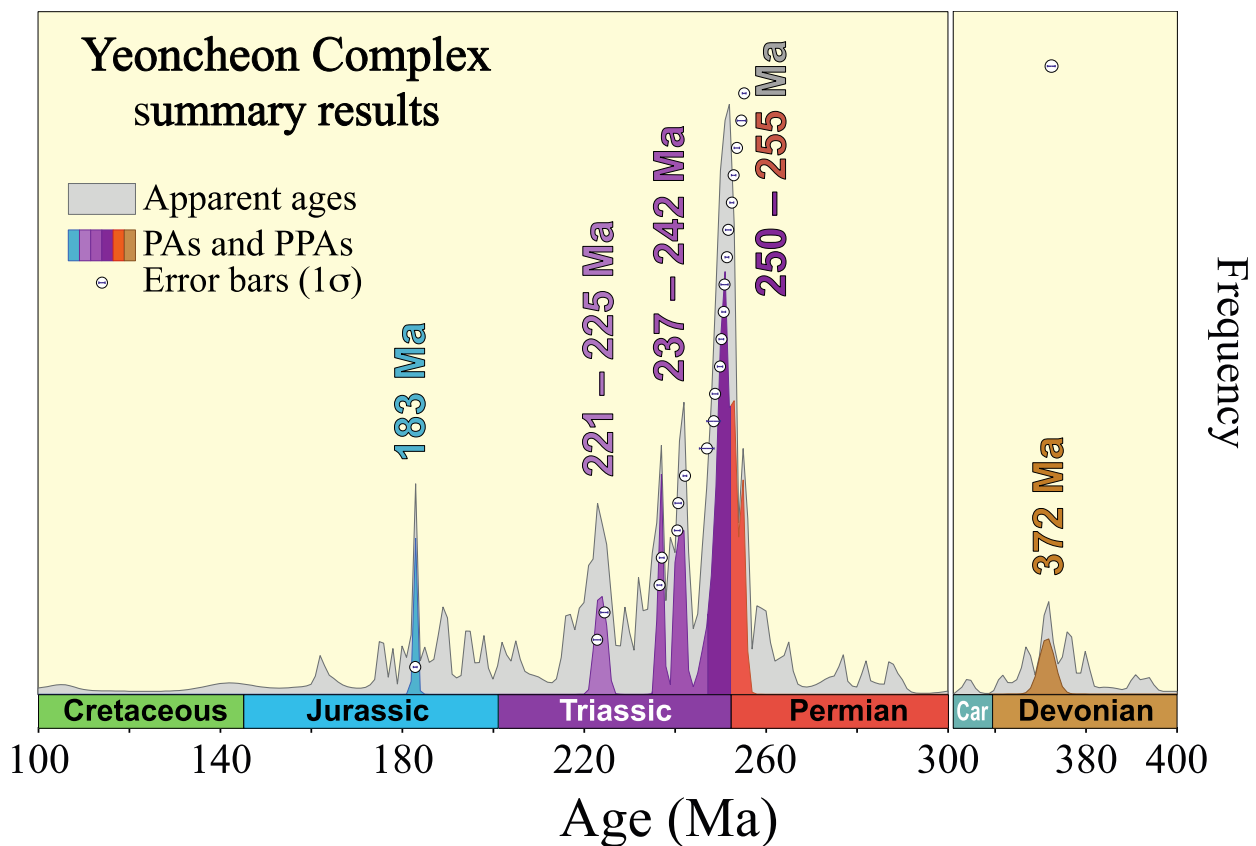


**Figure 10** - Density probability diagrams displaying the relative occurrence of apparent ages (grey) and PA/PPAs (colored) and a cumulative diagram of PAs and PPAs (bullets) with their ages summarizing the  $^{40}\text{Ar}/^{39}\text{Ar}$  results from the Yeoncheon Complex in the Juksung–Yeoncheon–Baengmagoji area. Colors of isotopic dates, periods and epochs follow the ICS scheme (Cohen et al., 2013).

The oldest  $^{40}\text{Ar}/^{39}\text{Ar}$  (P)PAs for muscovite and biotite from rocks with the main tectono-  
 metamorphic plano-linear fabric  $S_m$  and the shear fabric  $S_{m+1}$  in the different metamorphic zones  
 of the Jingok Unit are tightly clustered:  $254.6 \pm 0.9$  Ma (biotite, garnet zone),  $251.7 \pm 0.6$  and  
 $250.9 \pm 0.8$  Ma (biotite),  $250.2 \pm 0.5$  Ma (muscovite) in the staurolite zone, as well as  $255.2 \pm$   
 $0.4$  Ma (biotite) and  $250.7 \pm 0.4$  Ma (muscovite) in the kyanite zone. Large randomly oriented  
 muscovite grains from variably deformed, in part andalusite-bearing, quartz veins cross cutting  
 $S_m$  and  $S_{m+1}$  have similar PAs of  $252.9 \pm 0.5$ ,  $252.5 \pm 0.4$  and  $249.9 \pm 0.6$  Ma (minimum saddle-  
 shaped spectrum with maximum ages of  $253.6 \pm 0.6$  Ma on both sides) in the staurolite zone, as  
 well as  $251.4 \pm 0.4$  Ma in the kyanite zone. We regard all (P)PAs as cooling ages as biotite and  
 muscovite closure temperatures are substantially higher than the metamorphic peak temperatures  
 in the Jingok Unit. The slightly older ages for the largest muscovite grains, including the crystals  
 in the texturally latest quartz veins, agree with this interpretation conform the relationship  
 between size of the diffusive domain and isotopic closure temperature. Tight clustering of  
 closely matching muscovite and biotite (P)PAs, which are highly similar in mica schists and  
 cross-cutting quartz veins, points to fast cooling in the 550–450°C temperature range in the 255–  
 250 Ma interval, following the main tectono-metamorphic phase  $D_m$ , the principally top-to-the  
 (S)SE directed shear phase  $D_{m+1}$  and the formation of the quartz vein system. Hornblendes in the  
 Samgot Unit, however, yielded significantly younger concordant cooling ages of  $248.8 \pm 0.6$  Ma  
 (PA) and 248.5 and 247.0, errors  $\pm 1.6$  Ma (PPAs), suggesting the presence of a tectonic contact  
 within the Yeoncheon Complex, as discussed in section 6.3.

In the late Middle (ca. 242–237 Ma) and middle Late (ca. 225–221 Ma) Triassic (Fig. 10)  
 the rocks were partially overprinted by two successive incidents, which were both more  
 pervasive in the deeper part of the Jingok Unit. Both biotite and muscovite in the staurolite and

kyanite zones have staircase-shaped age spectra but retain Early Triassic ages for most of the degassing.  $^{40}\text{Ar}^*$  degassing kinetics analysis with age spectrum weighting of a kyanite zone biotite (PPA ca. 255 Ma) points to the presence of a ca. 239–237-Ma-old secondary component, whereas the nearly perfectly flat age spectrum of muscovite in the sample (PA ca. 251 Ma) implies it was not affected by mid-Triassic partial resetting. Whereas resetting was only partial around 240 Ma for larger grains in the staurolite zone, it was complete for smaller biotite shown by a sample with a PA of ca. 241 Ma. In contrast to biotite, muscovite does not show significant mid-Triassic age components in the staurolite zone, but does so in the kyanite zone (cf. Fig. 9h and Fig. 9l), demonstrated by sidewall steps mean ages of 241–242 Ma and a PA of ca. 242 Ma. The mid-Triassic partial resetting is not linked to a specific tectono-metamorphic phase, so that its meaning is not immediately clear. It is striking that despite having dated a very substantial number of samples we did not obtain any (P)PA in the 233–228 Ma range (Fig. 10) that forms the characteristic age group in rocks of the Taean Formation and the Hongseong Belt. Yet, it is not excluded that the ca. 240–237 Ma ages and age components formed by recrystallization could be related to the 237–224-Ma-old post-collisional thermo-magmatic pulse (section 3). In contrast, Late Triassic ages and age components for biotite and for muscovite in the kyanite zone are mostly found in areas affected by retrogression and chloritization, and/or top-to-the-(N)NW  $D_{m+2}$  shear superimposed on  $S_m$  and  $S_{m+1}$ . Complete Late Triassic resetting of biotite, shown by 223–221 Ma (P)PAs, took place in chlorite–mica schists with strongly retrogressed Barrovian mineralogy in the kyanite and staurolite zones. However, muscovite never shows significant Late Triassic age components in the staurolite zone, and is reset only partially in the kyanite zone. Muscovite from two non-retrogressed kyanite zone samples in the same outcrop, a mica schist with the main foliation and an andalusite-bearing quartz vein crosscutting it, yielded saddle-



shaped age spectra (sidewall steps mean ages 241–242 Ma) with saddle minima PPAs of 225 Ma (main foliation) or of 237 Ma (quartz vein). Although both samples do not show such structures, the occurrence in the outcrop and neighboring areas of  $D_{m+2}$  shear bands that overprint the  $S_m$  and  $S_{m+1}$  implies that ductile deformation may have been instrumental in the Late Triassic partial resetting of mid-Triassic muscovite. We explained saddle-shaped age spectra by mixing of the original white mica with a chemically distinct, younger muscovite formed by partial recrystallization of the former. Consequently, the age spectrum's saddle minimum of ca. 237 Ma would overestimate the timing of resetting, as the larger vein muscovite would be much less affected by partial recrystallization. The occurrence of  $D_{m+2}$  in the kyanite zone is demonstrated by fine-grained mylonites with a top-to-the-NW sense of shear. Northerly shear, correlated with  $D_{m+2}$ , is indicated by CS-like cleavages in the Samgot Unit and in garnet-free mylonites in its lowermost part.  $D_{m+2}$  related retrogression thus increases structurally downwards in the Yeoncheon Complex. Late Triassic ages and structures with similar kinematics are also found in lithotectonic units at still deeper level, like the underlying Gyeonggi Shear Zone.

Only gneisses in the Samgot Unit seem to have registered a Late Devonian event implied by biotite with a PPA and main age components in the 380–365 Ma range. We regard these Late Devonian ages as indicating geologically significant pre-collisional events, as discussed in detail in section 6.1. However, the older high-temperature steps in some experiments on biotite and muscovite single-grains from the Yeoncheon Complex are best explained by degassing of contaminants like accessory minerals because the thorough fluid-assisted tectono-metamorphic recrystallization at peak temperature, shown by the intensity of the ductile deformation fabrics and quartz veining, should have fully reset the K–Ar isotopic system of the micas.

The kyanite zone recorded an Early Jurassic event that appears to be fairly widespread in other lithotectonic units, as will be discussed in the following sections (5.3.6 to 5.3.9).

#### 5.3.6. Taeon Formation

Two muscovites from meta-sandstones in Anmyeon Island yielded saddle-shaped age spectra that resemble each other regarding mean ages for saddle sidewall steps of  $240.6 \pm 0.8$  Ma (12JK28) and  $242.8 \pm 0.6$  Ma (12JK79), as well as saddle minima pseudo-plateau or apparent ages converging towards ca. 222–220 Ma (Fig. 11a). Following the argumentation set out earlier, we interpret both spectra as due to differential degassing of two mixed differently-aged muscovite generations: an older component of at least ca. 241 Ma old and a secondary component formed by partial recrystallization around 222–220 Ma.

Four randomly oriented pluri-millimeter-diameter muscovite grains from two samples of layer-parallel quartz veins in meta-sandstones on the islands of Anmyeon (12JK76) and Yeongheung (13JK20) have disturbed age spectra (Fig. 11c). Grains 13JK20-b and 12JK76-b have highly irregular uncommon, hence difficult to interpret, age spectra in part with excessively old ages for initial degassing of muscovite 12JK76-b, most likely due to degassing of inclusions as already suggested. Yet, the last two steps of muscovite 13JK20-b equivalent to about half of the degassing yielded a concordant apparent age of about 241 Ma (Fig. 11c). The two other grains (12JK76-a and 13JK20-a) have asymmetric, slightly saddle-shaped age spectra with significant apparent ages ranging from ca. 241 Ma to ca. 232 Ma. Age spectrum weighting reveals a weighted mean age of  $244.6 \pm 0.8$  Ma for two principal age steps in grain 12JK76-a

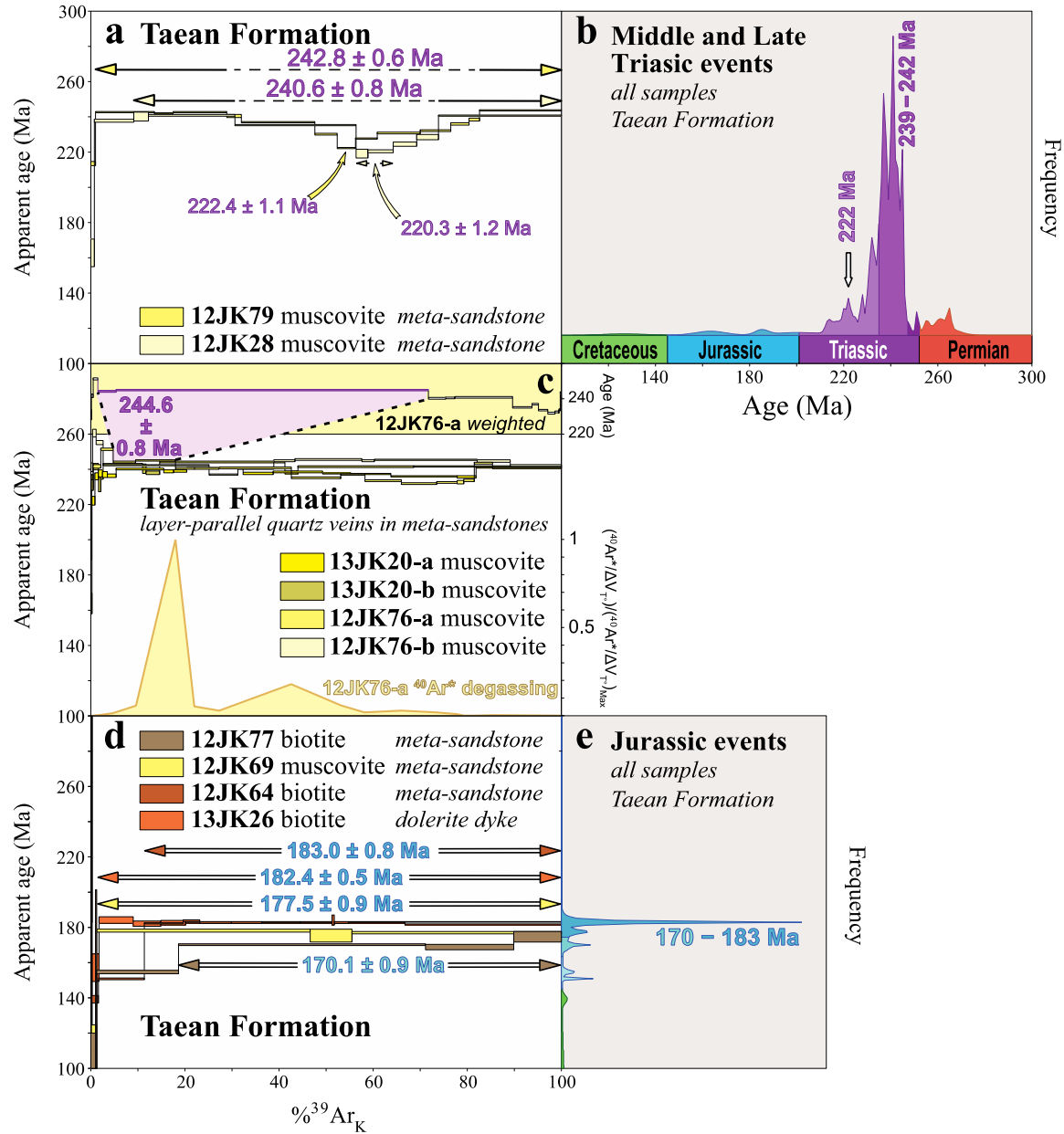


**Figure 11 - (a, c, d)**  $^{40}\text{Ar}/^{39}\text{Ar}$  laser step-heating age spectra for muscovite and biotite single-grains in different rocks of the Taean Formation on Anmyeon and Yeongheung islands (Figs. 1, 6); error bars at  $1\sigma$ , and **(b, e)** corresponding density probability diagrams with the relative occurrence of apparent ages. **(c)** Degassing diagram and conventional age spectrum of muscovite 12JK76-a (lower panel) compared with the corresponding weighted age spectrum (upper panel). See caption Fig. 9 for details.

(Fig. 11c). Importantly, despite the complexity of the age spectra, the fusion steps of all four muscovites are concordant at ca. 242–240 Ma. Because of the similarity of the age spectra of muscovite grains in samples 13JK20 and 12JK76, the convergence of apparent ages of saddle sidewalls and minima, as well as the concordance of fusion steps, we interpret these spectra too by differential degassing of a mix of two muscovite generations with different ages. This could indicate that a regionally consistent older component with a maximum age of 245–240 Ma (Fig. 11c) was partially recrystallized during a subsequent event, at least as young as about 232 Ma. The timing of this partial recrystallization of Middle Triassic muscovite agrees with the characteristic concordant isotopic ages of 233–229 Ma for metamorphic mica and titanite, as well as syenite and associated dolerites intruding the Taean Formation after two folding phases, as noted earlier by de Jong et al. (2014, 2015). This corroborates their suggestion that ca. 243–237-Ma-old steps in their saddle-shaped age spectra for muscovite grains are relics of an isotopic system related to an earlier tectono-metamorphic phase. The occurrence of 243–234-Ma-aged overgrowths on detrital zircon (S.W. Kim, Park, Jang, Kwon, Kim, & Santosh, 2017) further strengthens our interpretation. The fact that ca. 245–240 Ma ages are found for the Taean Formation in Anmyeon Island (12JK76) and for the slightly higher metamorphic grade rocks in Yeongheung Island (13JK20) points to a regionally significant mid-Triassic event. The Yeoncheon Complex experienced a mid-Triassic resetting of the 255–250-Ma-old peak metamorphic assemblage (previous sub-section). The peak of the amphibolite-facies conditions of the Taean Formation on the islets of Gukhwa and Ippa, farther north, is constrained by ca. 252–251-Ma-old metamorphic zircons (section 3). The ca. 245–240 Ma ages obtained in the current study are, hence, likely to be similarly due to mid-Triassic resetting following the Early Triassic event, the isotopic signal of which is, apparently, no longer present in muscovite. Also,

the partial recrystallization around 222–220 Ma of the least ca. 241-Ma-old component (12JK28 and 12JK79) is recorded in the youngest samples in the Yeoncheon Complex.

The density probability diagrams of all  $^{40}\text{Ar}/^{39}\text{Ar}$  step ages of muscovite grains discussed above show a number of main mid-Triassic and some minor Late Triassic clusters but only negligible Jurassic ages (Fig. 11b). But other samples yielded a significant number of Jurassic PAs (Fig. 11d and e) for biotite:  $183.0 \pm 0.8$  Ma (12JK64),  $182.4 \pm 0.5$  Ma (13JK26) and  $170.1 \pm 0.9$  Ma (12JK77), as well as muscovite:  $177.5 \pm 0.9$  Ma (12JK69), which are comparable to the timing of Jurassic granitic magmatism in the Taean Formation.

### 5.3.7. Gonam Complex

The density probability diagram of the step ages of all muscovite, biotite and amphibole single-grains shows distinct clusters, the ones of ca. 195 Ma and 220 Ma being the most significant, whereas Middle and Early Triassic peaks are subordinate (Fig. 12a).

Hornblende 13JK35 from an amphibolite with a well-developed tectono-metamorphic fabric within a quartzite–mica schist sequence with highly attenuated isoclinal, northward plunging D<sub>2</sub> folds, yielded corresponding saddle-shaped age and  $^{37}\text{Ar}_{\text{Ca}}/^{39}\text{Ar}_{\text{K}}$  spectra (Fig. 12b). The data suggest the presence of a primary amphibole ( $^{37}\text{Ar}_{\text{Ca}}/^{39}\text{Ar}_{\text{K}}$  ratios  $\geq 4.5$ ), as old as ca. 314.5 Ma (Late Carboniferous) that was partially recrystallized during a subsequent event around or after 251.0 Ma forming a secondary amphibole component with  $^{37}\text{Ar}_{\text{Ca}}/^{39}\text{Ar}_{\text{K}}$  ratios as low as about 3.1 (Fig. 12b, top panel). A concordant SHRIMP U–Pb age of about 320 Ma on an inner core of a zircon grain in a meta-sandstone in the complex that also yielded a concordant age of  $250 \pm 4$  Ma for the metamorphic outer rim (Kee, 2011) lends support to this interpretation. An average metamorphic outer rim age of  $262 \pm 3$  Ma around detrital zircons in another meta-



sandstone (Kee, 2011) further strengthens the argument that the Early Triassic hornblende date could record an initial tectono-metamorphic event in the complex. Minor Permian age peaks in the density probability diagram (Fig. 12a) may point to this too.

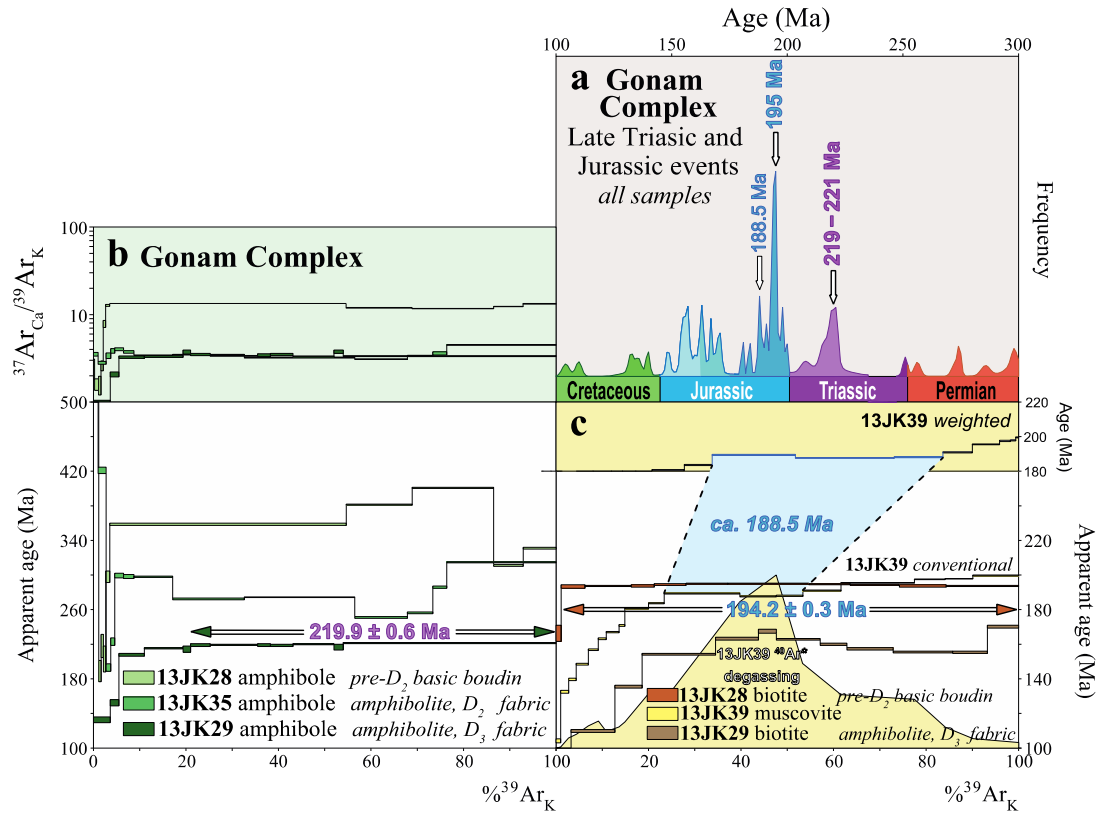


**Figure 12 - (a)** Density probability diagrams of all Gonam Complex samples on Anmyeon Island, with the relative occurrence of apparent ages. **(b, c)**  $^{40}\text{Ar}/^{39}\text{Ar}$  laser step-heating age spectra for amphibole, biotite and muscovite single-grains of the Gonam Complex (Fig. 6); error bars at  $1\sigma$ ; corresponding  $^{37}\text{Ar}_{\text{Ca}}/^{39}\text{Ar}_{\text{K}}$  ratios (# Ca/K ratios) of amphibole are plotted in the upper panel **(b)**. **(c)** Degassing diagram and conventional age spectrum of muscovite 13JK39 (lower panel) compared with the corresponding weighted age spectrum (upper panel). See caption Fig. 9 for details.

Strongly foliated and lineated amphibolite 13JK29 from a section with pervasive top-to-the-NNE  $D_3$  shear yielded biotite with a hump-shaped age spectrum, characteristic of chloritization (see above), and amphibole with a flat age spectrum with a PA of  $219.9 \pm 0.6$  Ma and a flat  $^{37}\text{Ar}_{\text{Ca}}/^{39}\text{Ar}_{\text{K}}$  spectrum averaging 3.4 (Fig. 12b). In view of the strong  $D_3$  shear in

neighboring rocks we regard the Late Triassic amphibole age as dating a final ductile deformation phase in the Gonam Complex. Because of the similar kinematics and timing we correlate D<sub>3</sub> in the Gonam Complex with D<sub>m+2</sub> in the Yeoncheon Complex, an event also provoking partial recrystallization of muscovite in some samples in the Taean Formation.

Hornblende 13JK28 from a basic boudin with a crude tectonic fabric that is wrapped by the main tectonic foliation in D<sub>2</sub>-folded meta-sediments has a hump-shaped age spectrum, with virtually all apparent ages far in excess of 300 Ma, which is difficult to interpret as it is uncorrelated to the saddle-shaped <sup>37</sup>Ar<sub>Ca</sub>/<sup>39</sup>Ar<sub>K</sub> spectrum (Fig. 12b). Biotite from this sample yielded a PA of 194.2 ± 0.3 Ma (Fig. 12b), although its slight hump-shape could reflect some chloritization (see above). Because the boudin also contains retrograde actinolite-rich amphibole, epidote and chlorite, the biotite plateau age and the strongly disturbed hornblende age spectrum point to Early Jurassic recrystallization, in agreement with the increments of 170–150 Ma in the hump-shaped age spectrum of biotite 13JK29 (Fig. 12b). A large muscovite grain from a layer-parallel quartz vein in a tourmaline-quartzite (13JK39) yielded a staircase-shaped age spectrum with a slope break around ca. 20–50% of <sup>39</sup>Ar<sub>K</sub> release (Fig. 12c, lower panel), suggesting degassing of a secondary component. The slope discontinuity is followed by an increase of apparent ages up to ca. 199.5 Ma at fusion. <sup>40</sup>Ar\* degassing kinetics analysis clearly shows a huge peak in this degassing range (Fig. 12c, lower panel) largely overlapping the degassing domain of the primary component, probably older than about 199.5 Ma. Age spectrum weighting highlights a disturbance related to degassing of a secondary component (partial recrystallization?) younger than ca. 188.5 Ma (Fig. 12c, upper panel), implying a significant Jurassic event affected the rocks of the Gonam Complex too, agreeing with a nearby outcrop of a ca. 175-Ma-old granite.

### 5.3.8. Gyeonggi Shear Zone

Muscovite and biotite from three tectonites from the Gyeonggi Shear Zone exclusively yielded Late Early to Middle Jurassic ages and age components. Biotite 12JK36 from a biotite–feldspar augen gneiss with well-developed foliation and lineation expressed by biotite and feldspar aggregates yielded a perfectly flat age spectrum with a PA of  $165.2 \pm 0.2$  Ma (Fig. 13a), validated by a concordant inverse isochron ( $165.1 \pm 0.7$  Ma, MSWD=0.72) with an atmospheric  $^{36}\text{Ar}/^{40}\text{Ar}$  intercept (Fig. 13b). In contrast, muscovites from a mica-rich fine-grained (ultra-)mylonitic gneiss (12JK35; Fig. 13a) and a foliation-parallel quartz vein (12JK39; Fig. 13c) display complex, but mostly saddle-shaped age spectra. Duplicate experiments (grains b) could not reproduce the complexity of the age spectrum of 12JK35 (Fig. 13a), but provided a closely matching spectrum for 12JK39, with similarities in form and identical PPAs or apparent ages for the sidewalls at ca. 181 Ma and the saddle bases at ca. 167 Ma (Fig. 13c). Such concordance between duplicated experiments suggests that the primary and secondary components were completely separated during the experimental degassing process. This could indicate that muscovite initially crystallized at about 181 Ma and was partly recrystallized during a subsequent event around 167 Ma. In contrast, the mismatch of step-heated duplicate of muscovite grains in 12JK35 suggests that the two components evoked above were not fully separated. Yet, muscovite grain b in this sample yielded the strongest disturbed and hump-shaped age spectrum with maximum apparent ages around 163 Ma. The ca. 163 Ma and 167 Ma age components in both muscovites are almost identical to the ca. 165 Ma PA of biotite 12JK36. The  $^{40}\text{Ar}/^{39}\text{Ar}$  ages of about 181 Ma to 165 Ma contrast with the ca. 226 Ma Rb–Sr age obtained by J.N. Kim et al. (2000) on synkinematic muscovite in a mylonite. The occurrence of late-stage

shear bands superimposed on the earlier mylonite foliation (Fig. 8b) may point to late Early to Middle Jurassic reactivation of the Late Triassic shear zone.

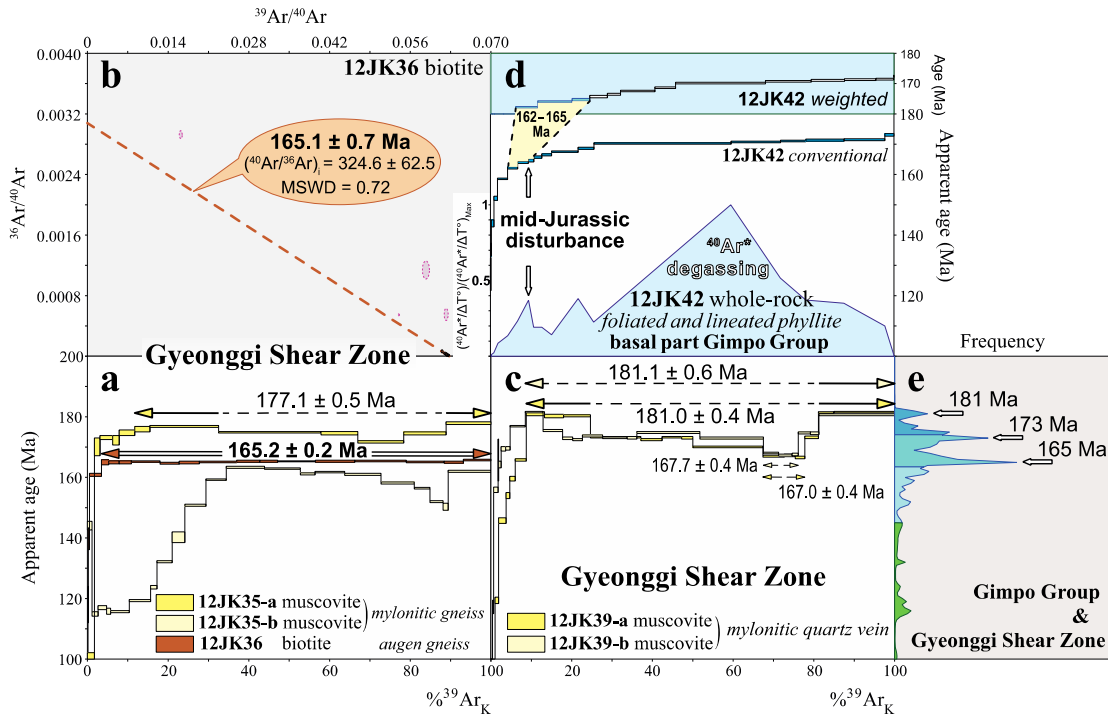


**Figure 13 - (a, c)**  $^{40}\text{Ar}/^{39}\text{Ar}$  laser step-heating age spectra for micas in tectonites from the Gyeonggi Shear Zone (Fig. 3); error bars at  $1\sigma$ , **(b)** inverse isochron ( $^{36}\text{Ar}/^{40}\text{Ar}$  vs.  $^{39}\text{Ar}/^{40}\text{Ar}$ ) for biotite 12JK36; grey ellipses are excluded from isochron regression, (MSWD; Mean Squares of Weighted Deviates). **(d)** Degassing diagram and conventional age spectrum of whole-rock 12JK42, a mylonitic phyllite (Fig. 8d) of the Gimpo Group's basal part on top of the Gyeonggi Shear Zone (lower panel), compared with the corresponding weighted age spectrum (upper panel). **(e)** Density probability diagram with the relative occurrence of apparent ages of all samples from the Gyeonggi Shear Zone and the Gimpo Group's basal part in the area south of Jeongok (Fig. 3). See caption Fig. 9 for details.

### 5.3.9. Gimpo Group

Sample 12JK42 is a foliated and lineated phyllite with isolated shear band boudins and low-angle shear bands (Fig. 8d) from the lowermost part of the Gimpo Group situated directly on the Gyeonggi Shear Zone. Laser step-heating of a single whole-rock fragment provided an age

spectrum with monotonously increasing apparent ages from ca. 140 Ma for low-temperature degassing up to ca. 172.5 Ma at fusion (Fig. 13d).  $^{40}\text{Ar}^*$  degassing kinetics analysis with age spectrum weighting reveals a disturbance related to degassing of a ca. 162–165-Ma-old secondary component (Fig. 13d), possibly formed by partial recrystallization of the first mica generation that was older than about 172.5 Ma. The strong deformation fabric in the phyllites of the Gimpo Group's basal part that yielded the 173–162 Ma  $^{40}\text{Ar}/^{39}\text{Ar}$  whole-rock ages wraps around large K-Fsp crystals, gneiss pebbles and a boulder with an internal shear fabric similar to the one present in the underlying Gyeonggi Shear Zone (Fig. 8c).

Apparent  $^{40}\text{Ar}/^{39}\text{Ar}$  ages for the Gimpo Group and the Gyeonggi Shear Zone form clusters at 181, 173 and 165 Ma in a combined density probability diagram (Fig. 13e). Also, planar and linear fabric elements in the Gimpo Group and the Gyeonggi Shear Zone have a highly similar orientation (Figs. 7b and c); their asymmetry implies top-to-the-North shear in both (Figs. 8b and d). This is likely due to similar tectonism, as will be discussed in section 6.6.

## 6. Interpretation and Discussion

Our  $^{40}\text{Ar}/^{39}\text{Ar}$  dating results and structural data demonstrate that the different litho-tectonic units to the north and west the Gyeonggi Massif experienced a polyphase orogenic evolution lasting at least 35 Myr, comprising mainly correlated episodic deformation and thermal activity in the ca. 255–247 Ma (exclusively in the Yeoncheon Complex, probably Gonam Complex), 245–240 Ma and 225–220 Ma periods, followed by an orogen-wide 194–165 Ma-aged partial rejuvenation event. In this section we develop the concept that the Korean Collision Belt's tectono-metamorphic evolution has taken place in a simple, yet well-constrained, tectonic system with the South China Block subducting beneath the Sino–Korean Craton and southern margin



(Gyeonggi Massif) from the latest Permian to the Late Triassic. This led to accretion into an orogenic wedge of mid-Paleozoic Qinling-derived turbiditic sediments (Taeon Formation, Yeoncheon Complex, Okcheon Zone) deposited along the Sino–Korean Craton’s southern margin, inducing their syn-tectonic Barrovian metamorphism, fast cooling and partial exhumation. Post-collisional reactivation, reworking and step-wise exhumation of the Korean Collision Belt in the Middle to Late Triassic, Jurassic and Cretaceous distorted and strongly modified the original architecture. Moreover, we identified rare Late Carboniferous (Gonam Complex, Hongseong Belt) and Late Devonian (Samgot Unit, Yeoncheon Complex) mineral ages or age components related to the belt’s Late Paleozoic pre-collisional setting.

### **6.1. Late Paleozoic Pre-collisional Setting of the Yeoncheon Complex, Taeon Formation and Hongseong Belt**

Detrital zircon populations in mature quartzites in the Yeoncheon Complex, as well as in the Taeon Formation and the upper Pibanryeong Unit (Okcheon Zone), are strikingly similar to those of the Middle to Late Devonian Liuling, Nanwan and Foziling groups in the Paleozoic Qinling–Tongbai–Hong'an–Dabie Belt ([S.Y. Han et al., 2017](#)). They argued that these Devonian sandstones could have formed the distant equivalent of the similar-aged Korean sedimentary series, which were deposited along the southern margin of the Sino–Korean Craton in the distal part of a deep-water turbidite system. The Liuling, Nanwan and Foziling groups were deposited in basins primarily formed on mid-Neoproterozoic basement of the South Qinling Belt, mainly receiving clastic material from the uplifting and eroding Paleozoic arc of the North Qinling Belt and its early Neoproterozoic substratum bordering the Sino–Korean Craton’s the southern margin ([Dong & Santosh, 2016](#)). Metamorphism of the Devonian basins took place around 270–

250 Ma during initial collision of the South China Block with the southern Qinling–Tongbai–Hong’an–Dabie Belt ([Liu et al., 2015](#)). The comparable timing of metamorphism of the Liuling, Nanwan and Foziling groups and the ca. 255–250 Ma  $^{40}\text{Ar}/^{39}\text{Ar}$  (P)PA’s on mica (this study) and 253–249-Ma-old metamorphic overgrowths on detrital zircon from the Yeoncheon Complex, as well as concordant ca. 277–250 Ma SHRIMP U–Pb ages on detrital and metamorphic zircon in the Taean Formation (Section 3) is striking and reinforces correlations based on detrital zircon characteristics. We identified an approximately 315-Ma-old primary hornblende in an amphibolite from the Gonam Complex, which was partially recrystallized around or after ca. 251 Ma. Blocks in the Weolhyeonri Complex mélange (Hongseong Belt) reveal an important episode of essentially coeval Late Ordovician to Late Devonian (ca. 450–375 Ma) intermediate- to high-grade metamorphism, anatexis and magmatism produced in an arc–fore-arc environment, continuing into the Carboniferous (ca. 330–310 Ma) ([Kee, 2011](#); [S.W. Kim et al., 2006](#); [S.W. Kim, Kwon, Park, Yi, Santosh, & Kim, 2017](#); [Kwon et al., 2013](#); [Oh et al., 2017](#); [S.-I. Park, Kim, Kwon, Thanh, Yi, & Santosh, 2014](#); [S.-I. Park, Kwon, Kim, Yi, & Santosh, 2014](#)). The different litho-tectonic units of the Hongseong Belt furthermore experienced arc-related magmatism between about 900 Ma and 770 Ma, as well as rift-related bi-modal magmatism at ca. 750–740 Ma. The quite similar 920–685 Ma igneous activity in the South Qinling Belt (see, [Dong and Santosh, 2016](#)), in combination with the comparable Ordovician to Carboniferous tectonic evolution, has been used as argument for a links between both belts ([de Jong et al., 2015](#); [S.Y. Han et al., 2017](#); [Kee, 2011](#); [S.W. Kim, Kwon, Park, Yi, Santosh, & Kim, 2017](#); [Kwon et al., 2013](#); [Oh et al., 2017](#); [S.-I. Park, Kim, Kwon, Thanh, Yi, & Santosh, 2014](#); [S.-I. Park, Kwon, Kim, Yi, & Santosh, 2014](#)). The lower mélange-like part of the Yeoncheon Complex (Samgot Unit) contains lenses of an Early Triassic (PA ca. 249 Ma) mylonitic gneiss with an

approximately 372–373-Ma-old granite protolith and ca. 361–371-Ma-old amphibolites (4.1) and amphibolites and gneisses with biotites having 380–365 Ma  $^{40}\text{Ar}/^{39}\text{Ar}$  age components, including a ca. 372 Ma PPA (this study). Moreover, this unit contains mafic rocks with ca. 860-Ma-old basaltic protoliths (4.1). The Yeoncheon Complex, thus, like the Qinling Belt, comprises siliciclastic rocks mainly derived from Neoproterozoic terranes and Paleozoic magmatic arcs (Jingok Unit) with its lower part also containing rocks with a South Qinling-like signature (Samgot Unit). Moreover, the Samgot Unit occurs on a heterogeneous zone above the Gyeonggi Massif that contains variably deformed gneisses with 742–731-Ma-old granitoid protoliths (Gyeonggi Shear Zone). We infer from this that the sedimentary series currently forming the Yeoncheon Complex, Taean Formation and upper Pibanryeong Unit received detritus from earlier accreted Qinling-type terranes along the margin of the Sino–Korean Craton, and were accreted in an orogenic wedge on the Gyeonggi Massif along the craton’s southern margin, experiencing syn-tectonic Barrovian metamorphism during late Paleozoic to early Mesozoic collisional tectonism (Fig. 14 a-d).

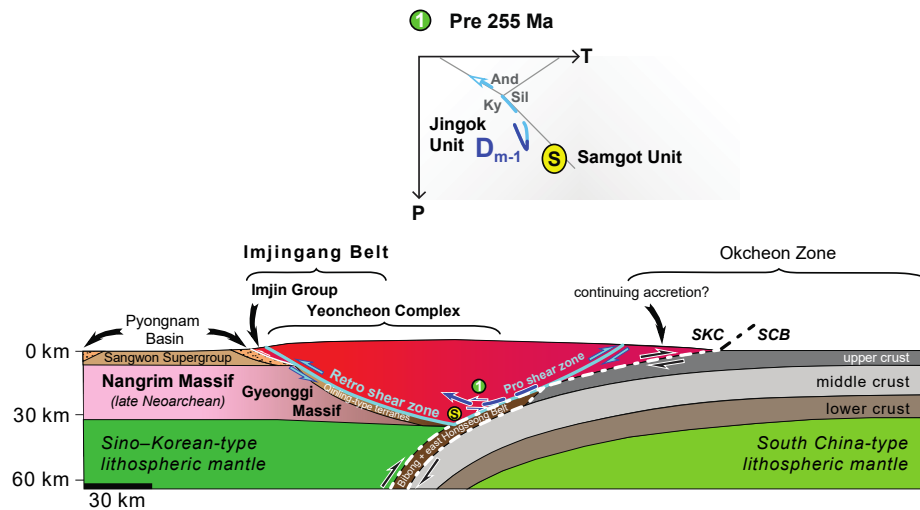
## 6.2. Collisional Architecture and Timing

During continent–continent collision a crustal-scale orogenic wedge forms by the mechanical decoupling of supracrustal units from the subducting plate and their stacking as thrust sheets on the cold and less deformable upper plate (Batt & Braun, 1997; Jamieson et al., 1998; Platt, 1986; Vanderhaeghe, 2012). This relatively rigid continental crust supports the wedge on the hinterland side, forming a backstop – in the Korean Collision Belt the Nangrim Massif (Fig. 14a). Depths of at least 55 km up to about 75 km needed to produce mid-Triassic HP eclogite metamorphism (section 3; Fig. 2) are best explained by subduction beneath a margin

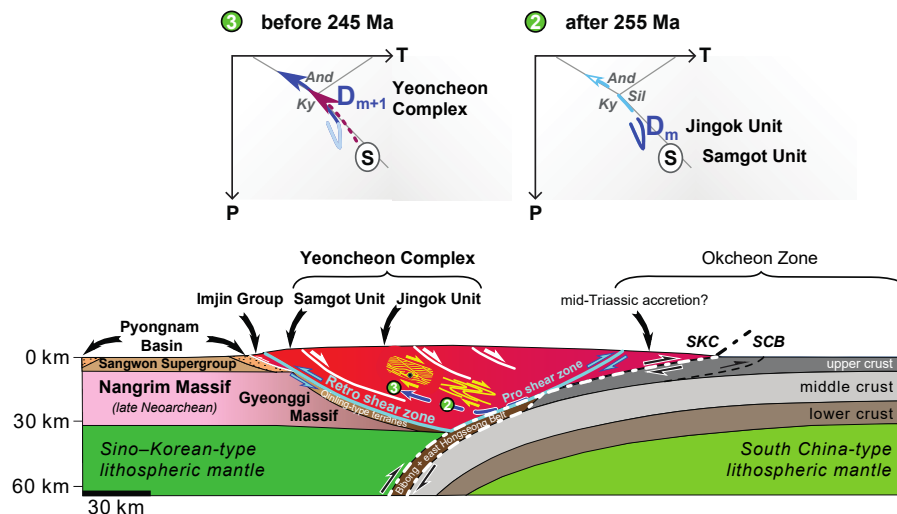
formed by the Nangrim Massif and its southward-thinning wedge-shaped mid-crustal segment forming the Gyeonggi Massif (Fig. 14a). Although subduction polarity cannot be established independently as geodynamic processes did not produce a magmatic arc, the crescent-shaped distribution of intrusions in the overriding plate around the South China promontory of the Late Triassic post-collisional bimodal magmatic suite due to slab break-off and/or lower crust and uppermost mantle delamination (section 3; Fig. 1) matches such a model.

**Figure 14 a-b** (caption: two pages below)

**(a)** Late Permian - Initial collision; Underthrusting; Early exhumation; Top-to-N-shear ( $D_{m-1}$ )

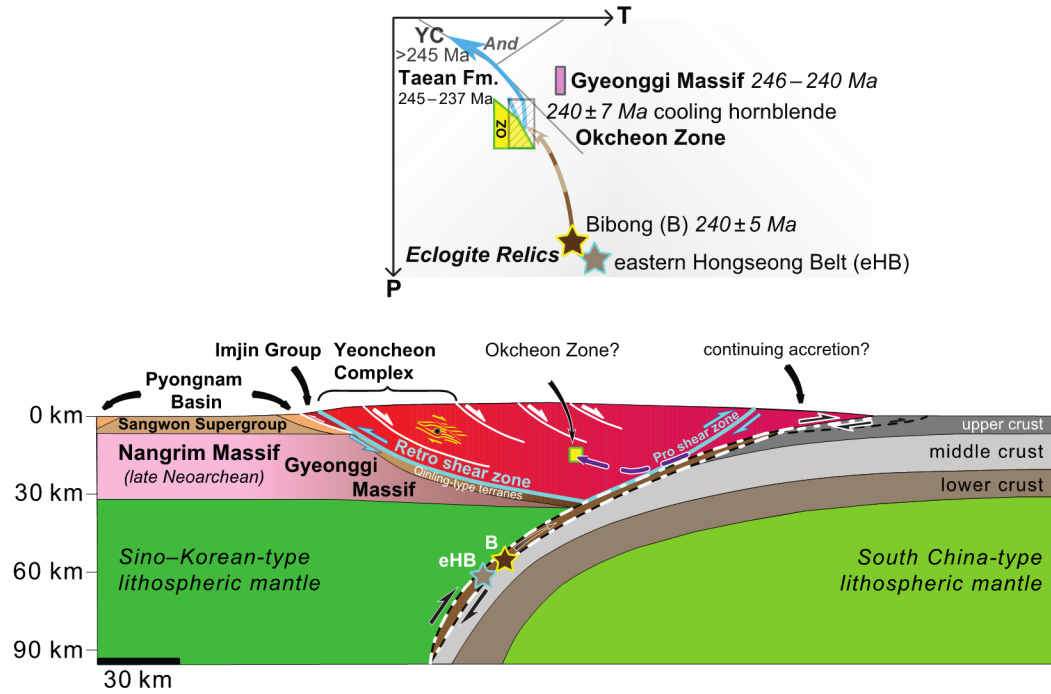
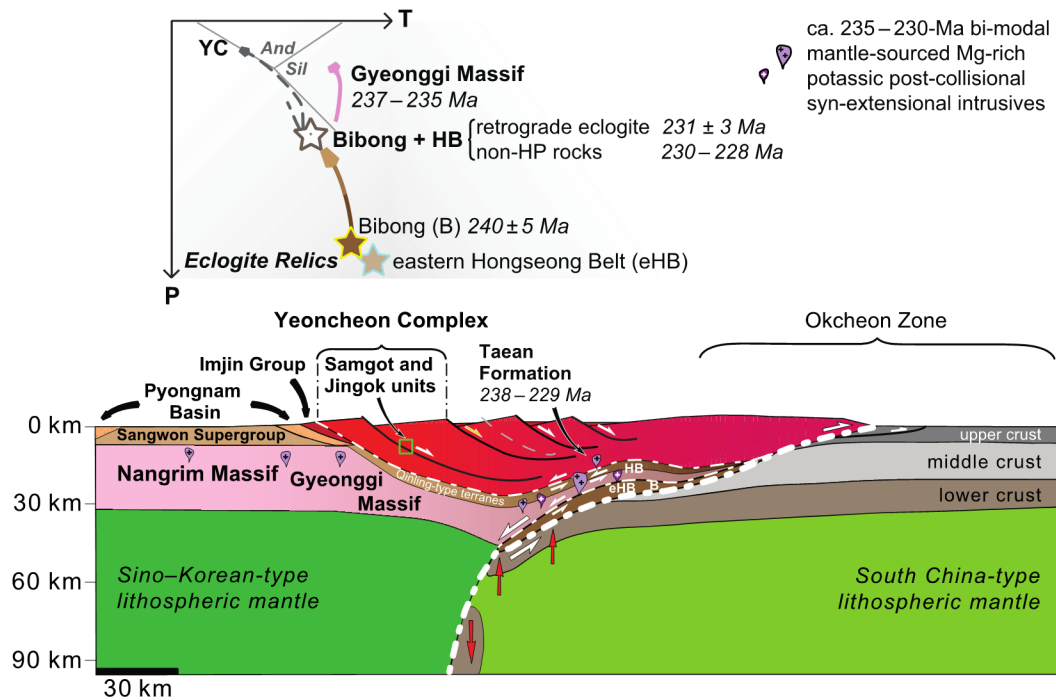


**(b)** latest Permian – Early Triassic - Extension; Exhumation; Top-to-S-shear ( $D_m - D_{m+1}$ )



1265 **Figure 14 c-d** (caption: next page)

(c) Middle Triassic - Resetting Yeoncheon Complex, Tae'an Formation; Exhumation HP rocks

(d) Late Triassic - Slab Detachment; Core Complex; Top-to-N-shear ( $D_{m+2}$ )

1266

1267



**Figure 14** - Cross-sections a-d in the present-day geographic reference frame (NNW, left; SSE, right) illustrating the tectonic evolution of the Korean Collision Belt in the late Paleozoic to early Mesozoic, insert *P-T-t* paths are from [Fig. 2](#) (And, andalusite; Ky, kyanite; Sil, sillimanite). **(a)** Late Permian initial collision and underthrusting of the rocks of the Yeoncheon Complex and Taeon Formation that were incorporated into the tectonic wedge by accretion onto the Gyeonggi Massif and previously accreted Qinling-type terranes leading to top-to-N-shear ( $D_{m-1}$ ) followed by early exhumation; **(b)** Permian–Triassic boundary times, rapid exhumation of rocks in the internal parts of the tectonic wedge; contact of the Jingok and Samgot units formed during top-to-S-shear under extension ( $D_m$ – $D_{m+1}$ ); **(c)** Middle Triassic exhumation of high-pressure metamorphic rocks (Bibong body, eastern Hongseong Belt) induced recrystallization and isotopic resetting (245–240 Ma) in the overlying crustal segments; accretion, deformation and Barrovian metamorphism of the Okcheon Zone may have occurred; **(d)** Late Triassic (240–220 Ma) thermal and magmatic pulse due to slab detachment; core complex formation and doming, top-to-N-shear ( $D_{m+2}$ ) lower part Yeoncheon Complex and upper Gyeonggi Massif. Isotopic ages in italics are from the literature ([Fig. 2](#)). HB, Hongseong Belt; OZ, Okcheon Zone; SCB, South China Block; SKC, Sino–Korean Craton; TF, Taeon Formation; YC, Yeoncheon Complex.

Many of the essential features of the tectono-metamorphic and geochronologic evolution of the Korean Collision Belt and its possible crustal-scale architecture can be recognized in the results of fully coupled thermo-mechanical modeling of small convergent, wedge-shaped, orogenic belts, focusing on the interactions between heat and tectonics (e.g., [Batt & Brown, 1997](#); [Jamieson et al., 1998](#); [Vanderhaeghe, 2012](#)). Such modeling studies revealed that broad regions of the middle crust can attain Barrovian P–T conditions following accretion of rocks enriched in heat-producing radioactive elements (U, Th and K), like granitoids and/or pelites formed by their erosion (like the Taeon Formation, Yeoncheon Complex and Okcheon Zone), present in accretionary wedges or continental margin sequences. In such model orogens these syn-collisional medium P/T conditions are only reached after initial incubation for at least 10–20 Myr following the onset of continental collision. Heating via radioactive decay in accreted crustal rocks in the wedge-shaped prism, hence, ultimately outweighs the initial depression of isotherms

by subduction (e.g., [Vanderhaeghe, 2012](#)). Using the latest Permian to Early Triassic timing for cooling of the main Barrovian tectono-metamorphic phase in the Yeoncheon Complex (present study), this would imply that continental collision in the Korean Peninsula could have started as early as about 275–265 Ma (mid-Permian). Metamorphic overgrowth rims on detrital zircon in meta-sandstones in the Taean Formation (ca. 277–260 Ma; [S.W. Kim, Park, Jang, Kwon, Kim, & Santosh, 2017](#)) and the Gonam Complex ( $262 \pm 3$  Ma; [Kee, 2011](#)), as well as a U–Pb age on garnet in mid-Paleozoic meta-sediments of the Gyeonggi Massif ( $265 \pm 8$  Ma; [Sagong et al., 2003](#)) could record this initial event. This timing is comparable to the estimate of collision using time-lags of about 10–30 Myr between post- or late-collisional delamination of the lower crust and uppermost mantle and/or oceanic slab break-off, and the occurrence of a magmatic and metamorphic pulse around 237–224 Ma ([de Jong et al., 2015](#); section 3). The P–T paths for the Yeoncheon Complex ([Kim & Jung, 2010](#); [B.C. Lee et al., 2019](#)) and the amphibolite-facies Taean Formation ([H.S. Kim et al., 2022](#)) show progressively increasing thermal and baric conditions implying their progressive underthrusting through collision, ultimately leading to peak metamorphism under Barrovian conditions during near isothermal decompression ([Figs. 2 and 14a](#)). Such characteristics agree with modeling results by e.g., [Batt and Braun \(1997\)](#) and [Jamieson et al. \(1998\)](#) who obtained P–T–t paths with an initial moderate increase in pressure and temperature, as material enters the orogen from the pro-side, followed by a rapid isothermal decompression as rocks are swiftly exhumed inside the orogen, and a final almost isobaric short lived ( $<1$  Ma) and very rapid (up to  $500^{\circ}\text{C}/\text{Myr}$ ) cooling as the earth surface is neared. The retro-shear zone is the principal tectonic discontinuity in such compressional model orogens. It has a dip opposite to that of the subduction zone on the orogen’s pro-side, and is situated between the overriding stable plate – in our case containing the Nangrim and Gyeonggi massifs and earlier

accreted Qinling-type terranes – and the orogen (Fig. 14a). Though the original orientation of the  
 main crustal shear zone during the continental collision cannot be established, all previous  
 studies of the Korean Collision Belt adopted the overall northward subduction and  
 underthrusting direction in the Qinling–Tongbai–Hong'an–Dabie–Sulu Belt. Studies by for  
 instance Kwon et al. (2009), B.C. Lee et al. (2019) and Ree et al. (1996) regarded the dominant  
 top-to-the-(E)SE vorticity of structures on northward dipping foliations as pointing to southward  
 overthrusting during continental collision. Such a tectonic regime, however, does not lead the  
 observed strong decompression during the dominant tectono-metamorphic phases  $D_m$  and  $D_{m+1}$ .  
 We observed mesoscopic structures in both the Jingok and Samgot units point to northerly pre-  
 main phase,  $D_{m-1}$  or  $D_m$ , shear. In addition, Jung et al. (2002) established early top-to-the-NE  
 kinematics based on lattice preferred orientation fabrics of quartz grains in straight inclusion  
 trails within interkinematic  $D_{m-1}$ – $D_m$  garnets in the Jingok Unit. The normal grading in quartzites  
 (S.Y. Han et al., 2017) and normal Barrovian zonation show that, overall, the Yeoncheon  
 Complex is not overturned. Collectively, these observations indicate that top-to-the-N shear  
 concomitant with progressive metamorphism during underthrusting (Fig. 14a) occurred before  
 the dominant  $D_m$  and  $D_{m+1}$  top-to-the-(E)SE shear during decompression, partial exhumation and  
 fast cooling (Fig. 14b; next section). In the model orogens (Batt & Braun, 1997; Jamieson et al.,  
 1998) the changes of shear sense and orientation of the main shear plane are associated with the  
 detachment of rocks from the subduction slab and their accretion to the overriding plate at the  
 onset of progressive exhumation and transport along the retro-shear zone (Fig. 14a). These  
 observations can only be reconciled when both major tectono-metamorphic phases occurred on a  
 main S(E)-ward dipping crustal-scale shear zone (Fig. 14a to c). Accretion of the Yeoncheon  
 Complex onto the Gyeonggi Massif (Fig. 14a) agrees with: (1) the occurrence of late stage

metamorphism in the northern Gyeonggi Massif in the Middle Triassic under higher pressure ( $P = 0.6\text{--}0.3$  GPa; Jeong et al., 2021; Lee & Cho 2003; Yi & Cho 2009), and (2) far higher metamorphic pressures experienced by ca. 229-Ma-old post-collisional granulites in the Gyeonggi Massif (section 3) compared to the ca. 253–250-Ma-old post-main phase andalusite-bearing quartz veins in the already partly exhumed Yeoncheon Complex (Figs. 2 and 14d).

### 6.3. Late Permian to Early Triassic Tectonism and Exhumation of the Yeoncheon Complex

The present study in combination with a literature review earlier in this paper (section 3) shows that a number of the litho-tectonic units in the Korean Collision Belt experienced metamorphism in Late Permian to Early Triassic time: (1) the Yeoncheon Complex (255–247-Ma-old main tectono-metamorphic phase), (2) the Taean Formation (252–251 Ma), (3) the Gonam Complex of the western Hongseong Belt (ca. 251-Ma-old secondary amphibole component; 262–251-Ma-old metamorphic rims of detrital zircon), and (4) metasediments and metabasites in the Gyeonggi Massif (ca. 265–247 Ma). Because the eclogite-facies metamorphism in the Korean Collision Belt took place in the mid-Triassic (section 3) these latest Permian to Early Triassic isotopic ages refer to an early tectonic phase. Interestingly, also the metamorphism of the probable lateral equivalents of the Yeoncheon Complex and Taean Formation in the Qinling–Tongbai–Hong’an–Dabie Belt took place around 270–250 Ma during the initial collisional stages, well before the 245–215-Ma-aged HP–UHP events in the belt (Liu et al., 2015; Wu & Zheng, 2013).

Principal staurolite and kyanite porphyroblastesis in the Jingok Unit occurred concomitant with near isothermal decompression after the metamorphic peak (M. Cho et al., 2007; Kim & Jung, 2010), following  $D_m$  and during the early stages of  $D_{m+1}$ . The occurrence of

andalusite in syn-metamorphic quartz veins in kyanite–mica schists demonstrates decompression to at least aluminosilicate triple point pressures (Fig. 2); rare kyanite-bearing veins probably record earlier stages. This implies that veining and flow of large amounts of fluids took place during partial exhumation to a depth of at least about 12.5 km concomitant with extension. The similar range of  $^{40}\text{Ar}/^{39}\text{Ar}$  (P)PAs (ca. 255–250 Ma) for muscovite and biotite in rocks with the  $D_m$  and  $D_{m+1}$  fabrics in all mineral zones, as well as the comparable ages of muscovite from the main tectono-metamorphic foliation (ca. 251–250 Ma) and from the texturally late quartz veins (ca. 253–250 Ma) implies very fast cooling in the latest Permian to Early Triassic after or in the waning stages of  $D_{m+1}$ . The ca. 255 Ma CHIME monazite age (kyanite zone) (D.L. Cho et al., 1996) corroborates fast cooling, but cannot be used to constrain a cooling rate due to the fairly large error of about 3%. In the Samgot Unit the asymmetry of the deformation structures deflecting the main foliation  $S_m$  usually also indicates top-to-the-SSE shear, which we correlate with  $D_{m+1}$  in the Jingok Unit showing the same kinematics. Yet, ca. 249–247 Ma hornblende  $^{40}\text{Ar}/^{39}\text{Ar}$  (P)PAs, in part from rocks with pervasive top-to-the-SSE shear, show that cooling of the Samgot Unit occurred significantly later than that of the overlying Jingok Unit. A slower cooling is suggested by the age difference between these hornblendes and ca. 253–249-Ma-old zircon overgrowth rims (errors: 1–3 Ma), interpreted as dating the metamorphic peak in this unit (section 3). It may suggest that when metamorphism in the Samgot Unit peaked, the Jingok Unit had already started to cool, and thus being tectonically exhumed. The difference of a about 2 to 7 million years in the timing of cooling following the main tectono-metamorphic events in both units and the jump in maximum metamorphic pressures and temperatures between the higher grade Samgot Unit and the Jingok Unit point to their separation by a low-angle ductile normal fault. Final fast cooling subsequent to the Barrovian metamorphism in the Jingok Unit may, thus,

have been driven by tectonic exhumation during and after  $D_{m+1}$ , also juxtaposing it with the Samgot Unit (Fig. 14a and b). In the Scottish type locality of the Barrovian metamorphism [Viète et al. \(2011\)](#) established that  $^{40}\text{Ar}/^{39}\text{Ar}$  plateau ages in the sillimanite zone are about 5 million years younger than in the biotite zone. Sillimanite zone mineral assemblages were never found in the Yeoncheon Complex. This may mean that rocks with these higher-grade assemblages could have been excised by ductile normal faulting, although such a high-metamorphic conditions may very well never have been attained. It appears from modeling studies that mineral assemblages of the sillimanite zone only form if collisional orogeny is accompanied by advective heating by syn-tectonic magmatism (e.g., [Vorhies & Ague, 2011](#), and references therein), which has never been described from the Korean Collision Belt. Yet, the widespread occurrence of such syn-metamorphic veins in the Yeoncheon Complex could be related to higher thermal conditions and possibly magmatism at deeper levels. Extensive syn-metamorphic aluminosilicate-bearing quartz vein systems are, regularly observed in amphibolite-facies rocks, reflecting fluid mobilization, and possibly advective heat transport, near peak thermal conditions when devolatilization reaches a maximum, generating substantial fluid overpressure and hydro-fracturing in the ductile regime (e.g., [Allaz et al., 2005](#); [Lancaster et al., 2008](#); [Whitney & Dilek, 2000](#)).

The reconstructed switch from a northerly shear during underthrusting to an opposite direction during extension, decompression, partial exhumation and fast cooling of the Jingok and Samgot units, and their juxtaposition, relates to the dynamics of accretionary wedges formed at convergent margins (Fig. 14a and b). Crustal rocks carried down under an orogenic wedge will accrete to its base, tending to thicken it and increase its surface slope, which is compensated by internal thinning and extension by ductile low-angle listric normal faulting with a top-to-foreland sense of movement, which may pass into zones of distributed shear (e.g., [Platt, 1986](#)).



Occurrence of highly attenuated  $D_m$  folds shows that foliations were once located in the compressional sector of the flow field probably during underplating and initial accretion. Their overprinting by extensional fabrics and ductile normal faults during and after the  $D_{m+1}$  exhumation during top-to-the-(S)SE shear (Fig. 14b) in all mineral zones of the Jingok Unit, also affecting late stage discordant in part aluminosilicate-bearing quartz veins, and in the Samgot Unit at least during  $D_{m+1}$  agrees with this mechanism. Barrovian metamorphism in the Scottish Highlands similarly took place after early large-scale folding and concomitant with large-scale extension by mid-crustal ductile shear zones with kinematics opposite to that of the subduction direction (Viete et al., 2011, and references therein). The local conjugate and occasional opposite shear may point to a deformation regime characterized by heterogeneous general non-coaxial, or sub-simple, shear, with components of both simple and pure shear. The vertical thinning and lateral extension of a wedge may induce the observed component of coaxial deformation during the exhumation and extrusion of the Yeoncheon Complex. Sub-simple shear, with multiple reversals of ductile shear direction under Barrovian-type metamorphic conditions, also occurs in the High Himalayan Crystalline Series - when it was extruded between normal (top) and thrust (bottom) fault systems (Harris, 2007) - and in the Paleoproterozoic Lapland–Kola Orogen of the northern Fennoscandian Shield (Mudruk et al., 2022).

Isoclinal folding and formation of a transposition foliation in the amphibolite-facies metamorphic Taean Formation on the islets of Gukhwa and Ippa (sections 2, 3, and 5.3.6) took place under peak conditions (0.9–1.1 GPa at 600–620°C) that are strikingly similar to those of the Yeoncheon Complex (H.S. Kim et al., 2022). The P–T–t path constrained by ca. 252–251 Ma U–Pb zircon ages is also comparable (Fig. 2). The two phases of folding and formation of associated cleavages in the lower-grade metamorphic Taean Formation on the islands of

Anmyeon and Yeongheung are probably also related the earliest Triassic tectono-metamorphic phase, for two reasons. Firstly, mafic dykes and associated ca. 230-Ma-old syenites truncate these contractional structures (sections 3, 4.2), and secondly, the mid-Triassic ages obtained in the present and earlier studies are related to a regional phase of resetting (next section). Accretion of the Taean Formation and exhumation in the orogenic wedge, thus, occurred broadly in the same way as for the Yeoncheon Complex (Fig. 14a and b).

#### 6.4. Middle Triassic Tectono-Thermal Events and Initial Exhumation of the Gyeonggi Massif

The 245–237 Ma  $^{40}\text{Ar}/^{39}\text{Ar}$  muscovite ages in the Taean Formation are virtually identical to the ca. 242–237 Ma ages in the Yeoncheon Complex that result from a second event that partially or completely reset the K–Ar isotopic system in whole-rock (garnet zone), biotite and muscovite (staurolite and kyanite zones). Highly deformed platy meta-sediments in the mélange zone along the northern margin of the Gyeonggi Massif and tectonically situated below the Samgot Unit, similarly yielded muscovite with ca. 243 and 240 Ma PPAs (de Jong & Ruffet 2014b; de Jong et al., 2015). Mid-Triassic isotopic ages are also recorded in the Paleoproterozoic Hwacheon Granulite Complex, about 100 km to the ENE in the northern Gyeonggi Massif (Fig. 1), which experienced localized late-stage metamorphism ( $P = 0.4\text{--}0.6$  GPa,  $T = \text{ca. } 750^\circ\text{C}$ ; Lee & Cho 2003; Yi & Cho 2009). CHIME monazite ages in mylonitized granulites ( $255 \pm 14$  and  $241.4 \pm 7.8$  Ma) and paragneisses of its Marginal Zone Gneiss Complex ( $245.3 \pm 5.5$  and  $245 \pm 3$  Ma) are concordant (D.L. Cho et al., 1996; Suzuki, 2009). Gneiss in the central Gyeonggi Massif yielded a zircon with a concordant rim age of  $246 \pm 4$  Ma (B.C. Lee et al., 2014), probably dating intermediate-P/T metamorphism (Yengkhom et al., 2014). The mid-Triassic  $^{40}\text{Ar}/^{39}\text{Ar}$

ages we obtained are neither linked to specific structures in the rocks, nor to a characteristic type of metamorphism. We argue that eclogite-facies metamorphism in some rocks associated with the eastern Hongseong Belt (sections 2 and 3) occurred during their subduction below the wedge-shaped mid-crustal segment constituting the Gyeonggi Massif and the Nangrim Massif (6.2; [Fig. 14b](#) and [c](#)). Apparently, subduction causing the eclogite-facies metamorphism and/or the incipient exhumation of the HP metamorphic rocks around about 240 Ma induced strong mid-crustal tectono-metamorphic reworking of the overriding plate (Gyeonggi Massif, Yeoncheon Complex and Taean Formation) that was actively exhumed in the 245–240 Ma time slice ([Fig. 14c](#)).

## **6.5. Late Triassic Tectono-Thermal Events and Advanced Exhumation of the Gyeonggi Massif**

225–221 Ma  $^{40}\text{Ar}/^{39}\text{Ar}$  ages and age components reveal complete and partial resetting of biotite and muscovite, respectively, in parts of the kyanite and staurolite zones affected by strong chloritization and retrogression of the Barrovian mineralogy or ductile top-to-the-(N)NW  $D_{m+2}$  shear. A similar late-stage ductile shear has been observed in some of the fine-grained, low-grade mylonites associated with near layer-parallel cataclasite in the kyanite zone, as well as in garnet-free meta-calc-silicate mylonites in the lowermost Samgot Unit. Titanite from amphibolites affected by retrogression in the unit yielded U–Pb ages of ca. 229 and 214 Ma (errors 13–16%) ([B.C. Lee et al., 2019](#)). Muscovite in mylonitic quartzite below the Samgot Unit along the northern margin of the Gyeonggi Massif yielded a  $^{40}\text{Ar}/^{39}\text{Ar}$  plateau age of  $219.7 \pm 0.9$  Ma ([de Jong & Ruffet 2014b](#); [de Jong et al., 2015](#)), which is identical to the hornblende plateau age of  $219.9 \pm 0.6$  Ma from a strongly deformed amphibolite in the Gonam Complex in the Hongseong

Belt. This implies that the D<sub>3</sub> mylonitic fabrics in the latter complex with an overall top-to-the-NNE sense of shear and the top-to-the-(N)NW D<sub>m+2</sub> shear in the Yeoncheon Complex can be correlated and are both of Late Triassic age. This would agree with the estimated timing of the movement on the Gyeonggi Shear Zone by [J.N. Kim et al. \(2000\)](#) based on a  $226 \pm 1$  Ma Rb–Sr mineral–whole-rock isochron age, which they regarded as dating top-to-the-N extensional shear. Because the shear zone was strongly reactivated in the Jurassic (next section), we regard the Late Triassic isotopic age as probably representing the early original translation phase. Furthermore, SHRIMP dating of recrystallized monazite in amphibolite-facies mylonitic schist in the ductile shear zone separating the Hwacheon Granulite Complex from its Marginal Zone Gneiss Complex gave U–Th–Pb ages of 224–223 Ma ( $2\sigma$  errors 1–1.5%; [Yi, 2010](#)), although the author did not establish its shear sense. A zircon from Paleoproterozoic gneiss in the central Gyeonggi Massif gave a lower discordant intercept age of  $226 \pm 7$  Ma, which may relate to NNE-ward translation along ductile shear zones ([Yengkhom et al., 2014](#)). This age is concordant with a weighted mean U–Pb age of  $224 \pm 14$  Ma on titanite from the Chuncheon amphibolite in the central Gyeonggi Massif ([J.M. Kim et al., 2008](#)). This may imply that many of the currently exposed contacts between the different litho-tectonic packages have a Late Triassic displacement component. [de Jong et al. \(2015\)](#) argued that all rocks along the northern margin of the Gyeonggi Massif, including the Gyeonggi Shear Zone, acquired a northern dip during its transformation into a metamorphic core complex in the early Late Triassic (section 3; [Fig. 14d](#)). North-directed kinematics in (ultra) mylonites could, thus, refer a Late Triassic phase of extensional tectonism and core complex formation of the Gyeonggi Massif during its advanced partial exhumation. It is probably not fortuitous that the timing of this northward ductile extensional shearing event in the northern Korean Collision Belt agrees with ca. 219 Ma ages in the Okcheon Zone for muscovite

(Rb–Sr, [Cliff et al., 1985](#)) and A-type alkali granite ([Williams et al., 2009](#)) manifesting the youngest post-collisional extension-related magmatism.

## 6.6. Jurassic Fluid Flow, Tectonism and Final Early Cretaceous Exhumation

Following the major Late Permian to Late Triassic orogenic activity, the Korean Peninsula's crust has been affected by non-collisional tectonism in the Early Jurassic to Early Cretaceous (Daebo Orogeny) (e.g., [Chough, 2013](#); [S.I. Park et al., 2019](#)). The Daebo Orogeny comprises an Early–Middle Jurassic magmatic phase in a continental arc setting linked to subduction of Paleo-Pacific oceanic lithosphere below East Asia, followed by a Late Jurassic to Early Cretaceous non-magmatic tectonic phase ([S.I. Park et al., 2019](#)). The magmatic stage is characterized by widespread intrusion of granitoids, forming coalesced Cordilleran-type batholiths ([Fig. 1](#)), volcanism, formation of sedimentary basins providing depocenters for the Daedong Supergroup, as well as strike-slip deformation that mainly affected the southern Okcheon Zone and the Yeongnam Massif (namely, Honam Shear Zone System; [Fig. 1](#)) ([Egawa, 2013](#); [Jeong, Cheong, Park, & Shin, 2008](#); [S.W. Kim et al., 2009](#); [H.-j. Lee et al., 2021](#); [Lim & Cho, 2012](#); [K.H. Park et al., 2010](#); [Sagong et al., 2005](#)). Contraction during the non-magmatic late stage of the Daebo Orogeny ended deposition of the Daedong Supergroup, leading to reactivation of preexisting structures and basin inversion, folding, imbrication and uplift of these sediments in the ca. 160–110 Ma period ([Egawa, 2013](#); [H.-j. Lee et al., 2021](#); [Lim & Cho, 2012](#); [S.I. Park et al., 2019](#)).

A significant number of micas yielded Early–Middle Jurassic  $^{40}\text{Ar}/^{39}\text{Ar}$  ages (biotite, PPA ca. 183 Ma, Jingok Unit; muscovite and biotite PAs 183–170 Ma, Taean Formation; biotite, PA ca. 194 Ma, muscovite age components of 200 Ma and 189 Ma, Gonam Complex). The

1526 emplacement of 195–160-Ma-aged granites at depths between 28 and 12 km (Cho & Kwon,  
1527 1994; K.H. Park et al., 2010; Sagong et al., 2005) coincides with these mica ages. Micas with  
1528 200–189 Ma ages and age components in the Gonam Complex occur at 1–2 km from a late Early  
1529 Jurassic granite (Fig. 6). But, the nearest Jurassic intrusives are over 10 km away from the  
1530 sample sites in the Taean Formation and the Yeoncheon Complex (Figs. 3 and 6). Therefore, it  
1531 unlikely that intruding granites induced simple (partial) thermal resetting of the K–Ar isotopic  
1532 system by contact metamorphism. It is well-documented that partial or complete resetting of  
1533 radiogenic isotopic systems of muscovite below their conventional blocking temperatures may  
1534 occur by progressive chemical recrystallization by fairly low-temperature magmatic and  
1535 meteoric fluids in the middle and upper crust rather than by thermal overprinting (e.g., de Jong et  
1536 al., 1992; Alexandrov et al., 2002; Tartèse et al., 2011). The Taean Formation's meta-sandstone  
1537 12JK64 (PA: 183 Ma) has randomly oriented muscovite grains on the bedding plane, implying  
1538 new mica growth during the Jurassic. Two meta-sandstones sampled from the same outcrop at  
1539 300 m from a ca. 177-Ma-old leucocratic dike that lacks a thermal aureole in the country rocks  
1540 also contain newly formed muscovite along the bedding with an age of about 177.5 Ma, whereas  
1541 texturally older fabric-forming white mica in one of the samples is about 231 Ma old (de Jong et  
1542 al., 2014). Similarly, processes leading to the formation of a ca. 170-Ma-old biotite in the Taean  
1543 Formation did not affect the muscovite grain with significant apparent ages between ca. 241 and  
1544 232 Ma in the same outcrop. Apparently, new growth of Jurassic mica did not lead to partial or  
1545 complete resetting of already existing muscovite. This suggests that hydrothermal processes in  
1546 the Early to Middle Jurassic might be responsible for growth of new mica with or without fluid-  
1547 assisted resetting of preexisting muscovite by recrystallization.



Also, tectonic recrystallization of muscovite and biotite has resulted in Early–Middle Jurassic ages. The combined density probability diagram displaying the relative occurrence of apparent  $^{40}\text{Ar}/^{39}\text{Ar}$  ages we obtained on tectonites from the Gyeonggi Shear Zone and a low-grade metamorphic mylonitic phyllite from the basal of the Gimpo Group directly above it reveals coinciding clusters at 181, 173 and 165 Ma (Fig. 13e). Moreover, the matching orientations of foliation, lineation (Figs. 7b and c) and shear sense (Figs. 8b and d) shown by deformation structures in the contact zone between both point to a linked tectonic activity. J.N. Kim et al. (2000) considered the Gimpo Group as being deposited unconformably on the Gyeonggi Shear Zone after its Late Triassic activity. However, this original unconformity clearly has been reactivated in the Middle Jurassic. This is indicated by the occurrence of clasts of gneiss with a fabric similar to the gneissosity of the underlying Gyeonggi Shear Zone that are wrapped by the strong deformation fabric of the phyllites (Fig. 8c) that yielded the 173–162 Ma  $^{40}\text{Ar}/^{39}\text{Ar}$  whole-rock ages. The downward intensification of metamorphism and deformation in the Gimpo Group's lowermost part is thus a mid-Jurassic tectonic feature and not due to fluid-assisted recrystallization and/or new growth intrinsically linked to regional granitic magmatism. It does imply that the gneiss substratum of the sediments was still at an elevated temperature. Although kinematic and isotopic age constraints are lacking, comparable observations from the Daedong Supergroup elsewhere (de Jong, personal observation, 2013; Egawa, 2013; Lim & Cho, 2012) point to a regionally coherent tectonic and thermal regime. Therefore, our dating results imply that the latest shearing activity of the Gyeonggi Shear Zone occurred around 165 Ma. If the age of ca. 181 Ma for the primary muscovite component also characterizes a period of dynamic recrystallization during displacement on the ductile shear zone, these results indicate that its activity was discontinuous over a period that lasted at least 16 Myr. In this case the

apparent ages of about 177 Ma for the sidewalls in the age spectrum for muscovite 12JK35-a, (Fig. 13a) could relate to an intermediate shearing episode. As the original Gyeonggi Shear Zone was most likely formed around about 226 Ma (J.N. Kim et al., 2000), its Jurassic activity between about 181 Ma and 165 Ma occurred during reactivation too, in agreement with the occurrence of late-stage shear bands superimposed on the earlier mylonite foliation (Fig. 8b).

A ductile normal shear zone with top-to-the-South kinematics along the southern boundary of the Gyeonggi Massif yielded a ca. 188-Ma-old syn-tectonic muscovite from a mylonite (R. Han et al., 2014). These authors argued this Early Jurassic deformation with opposite kinematics to the ca. 226-Ma-old Gyeonggi Shear Zone was a late increment in the exhumation of the Gyeonggi Massif, which they viewed, hence, as a slow and prolonged tectonic process. Our current much younger age estimate of the shear zone's reactivation and final ductile movement implies that this probably is not the case, and instead points to a polyphase tectonic history of brief and rapid phases. Therefore, the 188 and 181 Ma  $^{40}\text{Ar}/^{39}\text{Ar}$  mica ages date the Early Jurassic phase of the Gyeonggi Massif's stepwise exhumation history, superimposed on an earlier Late Triassic phase. Contrasting K–Ar muscovite and biotite ages in the westernmost Gyeonggi Massif (182–154 Ma) and in the adjacent Hongseong Belt (198–220 Ma) (Kee, 2011) also imply Jurassic cooling linked to exhumation of the massif and, thus, probably a reactivation of the original tectonic contact between them. The 181–162 Ma  $^{40}\text{Ar}/^{39}\text{Ar}$  ages from the base of the Gimpo Group and the Gyeonggi Shear Zone compare well with U–Pb age constraints on the timing of the main right-lateral ductile strike-slip movement on the intra-arc Honam Shear Zone System (Fig. 1) in the 179–171 Ma period, possibly continuing to or reactivated around ca. 166 Ma (Jeong, Cheong, Park, & Shin, 2008; S.W. Kim et al., 2009, and references therein). The

Early–Middle Jurassic deformation, thus, seems to have occurred in similarly timed phases on the scale of the orogen.

The sharply downward increasing intensity of metamorphism and ductile deformation in the lowermost Gimpo Group has bearing on its depositional age and the nature of the ductile shear zone separating these low-grade metasediments from their substratum. The ca. 172.5 Ma minimum age of the first mica generation of the fabric wrapping the gneiss boulder with the Late Triassic fabric and sandstones with 229–219-Ma-old detrital zircons ([H.-j. Lee et al., 2021](#)) and 231–229-Ma-old detrital grains of intergrown muscovite–biotite ([de Jong et al., 2015](#)) constrain the sedimentation age of Gimpo Group’s basal part as Late Triassic to early Middle Jurassic. In other syntectonic subbasins farther South the age of the Daedong Supergroup’s stratigraphic upper levels is well constrained by the occurrence of 187–172-Ma-old tuffs and tuffaceous rocks ([H.-j. Lee et al., 2021](#); and references therein). Consequently, the early Middle Jurassic age estimate of the fabric-forming first generation mica in the Gimpo Group is at the upper end of the timing of sedimentation of the Daedong Supergroup. Although the Gimpo Group’s uppermost formation has not yielded Jurassic detrital zircons, the higher parts of the Daedong Supergroup elsewhere have a youngest ca. 164-Ma-old detrital zircon population and individual zircons as young as ca. 158 Ma ([H.-j. Lee et al., 2021](#); and references therein). The latter are, thus, younger than the deformation and metamorphism in the basal parts of the Gimpo Group linked to movement along the Gyeonggi Shear Zone. The most straightforward interpretation is that this tectono-metamorphic activity occurred while sedimentation at higher levels continued. This would imply that reactivation of the Gyeonggi Shear Zone occurred as a basin-forming extensional event, in relation to an exhumation increment of the Gyeonggi Massif. The metamorphic gradient in the basal part of the Gimpo Group shows that the temperatures in the

shear zone and the underlying massif were still elevated around the Early to Middle Jurassic boundary. Consequently, the ductile shear zone and the Gyeonggi Massif both cooled during the exhumation process. This is one of the reasons for the lack of  $^{40}\text{Ar}/^{39}\text{Ar}$  mineral ages younger than the Middle Jurassic in our regional study (Fig. 10).

Absence in sediments of the Gimpo Group of lithic fragments and detrital grains of medium-grade metamorphic minerals like staurolite, kyanite and garnet, attributable to erosion of the Yeoncheon Complex and deeper parts of the Taean Formation, shows that in Early–Middle Jurassic time erosion had not yet reached the medium P/T metamorphic deeper part of the Permian–Triassic Korean Collision Belt. This is supported by an apparent similar absence of detritus from the medium-grade metamorphic rocks in the Daedong Supergroup's basal conglomerate in North Korea (D.C. Lee et al., 2017). The widespread occurrence of Early–Middle Jurassic  $^{40}\text{Ar}/^{39}\text{Ar}$  ages in the metamorphic rocks we studied indeed also clearly demonstrates that deeper parts of the Korean Collision Belt were still subjected to magmatic and metamorphic processes and thus not exhumed or subjected to erosion at that time. This is supported by the observation that Late Triassic zircons account for just 2% of the detrital population of sandstones of the Gimpo Group (H.-j. Lee et al., 2021). The 231–229-Ma-old detrital grains of metamorphic intergrown muscovite–biotite in the Gimpo Group's sandstones (de Jong et al., 2015) could be due to erosion of lower-grade metamorphic upper levels of the tectonic wedge, like the Taean Formation. In stark contrast to the Daedong Supergroup, however, latest Early Cretaceous conglomerates, sandstones, volcanoclastic sediments and volcanic rocks, including 113–110-Ma-old calc-alkaline tuffs and basalts, that overlie the Yeoncheon Complex, Gonam Complex and Taean Formation (Figs. 1, 3, 6; Kee, 2011) contain the first clear influx of coarse sub-angular to sub-rounded detritus of their substratum. Our

reconnaissance studies showed that these locally slump-folded rocks have an ill-defined, sometimes chaotic layering with randomly oriented, pebbles and cobbles of laminated quartzite, (garnet–) mica schist and rare serpentinite, in addition to fragments of feldspar and other volcanic material. Final exhumation and deep erosion of the Korean Collision Belt did, thus, not occur before the latest Early Cretaceous, probably related to the non-collisional Bulguksa Orogeny.

## 7. Conclusions

Combined  $^{40}\text{Ar}/^{39}\text{Ar}$  single-grain geochronology and structural geological analysis of the northern Korean Collision Belt's main litho-tectonic units implies that the mid-Paleozoic sediments (Yeoncheon Complex and its equivalent the Taean Formation) along the Sino–Korean Craton's southern margin (Nangrim Massif) accreted in a tectonic wedge on its southern extension (Gyeonggi Massif). Peaks in density probability diagrams of apparent ages coincide with (pseudo-)plateau ages ((P)PAs), defining three discrete age groups: 255–247 Ma (Yeoncheon Complex, one case in the Gonam Complex, Hongseong Belt), 245–237 Ma and 225–220 Ma. These reflect distinct, correlated tectonic episodes of rapid cooling and partial exhumation following syntectonic Barrovian metamorphism in Permian–Triassic boundary time and subsequent recrystallization and retrogression in the Middle and Late Triassic during continuing exhumation. The finding of biotites with a ca. 372 Ma PPA and main age components in the 380–365 Ma range (Samgot Unit, Yeoncheon Complex), and of a ca. 315-Ma-old primary hornblende (Gonam Complex) shows that parts of the Korean Collision Belt experienced Paleozoic tectono-metamorphic and magmatic processes before the Permian–Triassic main orogeny. This may point to the presence of earlier accreted Qinling-like terrane(s).

The three Barrovian mineral zones of the Yeoncheon Complex' tectonically upper Jingok Unit all yielded tightly clustered mica cooling ages regardless of the sample having a plano-linear tectono-metamorphic main fabric  $S_m$ , a superimposed shear band fabric  $S_{m+1}$ , or containing variably deformed, in part andalusite-bearing quartz veins cross cutting both foliations. The (near) concordance of all mica (P)PAs ( $255.2\text{--}249.9 \pm 0.4\text{--}0.9$  Ma,  $1\sigma$ ) points to final fast cooling concomitant with or following the quartz veining during exhumation from around 30 km to at least 12.5 km. The concordant hornblende (P)PAs ( $248.8\text{--}247.0 \pm 0.6\text{--}1.6$  Ma,  $1\sigma$ ) in the underlying higher-grade metamorphic, deeper underthrust Samgot Unit are significantly younger. Hence, the deeper underthrust Samgot Unit cooled later than the overlying Jingok Unit and was exhumed along the low-angle extensional ductile shear zone separating them.  $S_m$  and  $S_{m+1}$  in the Yeoncheon Complex were formed during heterogeneous non-coaxial shear with a principal top-to-the-(S)SE component. Fast cooling and decompression around the Permian–Triassic boundary were initiated by (S)SE-ward exhumation along low-angle ductile normal faults in a southward tapering tectonic wedge. Resetting of biotite (completely) and muscovite (partly) in the Jingok Unit resulted in complex staircase- and saddle-shaped age spectra, and increased structurally downwards in tandem with increasing retrogression during two successive events around 242–237 Ma and 225–221 Ma, only the latter linked to overprinting of  $S_m$  and  $S_{m+1}$  by top-to-the-north  $D_{m+2}$  shearing. Ductile shear with a similar sense dominates in the Samgot Unit's retrograde lowermost part and in the underlying highly deformed and strongly retrogressed *mélange*-like shear zone on top of the Gyeonggi Massif that contains muscovite with ca. 243, 240 and 220 Ma (P)PAs. A mylonitic amphibolite in the Gonam Complex with principal top-to-the-north kinematics yielded a hornblende with a PA of  $219.9 \pm 0.6$  Ma ( $1\sigma$ ). Also, the Taean Formation's greenschist facies metamorphic part yielded complicated in part



saddle-shaped age spectra pointing to a 245–240-Ma-old component subsequently partially recrystallized around about 232 Ma during the core complex-related main metamorphism and/or at ca. 222–220 Ma. The oldest age component we found is virtually as old as the mid-Triassic second event in the Yeoncheon Complex. Because the Yeoncheon Complex, Taean Formation and Gyeonggi Massif were situated in the overriding plate, formation of the HP-metamorphic rocks by subduction/underthrusting beneath the Sino–Korean Craton and/or their incipient exhumation in mid-Triassic time could have induced the observed strong tectono-metamorphic reworking at higher crustal level. A change from a southern to a northern dip of the tectonic foliations in the Yeoncheon Complex was due to the transformation of the underlying Gyeonggi Massif into a core complex around 237–224 Ma following mantle delamination and/or slab break-off. Late Triassic top-to-the-north ductile extensional shear during advanced retrogression could also relate to the final phase of core complex formation.

The widespread occurrence in all litho-tectonic units of biotite and muscovite with (P)PAs in the 194–170 Ma range reflects their fluid-assisted recrystallization and new growth during the Early–Middle Jurassic episode of regional granitic magmatism. Ductile top-to-the-north shear induced mid-Jurassic partial recrystallization of biotite and muscovite in (ultra) mylonites during reactivation of the original Late Triassic Gyeonggi Shear Zone (180–165 Ma PAs and age components) and in the low-grade metamorphic mylonitic basal part of the Jurassic post-collisional sedimentary Gimpo Group directly on the shear zone (173–163 Ma age components). This Jurassic basin-forming extensional event provided depocenters for sediments of the Gimpo Group and induced the second major exhumation phase of the Gyeonggi Massif. Final exhumation and deep erosion of the Korean Collision Belt occurred not earlier than the

latest Early Cretaceous implied by the omnipresence of detritus of medium-grade metamorphic rocks of the substratum.

### **Data Availability Statement**

The Supporting Information data can be found at:

<https://data.mendeley.com/datasets/x2x5h8p6wj/1>

### **Acknowledgments**

KdJ acknowledges support from the Basic Science Research Program through the National Research Foundation of Korea (NRF) funded by the Ministry of Education [NRF-2011-0012900], as well as subsequent grants from Seoul National University's Research Institute of Basic Sciences and the College of Natural Sciences during different stages of the project. The research on Taean Formation formed part of SH's M.Sc. thesis supervised by KdJ at Seoul National University. Aides-de-camp during sampling for this study were Mr. YANG Siho, as part of his B.Sc. research project in the Yeoncheon Complex, who also assisted with preparation of some samples, and Mr. KIM Daeyeong. Miss KIM YeonJoo provided indispensable administrative assistance in the project's initial phase.

### **Conflict of interest**

We declare there is no conflict of interest.

## References

- Alexandrov, P., Ruffet, G., & Cheilletz, A. (2002). Muscovite recrystallization and saddle-shaped  $^{40}\text{Ar}/^{39}\text{Ar}$  age spectra: example from the Blond granite (Massif Central, France). *Geochimica et Cosmochimica Acta*, 66, 1793–1807. [http://dx.doi.org/10.1016/S0016-7037\(01\)00895-X](http://dx.doi.org/10.1016/S0016-7037(01)00895-X)
- Allaz, J., Maeder, X., Vannay, J.-C., & Steck, A. (2005). Formation of aluminosilicate-bearing quartz veins in the Simano nappe (Central Alps): structural, thermobarometric and oxygen isotope constraints. *Schweizerische Mineralogische und Petrographische Mitteilungen*, 85, 191–214.
- Bakker, H. E., de Jong, K., Helmers, H., & Biermann, C. (1989). The geodynamic evolution of the Internal Zone of the Betic Cordilleras (SE Spain): a model based on structural analysis and geothermobarometry. *Journal of Metamorphic Geology*, 7, 359–381. <http://dx.doi.org/10.1111/j.1525-1314.1989.tb00603.x>
- Batt, G. E., & Braun, J. (1997). On the thermomechanical evolution of compressional orogens. *Geophysical Journal International*, 128, 364–382. <https://doi.org/10.1111/j.1365-246X.1997.tb01561.x>
- Bosse, V., Féraud, G., Ballèvre, M., Peucat, J.-J., & Corsini, M. (2005). Rb–Sr and  $^{40}\text{Ar}/^{39}\text{Ar}$  ages in blueschists from the Ile de Groix (Armorican Massif, France): Implications for closure mechanisms in isotopic systems. *Chemical Geology*, 220, 21–45. <https://doi.org/10.1016/j.chemgeo.2005.02.019>
- Cheong, C.-s., Kim, N. H., Hui, J. J., Cho, M., Choi, S. H., Zhou, H., & Geng, J.-Z. (2015). Lithospheric mantle signatures as revealed by zircon Hf isotopes of Late Triassic post-collisional plutons from the central Korean peninsula, and their tectonic implications. *Terra Nova*, 27, 97–105. <http://dx.doi.org/10.1111/ter.12135>
- Cheong, C.-s., Kim, N., Kim, J., Yi, K., Jeong, Y.-J., Park, C.-S., Li, H.-k., & Cho, M. (2014). Petrogenesis of Late Permian sodic metagranitoids in southeastern Korea: SHRIMP zircon geochronology and elemental and Nd–Hf isotope geochemistry. *Journal of Asian Earth Sciences*, 95, 228–242. <https://doi.org/10.1016/j.jseaes.2014.06.005>
- Cho D.-L. (2014). SHRIMP U-Pb zircon geochronology of the Guryong Group in Odesan area, east Gyeonggi Massif, Korea: A new identification of Late Paleozoic strata and its tectonic implication. *Journal of the Petrological Society of Korea*, 23, 197–208. <http://dx.doi.org/10.7854/JPSK.2014.23.3.197> (in Korean with English abstract)
- Cho, D.-L., & Kwon, S.-T. (1994). Hornblende geobarometry of the Mesozoic granitoids and evolution of crustal thickness. *Journal of the Geological Society of Korea*, 30, 41–61. (in Korean with English abstract)

- Cho, D.-L., Kwon, S.-T., Jeon, E.-Y., & Armstrong, R. (2005). SHRIMP U–Pb zircon ages of metamorphic rocks from the Samgot unit, Yeoncheon complex in the Imjingang belt, Korea: Implications for the Phanerozoic tectonics of East Asia. *Geological Society of America Abstracts with Programs*, 37(7), p. 388.
- Cho, D.-L., Suzuki, K., Adachi, M., & Chwae, U. (1996). A preliminary CHIME age determination of monazites from metamorphic and granitic rocks in the Gyeonggi Massif, Korea. *Journal of Earth and Planetary Sciences, Nagoya University*, 43, 49–65. (retrieved from: <https://nagoya.repo.nii.ac.jp/records/1420>)
- Cho, M., Cheong, W., Ernst, W. G., Yi, K., & Kim, J. (2013). SHRIMP U-Pb ages of detrital zircons in metasedimentary rocks of the central Ogcheon fold-thrust belt, Korea: Evidence for tectonic assembly of Paleozoic sedimentary protoliths. *Journal of Asian Earth Sciences*, 63, 234–249. <http://dx.doi.org/10.1016/j.jseaes.2012.08.020>
- Cho, M., & Kim, H. (2005). Metamorphic evolution of the Ogcheon Belt, Korea: A review and new age constraints. *International Geology Review*, 47, 41–57. <https://doi.org/10.2747/0020-6814.47.1.41>
- Cho, M., Kim, Y., & Ahn, J. (2007). Metamorphic evolution of the Imjingang Belt, Korea: Implications for Permo-Triassic collisional orogeny. *International Geology Review*, 49, 30–51. <http://dx.doi.org/10.2747/0020-6814.49.1.30>
- Cho, M., Kim, T., Yang, S.-y., & Yi, K. (2017). Paleoproterozoic to Triassic crustal evolution of the Gyeonggi Massif, Korea: Tectonic correlation with the North China craton. In R.D. Law, J.R. Thigpen, A.J. Merschat, H.H. Stowell (Eds.), *Linkages and Feedbacks in Orogenic Systems, Geological Society of America Memoir* (Vol. 213, pp. 165–197). [http://dx.doi.org/10.1130/2017.1213\(09\)](http://dx.doi.org/10.1130/2017.1213(09))
- Cho, M., Lee, Y., Kim, T., Cheong, W., Kim, Y., & Lee, S. R. (2017). Tectonic evolution of Precambrian basement massifs and an adjoining fold-and-thrust belt (Gyeonggi Marginal Belt), Korea: An overview. *Geosciences Journal*, 21, 845–865. <http://dx.doi.org/10.1007/s12303-017-0044-2>
- Choi, D. K., Woo, J., & Park, T.-Y. (2012). The Okcheon Supergroup in the Lake Chungju area, Korea: Neoproterozoic volcanic and glaciogenic sedimentary successions in a rift basin. *Geosciences Journal*, 16, 229–252. <http://dx.doi.org/10.1007/s12303-012-0031-6>
- Choi, S. G., Rajesh, V. J., Seo, J., Park, J. W., Oh, C. W., Park, S. J., & Kim, S. W. (2009). Petrology, geochronology and tectonic implications of Mesozoic high Ba–Sr granites in the Haemi area, Hongseong Belt, South Korea. *Island Arc*, 18, 266–281. <http://dx.doi.org/10.1111/j.1440-1738.2008.00622.x>
- Chough, S. K. (2013). *Geology and sedimentology of the Korean Peninsula*. Amsterdam: Elsevier, 363 p.

- Cliff, R. A., Jones, G., Choi, W. C., & Lee, T. J. (1985). Strontium isotopic equilibration during metamorphism of tillites from the Ogcheon Belt, South Korea. *Contributions to Mineralogy and Petrology*, 90, 346–352. <http://dx.doi.org/10.1007/BF00384713>
- Cohen, K. M., Finney, S. C., Gibbard, P. L., & Fa, J.-X. (2013). The ICS international chronostratigraphic chart. *Episodes*, 36, 199–204. Retrieved updated from <http://www.stratigraphy.org/ICSchart/ChronostratChart2021-07.pdf>
- Daoudene, Y., Ruffet, G., Cocherie, A., Ledru, P., & Gapais, D. (2013). Timing of exhumation of the Ereendavaa metamorphic core complex (north-eastern Mongolia) - U–Pb and  $^{40}\text{Ar}/^{39}\text{Ar}$  constraints. *Journal of Asian Earth Sciences*, 62, 98–116. <http://dx.doi.org/10.1016/j.jseaes.2011.04.009>
- de Jong, K., Han, S., & Ruffet, G. (2015). Fast cooling following a Late Triassic metamorphic and magmatic pulse: implications for the tectonic evolution of the Korean Collision Belt. In T. Kusky & W.J. Xiao (Eds.), *Comparative Tectonic and Dynamic Analysis of Cratons, Orogens, Basins, and Metallogeny, Tectonophysics*, 662, 271–290. <http://dx.doi.org/10.1016/j.tecto.2015.06.016>
- de Jong, K., Han, S., Ruffet, G., & Yi, K. (2014). First age constraints on the timing of metamorphism of the Tae'an Formation, Anmyeondo: concordant 233 Ma U–Pb titanite and 231–229 Ma  $^{40}\text{Ar}/^{39}\text{Ar}$  muscovite ages *Journal of the Geological Society of Korea*, 50, 593–609. <http://dx.doi.org/10.14770/jgsk.2014.50.5.593> (in Korean with English abstract). Original English version downloadable from [https://www.researchgate.net/profile/Koen\\_De\\_Jong/](https://www.researchgate.net/profile/Koen_De_Jong/)
- de Jong, K., Kurimoto, C., & Ruffet, G. (2009). Triassic  $^{40}\text{Ar}/^{39}\text{Ar}$  ages from the Sakaigawa unit, Kii Peninsula, Japan - implications for possible merger of the Central Asian Orogenic Belt with large-scale tectonic systems of the East Asian margin. *International Journal of Earth Sciences*, 98, 1529–1556. <http://dx.doi.org/10.1007/s00531-008-0340-1>
- de Jong, K., & Ruffet, G. (2014a). Tectonic implications of the very fast cooling shown by concordant 230–228 Ma  $^{40}\text{Ar}/^{39}\text{Ar}$  laser probe hornblende and biotite single-grain ages in the Hongseong area. *Journal of the Geological Society of Korea*, 50, 611–626. <http://dx.doi.org/10.14770/jgsk.2014.50.5.611> (in Korean with English abstract). Original English version downloadable from [https://www.researchgate.net/profile/Koen\\_De\\_Jong/](https://www.researchgate.net/profile/Koen_De_Jong/)
- de Jong, K., & Ruffet, G. (2014b). 243–220 Ma  $^{40}\text{Ar}/^{39}\text{Ar}$  laser probe muscovite single-grain ages in the northernmost Gyeonggi Massif (Juksung area) and their tectonic implications. *Journal of the Geological Society of Korea*, 50, 771–782. <http://dx.doi.org/10.14770/jgsk.2014.50.5.771> (in Korean with English abstract). Original English version downloadable from [https://www.researchgate.net/profile/Koen\\_De\\_Jong/](https://www.researchgate.net/profile/Koen_De_Jong/)
- de Jong, K., Wijbrans, J. R., & Féraud, G. (1992). Repeated thermal resetting of phengites in the Mulhacen Complex (Betic Zone, southeastern Spain) shown by  $^{40}\text{Ar}/^{39}\text{Ar}$  stepheating and single-

- grain laser probe dating. *Earth and Planetary Science Letters*, 110, 173–191.  
[http://dx.doi.org/10.1016/0012-821X\(92\)90047-Y](http://dx.doi.org/10.1016/0012-821X(92)90047-Y)
- de Jong, K., Xiao, W. J., Windley, B. F., Masago, H., & Lo, C. H. (2006). Ordovician  $^{40}\text{Ar}/^{39}\text{Ar}$  phengite ages from the blueschist-facies Ondor Sum subduction-accretion complex (Inner Mongolia) and implications for the early Paleozoic history of continental blocks in China and adjacent areas. *American Journal of Science*, 306, 799–845. <http://dx.doi.org/10.2475/10.2006.02>
- De Putter, Th., & Ruffet, G. (2020). Supergene manganese ore records 75 Myr-long Campanian to Pleistocene geodynamic evolution and weathering history of the Central African Great Lakes Region – Tectonics drives, climate assists. *Gondwana Research*, 83, 96–117.  
<https://doi.org/10.1016/j.gr.2020.01.021>
- Dong, Y. P., & Santosh, M. (2016). Tectonic architecture and multiple orogeny of the Qinling Orogenic Belt, Central China. *Gondwana Research*, 29, 1–40. <http://dx.doi.org/10.1016/j.gr.2015.06.009>
- Egawa, K. (2013). East Asia-wide flat slab subduction and Jurassic synorogenic basin evolution in West Korea. In Y. Itoh (Ed.), *Mechanism of Sedimentary Basin Formation - Multidisciplinary Approach on Active Plate Margins* (pp. 61–81). Rijeka: IntechOpen. <http://dx.doi.org/10.5772/56770>
- Fleck, R. J., Sutter, J. F., & Elliot, D. H. (1977). Interpretation of discordant  $^{40}\text{Ar}/^{39}\text{Ar}$  age-spectra of Mesozoic tholeiites from Antarctica. *Geochimica et Cosmochimica Acta*, 41, 15–32.  
[https://doi.org/10.1016/0016-7037\(77\)90184-3](https://doi.org/10.1016/0016-7037(77)90184-3)
- Han, R., Min, K., Ree, J.-H., & Foster, D. A. (2014). Extensional deformation along the southern boundary of the Gyeonggi Massif, South Korea: structural characteristics, age constraints, and tectonic implications. *International Journal of Earth Sciences*, 103, 757–776.  
<http://dx.doi.org/10.1007/s00531-013-0985-2>
- Han, S. Y., de Jong, K., & Yi, K. (2017). Detrital zircon ages in Korean mid-Paleozoic meta-sandstones (Imjingang Belt and Taean Formation): constraints on tectonic and depositional setting, source regions and possible affinity with Chinese terranes. *Journal of Asian Earth Sciences*, 143, 191–217.  
<http://dx.doi.org/10.1016/j.jseaes.2017.04.028>
- Harris, N. B. W. (2007). Channel flow and the Himalayan-Tibet orogen: a review. *Journal of the Geological Society London*, 164, 511–523. <https://doi.org/10.1144/0016-76492006-133>
- Harrison, T. M. (1981). Diffusion of  $^{40}\text{Ar}$  in hornblende. *Contributions to Mineralogy and Petrology*, 78, 324–331. <https://doi.org/10.1007/BF00398927>
- Harrison, T. M., C  lerier, J., Aikman, A. B., Hermann, J., & Heizler, M. T. (2009). Diffusion of  $^{40}\text{Ar}$  in muscovite. *Geochimica et Cosmochimica Acta*, 73, 1039–1051.  
<https://doi.org/10.1016/j.gca.2008.09.038>



- Jamieson, R. A., Beaumont, C., Fullsack, P., & Lee, B. (1998). Barrovian regional metamorphism: Where's the heat? In: P.J. Treloar & P.J. O'Brien (Eds.), *What drives metamorphism and metamorphic reactions, Geological Society of London Special Publications* (Vol. 138, pp. 23–51). <https://doi.org/10.1144/GSL.SP.1996.138.01.03>
- Jeon, E. Y., & Kwon, S.-T. (1999). Metamorphism of the Gonamsan area in the western Imjingang belt: Anti-clockwise P–T–t path. *Journal of the Geological Society of Korea*, 35, 49–72. (in Korean with English abstract)
- Jeong, J. W., Oh, C. W., & Cho, D.-L. (2021). The Neoproterozoic to Triassic tectonic evolution of Jangbong Island in the northwestern Gyeonggi Massif on the Korean Peninsula. *Lithos*, 390–391, 106102, <https://doi.org/10.1016/j.lithos.2021.106102>
- Jeong, Y.-J., Cheong, C.-S., Park, C.-Y., & Shin, I.-H. (2008). Geochemistry, isotope properties and U-Pb sphene age of the Jeongeup foliated granite, Korea. *Journal of the Korean Earth Sciences Society*, 29, 539–550.
- Jeong, Y.-J., Yi, K., Kamo, S. L., & Cheong, C.-S. (2008). ID-TIMS single zircon age determination of mangerite in the eastern Gyeonggi massif, Korea. *Journal of the Geological Society of Korea*, 44, 425–433. (in Korean with English abstract)
- Jourdan, F., Verati, C., & Feraud, G. (2006). Intercalibration of the Hb3gr  $^{40}\text{Ar}/^{39}\text{Ar}$  dating standard. *Chemical Geology*, 231, 177–189. <http://dx.doi.org/10.1016/j.chemgeo.2006.01.027>
- Jung, W.-S., Ree, J.-H., & Park, Y. (1999). Non-rotation of garnet porphyroblasts and 3-D inclusion trail data: an example from the Imjingang belt, South Korea. *Tectonophysics*, 307, 381–395. [https://doi.org/10.1016/S0040-1951\(99\)00105-5](https://doi.org/10.1016/S0040-1951(99)00105-5)
- Jung, W.-S., Ree, J.-H., Park, Y., & Choi, S.-H. (2002). Lattice preferred orientation of quartz inclusions within garnet porphyroblasts from the Imjingang belt, South Korea. *Journal of Structural Geology*, 24, 557–565. [https://doi.org/10.1016/S0191-8141\(01\)00083-9](https://doi.org/10.1016/S0191-8141(01)00083-9)
- Kee, W.-S. (Ed.) (2011). *Tectonic evolution of the upper crustal units in the mid-western part of the Korean peninsula*. (Basic Research Report, GP2009-012-01-2011(3)). Daejeon: Korea Institute of Geoscience and Mineral Resources (KIGAM) (In Korean with English summary).
- Kee, W.-S., Lim, S.-B., Kim, H., Hwang, S. K., Kim, B. C., Song, K.-Y., & Kihm, Y.-H. (2008). Yeoncheon Sheet, with explanatory text. In *The Korean Geological Map* (scale 1:50,000). (Geological Survey Report). Daejeon: Korea Institute of Geoscience and Mineral Resources (KIGAM) (In Korean with English summary).
- Kim, S. W. (2005). Amphibole  $^{40}\text{Ar}/^{39}\text{Ar}$  geochronology from the Okcheon Metamorphic Belt, South Korea and its tectonic implications. *Gondwana Research*, 8, 385–402. [https://doi.org/10.1016/S1342-937X\(05\)71142-4](https://doi.org/10.1016/S1342-937X(05)71142-4)

- Kim, J.-M., Cheong, C.-S., Lee, S.-R., Cho, M., & Yi, K. (2008). In-situ U–Pb titanite age of the Chuncheon amphibolite: Evidence for Triassic regional metamorphism in central Gyeonggi massif, South Korea, and its tectonic implication. *Geosciences Journal*, *12*, 309–316. <http://dx.doi.org/10.1007/s12303-008-0031-8>
- Kim, D., Cho, M., & Kim, H. (2009). *An electron backscatter diffraction (EBSD) study of garnet-bearing aggregate lineation in calc-silicate rocks, Imjingang belt, Korea*. Paper presented at 8<sup>th</sup> International Eclogite Conference, Xining, China.
- Kim, Y., & Cho, M. (2008). Two-stage growth of porphyroblastic biotite and garnet in the Barrovian metapelites of the Imjingang belt, central Korea. *Journal of Metamorphic Geology*, *26*, 385–399. <http://dx.doi.org/10.1111/j.1525-1314.2008.00767.x>
- Kim, H. S., & Jung, W.-S. (2010). The use of garnet porphyroblasts to resolve the metamorphic pressure–temperature–deformation (P–T–d) path: An example from the Imjingang belts, South Korea. *Geosciences Journal*, *14*, 111–126. <http://dx.doi.org/10.1007/s12303-010-0012-6>
- Kim, S. W., Kwon, S., Park, S.-I., Yi, K., Santosh, M., & Kim, H. S. (2017). Early to Middle Paleozoic tectonometamorphic evolution of the Hongseong area, central western Korean Peninsula: Tectonic implications. *Gondwana Research*, *47*, 308–322. <https://doi.org/10.1016/j.gr.2016.05.016>
- Kim, S. W., Kwon, S., Park, S.-I., Yi, K., Santosh, M., & Ryu, I.-C. (2015). Early to Middle Paleozoic arc magmatism in the Korean Peninsula: Constraints from zircon geochronology and geochemistry. *Journal of Asian Earth Sciences*, *113*, 866–882. <http://dx.doi.org/10.1016/j.jseas.2015.09.017>
- Kim, S. W., Kwon, S.-T., & Ryu, I.-C. (2009). Geochronological constraints on multiple deformations of the Honam Shear Zone, South Korea and its tectonic implication. *Gondwana Research*, *16*, 82–89. <http://dx.doi.org/10.1016/j.gr.2008.12.004>
- Kim, S. W., Oh, C.W., Williams, I. S., Rubatto, D., Ryu, I.-C., Rajesh, V. J., Kim, C.-B., Guo, J., & Zhai, M. (2006). Phanerozoic high-pressure eclogite and intermediate-pressure granulite facies metamorphism in the Gyeonggi Massif, South Korea: Implications for the eastward extension of the Dabie-Sulu continental collision zone. *Lithos*, *92*, 357–377. <http://dx.doi.org/10.1016/j.lithos.2006.03.050>
- Kim, S. W., Park, S.-I., Jang, Y., Kwon, S., Kim, S.-J., & Santosh, M. (2017). Tracking Paleozoic evolution of the South Korean Peninsula from detrital zircon records: Implications for the tectonic history of East Asia. *Gondwana Research*, *50*, 195–215. <https://doi.org/10.1016/j.gr.2017.05.009>
- Kim, H. S., Ree, J.-H., Kang, H.-C., & Yi, K. (2022). Pressure–temperature–time–deformation (P–T–t–d) path for Devonian forearc deposits in the Imjingang Belt, South Korea: Implications for Permian–Triassic collisional orogenesis on the eastern margin of Eurasia. *Journal of Metamorphic Geology*, *40*, 489–516. <https://doi.org/10.1111/jmg.12636>

- Kim, J.-N., Ree, J.-H., Kwon, S.-T., Park, Y., Choi, S.-J., & Cheong, C.-S. (2000). The Kyonggi shear zone of the central Korean Peninsula: late orogenic imprint of the North and South China collision. *Journal of Geology*, 108, 469–478. <http://dx.doi.org/10.1086/314412>
- Kim, K. H., Suzuki, K., Lee, J. I., & Jang, H. K. (2008). CHIME ages of monazites from metamorphic rocks from the Precambrian Gyeonggi Gneiss Complex in the Siheung and Seosan Group of the Gyeonggi Massif, South Korea. *Economic and Environmental Geology*, 41, 173–181. (In Korean with English summary)
- Kim, S. W., Williams, I. S., Kwon, S., & Oh, C. W. (2008). SHRIMP zircon geochronology, and geochemical characteristics of metaplutonic rocks from the south-western Gyeonggi Block, Korea: Implications for Paleoproterozoic to Mesozoic tectonic links between the Korean Peninsula and eastern China. *Precambrian Research*, 162, 475–497. <http://dx.doi.org/10.1016/j.precamres.2007.10.006>
- Kwon, S., Kim, S. W., & Santosh, M. (2013). Multiple generations of mafic–ultramafic rocks from the Hongseong suture zone, western South Korea: implications for the geodynamic evolution of NE Asia. *Lithos*, 160–161, 68–83. <http://dx.doi.org/10.1016/j.lithos.2012.11.011>
- Kwon, S., Sajeed, K., Mitra, G., Park, Y., Kim, S. W., & Ryu, I.-C. (2009). Evidence for Permo-Triassic collision in Far East Asia: The Korean collisional orogen. *Earth and Planetary Science Letters*, 279, 340–349. <http://dx.doi.org/10.1016/j.epsl.2009.01.016>
- Kwon, S., Samuel, V. O., Song, Y., Kim, S. W., Park, S.-I., Jang, Y., & Santosh, M. (2020). Eclogite resembling metamorphic disequilibrium assemblage formed through fluid-induced metasomatic reactions. *Science Report*, 10, 19869 <https://doi.org/10.1038/s41598-020-76999-y>
- Lancaster, P. J., Baxter, E. F., Ague, J. J., Breeding, C. M., & Owens, T. L. (2008). Synchronous peak Barrovian metamorphism driven by syn-orogenic magmatism and fluid flow in southern Connecticut, USA. *Journal of Metamorphic Geology*, 26, 527–538. <https://doi.org/10.1111/j.1525-1314.2008.00773.x>
- Lee, S.R., & Cho, K. (2012). Precambrian crustal evolution of the Korean Peninsula. *Journal of the Petrological Society of Korea*, 21, 89–112. <https://doi.org/10.7854/JPSK.2012.21.2.089> (in Korean with English abstract)
- Lee, S. R., & Cho, M. (2003). Metamorphic and tectonic evolution of the Hwacheon granulite complex, central Korea: composite P-T path resulting from two distinct crustal-thickening events. *Journal of Petrology*, 44, 197–225. <http://dx.doi.org/10.1093/petrology/44.2.197>
- Lee, B. C., Oh, C. W., Cho, D.-L., Zhai, M., Lee, B. C., Peng, P., & Yi, K. (2019). The Devonian back-arc basin and Triassic arc-continent collision along the Imjingang belt in the Korean Peninsula and their tectonic meaning. *Lithos*, 328–329, 276–296, <https://doi.org/10.1016/j.lithos.2019.01.011>

- 1964 Lee, B. C., Oh, C. W., Yengkhom, K. S., & Yi, K. (2014). Paleoproterozoic magmatic and metamorphic  
 1965 events in the Hongcheon area, southern margin of the Northern Gyeonggi Massif in the Korean  
 1966 Peninsula, and their links to the Paleoproterozoic orogeny in the North China Craton. *Precambrian*  
 1967 *Research*, 248, 17–38. <http://dx.doi.org/10.1016/j.precamres.2014.04.003>
- 1968 Lee, D.-C., Choh, S.-J., Lee, D.-C., Ree, J.-H., Lee, J.-H., & Lee, S.-B. (2017). Where art thou “the great  
 1969 hiatus?” – review of Late Ordovician to Devonian fossil-bearing strata in the Korean Peninsula and  
 1970 its tectonostratigraphic implications. *Geosciences Journal*, 21, 913–931.  
 1971 <http://dx.doi.org/10.1007/s12303-017-0046-0>
- 1972 Lee, H.-j., Park, S.-I., Choi, T.-j., & Sim, M. S. (2021). Post-collisional denudation of an orogenic belt  
 1973 traced from geochronological and bulk-rock geochemical records of the western Korean Peninsula.  
 1974 *International Geology Review*, 63, 87–108. <https://doi.org/10.1080/00206814.2019.1706649>
- 1975 Lee, J. Y., Marti, K., Severinghaus, J. P., Kawamura, K., Yoo, H. S., Lee, J. B., & Kim, J. S. (2006). A  
 1976 redetermination of the isotopic abundances of atmospheric Ar. *Geochimica et Cosmochimica Acta*,  
 1977 70, 4507–4512. <http://dx.doi.org/10.1016/j.gca.2006.06.1563>
- 1978 Lee, S. R., Cho, M., Cheong, C.-S., Kim, H., & Wingate, M. T. D. (2003). Age, geochemistry, and  
 1979 tectonic significance of Neoproterozoic alkaline granitoids in the northwestern margin of the  
 1980 Gyeonggi massif, South Korea. *Precambrian Research*, 122, 297–310.  
 1981 [http://dx.doi.org/10.1016/S0301-9268\(02\)00216-4](http://dx.doi.org/10.1016/S0301-9268(02)00216-4)
- 1982 Lim, C., & Cho, M. (2012). Two-phase contractional deformation of the Jurassic Daebo Orogeny,  
 1983 Chungnam Basin, Korea, and its correlation with the early Yanshanian movement of China.  
 1984 *Tectonics*, 31, TC1004. <http://dx.doi.org/10.1029/2011TC002909>
- 1985 Lister, G. S., & Baldwin, S. L. (1996). Modeling the effect of arbitrary P–T–t histories on argon diffusion  
 1986 in minerals using the MacArgon program for the Apple Macintosh. *Tectonophysics*, 253, 83–109.  
 1987 [https://doi.org/10.1016/0040-1951\(95\)00059-3](https://doi.org/10.1016/0040-1951(95)00059-3)
- 1988 Liu, X. C., Li, S. Z., & Jahn, B. M. (2015). Tectonic evolution of the Tongbai-Hong’an orogen in central  
 1989 China: From oceanic subduction/accretion to continent-continent collision. *Science China Earth*  
 1990 *Sciences*, 58, 1477–1496. <http://dx.doi.org/10.1007/s11430-015-5145-z>
- 1991 Mark, D. F., Stuart, F. M., & De Podesta, M. (2011). New high-precision measurements of the isotopic  
 1992 composition of atmospheric argon. *Geochimica et Cosmochimica Acta*, 75, 7494–7501.  
 1993 <http://dx.doi.org/10.1016/j.gca.2011.09.042>
- 1994 Mudruk, S. V., Balagansky, V. V., Raevsky, A. B., Rundkvist, O. V., Matyushkin, A. V., & Gorbunov, I.  
 1995 A. (2022). Complex shape of the Palaeoproterozoic Serpovidny refolded mega-sheath fold in  
 1996 northern Fennoscandia revealed by magnetic and structural data. *Journal of Structural Geology*,  
 1997 154, 104492. <https://doi.org/10.1016/j.jsg.2021.104492>

- Oh, C. W., Imayama, T., Jeon, J., & Yi, K. (2017). Regional Middle Paleozoic metamorphism in the southwestern Gyeonggi Massif, South Korea: Its implications for tectonics in Northeast Asia. *Journal of Asian Earth Sciences*, 145, 542–564. <http://dx.doi.org/10.1016/j.jseae.2017.06.030>
- Oh, C. W., Imayama, T., Lee, S. Y., Yi, S.-B., Yi, K., & Lee, B. C. (2015). Permo-Triassic and Paleoproterozoic metamorphism related to continental collision in Yangpyeong, South Korea. *Lithos*, 216–217, 264–284. <http://dx.doi.org/10.1016/j.lithos.2014.12.016>
- Oh, C. W., & Kusky, T. M. (2007). The Late Permian to Triassic Hongseong-Odesan collision belt in South Korea, and its tectonic correlation with China and Japan. *International Geology Review*, 49, 639–657. <https://doi.org/10.2747/0020-6814.49.7.636>
- Om, H. Y., Kim, Y. H., & Ryang, C. C. (1993). Devonian Strata (Rimjin System). In R.J. Paek, H.G. Kang, G.P. Jon, Y.M. Kim, Y.H. Kim (Eds.), *Geology of Korea*. (pp. 114–129). Pyongyang: Geological Institute Academy of Science DPRK, Foreign Languages Books Publishing House.
- Park, S.-I., Kim, S. W., Kwon, S., Thanh, N. X., Yi, K., & Santosh, M. (2014). Paleozoic tectonics of the southwestern Gyeonggi massif, South Korea: Insights from geochemistry, chromian-spinel chemistry and SHRIMP U-Pb geochronology. *Gondwana Research*, 26, 684–698. <http://dx.doi.org/10.1016/j.gr.2013.07.015>
- Park, K.-H., Kim, M. J., Yang, Y. S., & Cho, K. O. (2010). Age distribution of the Jurassic plutons in Korean Peninsula. *Journal of the Petrological Society of Korea*, 19, 269–281. (in Korean with English abstract)
- Park, S.-I., Kwon, S., Kim, S. W., Yi, K., & Santosh, M. (2014). Continental origin of the Bibong eclogite, southwestern Gyeonggi Massif, South Korea. *Journal of Asian Earth Sciences*, 95, 192–202. <http://dx.doi.org/10.1016/j.jseae.2014.08.024>
- Park, S.-I., Noh, J., Cheong, H. J., Kwon, S., Song, Y., Kim, S. W., & Santosh, M. (2019). Inversion of two-phase extensional basin systems during subduction of the Paleo-Pacific Plate in the SW Korean Peninsula: Implication for the Mesozoic “Laramide-style” orogeny along East Asian continental margin. *Geoscience Frontiers*, 10, 909–925. <https://doi.org/10.1016/j.gsf.2018.11.008>
- Pitra, P., Ballèvre, M., & Ruffet, G. (2010). Inverted metamorphic field gradient towards a Variscan suture zone (Champtoceaux Complex, Armorican Massif, France). *Journal of Metamorphic Geology*, 28, 183–208. <http://dx.doi.org/10.1111/j.1525-1314.2009.00862.x>
- Platt, J. P. (1986). Dynamics of orogenic wedges and the uplift of high-pressure metamorphic rocks. *Geological Society of America Bulletin*, 97, 1037–1053. [https://doi.org/10.1130/0016-7606\(1986\)97<1037:DOOWAT>2.0.CO;2](https://doi.org/10.1130/0016-7606(1986)97<1037:DOOWAT>2.0.CO;2)

- Purdy, J. W., & Jäger, E. (1976). K–Ar ages on rock-forming minerals from the Central Alps. *Memorie degli Istituti di Geologia e Mineralogia dell' Università di Padova*, 30, 1–31. (retrieved from: <https://phaidra.cab.unipd.it/detail/o:450665>).
- Ree, J.-H., Cho, M., Kwon, S.-T., & Nakamura, E. (1996). Possible eastward extension of Chinese collision belt in South Korea: The Imjingang belt. *Geology*, 24, 1071–1074. [https://doi.org/10.1130/0091-7613\(1996\)024<1071:PEEOCC>2.3.CO;2](https://doi.org/10.1130/0091-7613(1996)024<1071:PEEOCC>2.3.CO;2)
- Renne, P. R., Balco, G., Ludwig, R. L., Mundil, R., & Min, K. (2011). Response to the comment by W.H. Schwarz et al. on "Joint determination of  $^{40}\text{K}$  decay constants and  $^{40}\text{Ar}^*/^{40}\text{K}$  for the Fish Canyon sanidine standard, and improved accuracy for  $^{40}\text{Ar}/^{39}\text{Ar}$  geochronology" by P.R. Renne et al. (2010). *Geochimica et Cosmochimica Acta*, 75, 5097–5100. <http://dx.doi.org/10.1016/j.gca.2011.06.021>
- Renne, P. R., Mundil, R., Balco, G., Min, K., & Ludwig, R. L. (2010). Joint determination of  $^{40}\text{K}$  decay constants and  $^{40}\text{Ar}^*/^{40}\text{K}$  for the Fish Canyon sanidine standard, and improved accuracy for  $^{40}\text{Ar}/^{39}\text{Ar}$  geochronology. *Geochimica et Cosmochimica Acta*, 74, 5349–5367. <http://dx.doi.org/10.1016/j.gca.2010.06.017>
- Renne, P. R., Swisher, C. C., Deino, A. L., Karner, D. B., Owens, T. L., & DePaolo, D. J. (1998). Intercalibration of standards, absolute ages and uncertainties in  $^{40}\text{Ar}/^{39}\text{Ar}$  dating. *Chemical Geology*, 145, 117–152. [https://doi.org/10.1016/S0009-2541\(97\)00159-9](https://doi.org/10.1016/S0009-2541(97)00159-9)
- Ruffet, G., Féraud, G., & Amouric M. (1991). Comparison of  $^{40}\text{Ar}$ - $^{39}\text{Ar}$  conventional and laser dating of biotites from the North Trégor Batholith. *Geochimica et Cosmochimica Acta*, 55, 1675–1688. [https://doi.org/10.1016/0016-7037\(91\)90138-U](https://doi.org/10.1016/0016-7037(91)90138-U)
- Ruffet, G., Féraud, G., Ballèvre, M., & Kiénast, J. R. (1995). Plateau ages and excess argon in phengites: an  $^{40}\text{Ar}$ - $^{39}\text{Ar}$  conventional laser probe study of Alpine micas (Sesia zone, Western Alps, northern Italy). *Chemical Geology*, 121, 327–343. [https://doi.org/10.1016/0009-2541\(94\)00132-R](https://doi.org/10.1016/0009-2541(94)00132-R)
- Sagong, H., Cheong, C.-S., & Kwon, S.-T. (2003). Paleoproterozoic orogeny in South Korea: evidence from Sm–Nd and Pb step-leaching garnet ages of Precambrian basement rocks. *Precambrian Research*, 122, 275–295. [https://doi.org/10.1016/S0301-9268\(02\)00215-2](https://doi.org/10.1016/S0301-9268(02)00215-2)
- Sagong, H., Kwon, S.-T., & Ree, J.-H. (2005). Mesozoic episodic magmatism in South Korea and its tectonic implication. *Tectonics*, 24, TC5002. <http://dx.doi.org/10.1029/2004TC001720>
- Sajeev, K., Jeong, J., Kwon, S., Kee, W.-S., Kim, S. W., Komiya, T., Itaya, T., Jung, H.-S., & Park, Y. (2010). High P–T granulite relicts from the Imjingang belt, South Korea: Tectonic significance. *Gondwana Research*, 17, 75–86. <http://dx.doi.org/10.1016/j.gr.2009.07.001>
- Seo, J., Choi, S.-G., & Oh, C. W. (2010). Petrology, geochemistry, and geochronology of the post-collisional Triassic mangerite and syenite in the Gwangcheon area, Hongseong Belt, South Korea. *Gondwana Research*, 18, 479–496. <http://dx.doi.org/10.1016/j.gr.2009.12.009>



- So, Y., Rhee, C. W., Choi, P. Y., Kee, W. S., Seo, J. Y., & Lee, E. J. (2013). Distal turbidite fan/lobe succession of the Late Paleozoic Taean Formation, western Korea. *Geosciences Journal*, *17*, 9–25. <http://dx.doi.org/10.1007/s12303-013-0016-0>
- Suzuki, K. (2009). CHIME dating and age mapping of monazite in granulites and paragneisses from the Hwacheon area, Korea: implication to correlations to Chinese cratons. *Geosciences Journal*, *13*, 275–292. <http://dx.doi.org/10.1007/s12303-009-0027-z>
- Suzuki, K., Dunkley, D., Adachi, M., & Chwae, U. (2006). Discovery of a c. 370 Ma granitic gneiss clast from the Hwanggangri pebble-bearing phyllite in the Okcheon metamorphic belt, Korea. *Gondwana Research*, *9*, 85–94. <http://dx.doi.org/10.1016/j.gr.2005.06.004>
- Tartèse, R., Ruffet, G., Poujol, M., Boulvais, P., Ireland, T. R., & Bohn, M. (2011). Simultaneous resetting of the muscovite K–Ar and monazite U–Pb geochronometers: a story of fluids. *Terra Nova*, *23*, 390–398. <http://dx.doi.org/10.1111/j.1365-3121.2011.01024.x>
- Vanderhaeghe, O. (2012). The thermal–mechanical evolution of crustal orogenic belts at convergent plate boundaries: A reappraisal of the orogenic cycle. *Journal of Geodynamics*, *56–57*, 124–145. <http://dx.doi.org/10.1016/j.jog.2011.10.004>
- Viete, D. R., Forster, M. A., & Lister, G. S. (2011). The nature and origin of the Barrovian metamorphism, Scotland:  $^{40}\text{Ar}/^{39}\text{Ar}$  apparent age patterns and duration of metamorphism in the biotite zone. *Journal of the Geological Society London*, *168*, 133–146. <https://doi.org/10.1144/0016-76492009-164>
- Villa, I. M. (1998). Isotopic closure. *Terra Nova*, *10*, 42–47. <https://doi.org/10.1046/j.1365-3121.1998.00156.x>
- Villa, I. M., & Puxeddu, M. (1994). Geochronology of the Larderello geothermal field: new data and the 'closure temperature' issue. *Geochimica et Cosmochimica Acta*, *115*, 415–426. <https://doi.org/10.1007/BF00320975>
- Vorhies, S. H., & Ague, J. J. (2011). Pressure–temperature evolution and thermal regimes in the Barrovian zones, Scotland. *Journal of the Geological Society London*, *168*, 1147–1166. <https://doi.org/10.1144/0016-76492010-073>
- Whitney, D. L., & Dilek, Y. (2000). Andalusite-sillimanite-quartz veins as indicators of low-pressure-high temperature deformation during late-stage unroofing of a metamorphic core complex, Turkey. *Journal of Metamorphic Geology*, *18*, 59–66. <http://dx.doi.org/10.1046/j.1525-1314.2000.00234.x>
- Williams, I. S., Cho, D. L., & Kim, S. W. (2009). Geochronology, and geochemical and Nd–Sr isotopic characteristics of Triassic plutonic rocks in the Gyeonggi Massif, South Korea: Constraints on Triassic post-collisional magmatism. *Lithos*, *107*, 239–256. <http://dx.doi.org/10.1016/j.lithos.2008.10.017>

- Wu, Y.-B., & Zheng, Y.-F. (2013). Tectonic evolution of a composite collision orogen: an overview on the Qinling–Tongbai–Hong’an–Dabie–Sulu orogenic belt in central China. *Gondwana Research*, 23, 1402–1428. <http://dx.doi.org/10.1016/j.gr.2012.09.007>
- Xu, Z. Q., Yang, W. C., Ji, S. C., Zhang, Z. M., Yang, J. S., Wang, Q., & Tang, Z. M. (2009). Deep root of a continent–continent collision belt: Evidence from the Chinese Continental Scientific Drilling (CCSD) deep borehole in the Sulu ultrahigh-pressure (HP–UHP) metamorphic terrane, China. *Tectonophysics*, 475, 204–219. <http://dx.doi.org/10.1016/j.tecto.2009.02.029>
- Yengkhom, K. S., Lee, B. C., Oh, C. W., Yi, K., & Kang, J. H. (2014). Tectonic and deformation history of the Gyeonggi Massif in and around the Hongcheon area, and its implications in the tectonic evolution of the North China Craton. *Precambrian Research*, 240, 37–59. <http://dx.doi.org/10.1016/j.precamres.2013.10.016>
- York, D. (1969). Least squares fitting of a straight line with correlated errors. *Earth and Planetary Science Letters*, 5, 320–324. [https://doi.org/10.1016/S0012-821X\(68\)80059-7](https://doi.org/10.1016/S0012-821X(68)80059-7)
- York, D., Evensen, N., Lopez-Martinez, M., & De Basabe Delgado, J. (2005). Unified equations for the slope, intercept, and standard errors of the best straight line. *American Journal of Physics*, 72, 367–375. <https://doi.org/10.1119/1.1632486>
- Yi, K., (2010). *Recrystallization and SHRIMP U–Th–Pb geochronology of monazite in high-grade gneisses, Gyeonggi Massif, Korea*. (Doctoral dissertation). Seoul: Seoul National University.
- Yi, K., & Cho, M. (2009). SHRIMP Geochronology and reaction texture of monazite from a retrogressive transitional layer, Hwacheon Granulite Complex, Korea. *Geosciences Journal*, 13, 293–304. <http://dx.doi.org/10.1007/s12303-009-0028-y>